2017

Sediment Mobilization from Streambank Failures: Model Development and Climate Impact Studies

Jody Juniper Stryker
University of Vermont

SEDIMENT MOBILIZATION FROM STREAM BANK FAILURES: MODEL DEVELOPMENT AND CLIMATE IMPACT STUDIES.

A Dissertation Presented

By

Jody J. Stryker

To

The Faculty of the Graduate College

of

The University of Vermont

In Partial Fulfillment of the Requirements
for the Degree of Doctor of Philosophy
Specializing in Civil and Environmental Engineering

May, 2017

Defense Date: December 19, 2016
Dissertation Examination Committee:

Arne Bomblies, Ph.D., Advisor
Carol Adair, Ph.D., Chairperson
Beverley Wemple, Ph.D., Co-Advisor
Mandar Dewoolkar, Ph.D.
Cynthia J. Forehand, Ph.D., Dean of the Graduate College

ABSTRACT

This research incorporates streambank erosion and failure processes into a distributed watershed model and evaluates the impacts of climate change on the processes driving streambank sediment mobilization at a watershed scale. Excess sediment and nutrient loading are major water quality concerns for streams and receiving waters. Previous work has established that in addition to surface and road erosion, streambank erosion and failure are primary mechanisms that mobilize sediment and nutrients from the landscape. This mechanism and other hydrological processes driving sediment and nutrient transport are likely to be highly influenced by anticipated changes in climate, particularly extreme precipitation and flow events. This research has two primary goals: to develop a physics-based watershed model with more inclusive representation of sediment by including simulation of streambank erosion and geotechnical failure; and to investigate the impacts of climate change on unstable streams and suspended sediment mobilization by overland erosion, erosion of roads, and the erosion as well as failure of streambanks. This advances mechanistic simulation of suspended sediment mobilization and transport from watersheds, which is particularly valuable for investigating the impacts of climate and land use changes, as well as extreme events.

Model development involved coupling two existing physics-based models: the Bank Stability and Toe Erosion Model (BSTEM) and the Distributed Hydrology Soil Vegetation Model (DHSVM). This approach simulates streambank erosion and failure in a spatially explicit environment. The coupled model is applied to the Mad River watershed in central Vermont as a test case. I then use the calibrated Mad River model to predict the response in watershed sediment loading to future climate scenarios that specifically represent local temperature and precipitation trends for the northeastern US, particularly changing trends in the frequency and magnitude of extreme precipitation.

Overall the streambank erosion and failure processes are captured in the coupled model approach. Although the presented calibration of the model underestimates suspended sediment concentrations resulting from relatively small storm/flow events, it still improves prediction of cumulative loads and in some cases suspended sediment concentrations during elevated flow events in comparison to model results without including BSTEM. Increases in temperature affect the timing and magnitude of snow melt and spring flows, as well as associated sediment mobilization, in the watershed. Increases in annual precipitation and in extreme precipitation events produce increases in annual as well as peak discharge and sediment loads in the watershed.

This research adds to the body of evidence indicating that streambank erosion and failure can be a major source of suspended sediment, and thereby a major source of phosphorus as well. It also shows that local climate trends in the Northeast are likely to result in higher peak discharges and sediment yields from meso-scale, high-gradient watersheds that encompass headwater forested streams and agricultural floodplains. One limitation was that we could not drive the model with meteorological data that represented changes in both temperature and precipitation, highlighting the need for improved climate predictions. This coupled model approach could be parameterized for alternative watersheds and be re-applied to answer various questions related to erosion processes and sediment transport in a watershed. These findings have important implications for resource allocation and targeted watershed management strategies.

CITATIONS

Material from this dissertation has been submitted for publication to *Water Resources Research* on May 2, 2016 in the following form:

Stryker, J., Wemple, B., Bomblies, A.. Modeling sediment mobilization using a distributed hydrology model coupled with a bank stability model. *Water Resources Research*.

AND

Material from this dissertation is in the final stages of preparation and will be submitted for publication to *Geophysical Research Letters* in February 2017 in the following form:

Stryker, J., Wemple, B., Bomblies, A.. The impacts of climate change on sediment mobilization and transport in the Mad River watershed, Vermont. *Geophysical Research Letters.*

ACKNOWLEDGEMENTS

So many people supported me on my way to completing this research and degree. First, I would never have finished this without the hard work and dedication of my husband. In particular, he took on a lot of extra house and baby responsibilities near the end of my graduate work, and I am really appreciative. I am also thankful to my parents for all their support through the many years of school. My advisors, Dr. Arne Bomblies and Dr. Beverley Wemple, were invaluable and I am so grateful for their guidance and mentorship. I am also appreciative of the rest of my committee for their suggestions and input into this research. I cannot imagine a better group of people to have worked with and learned from.

TABLE OF CONTENTS

LIST OF TABLES

LIST OF FIGURES

CHAPTER 1: DISSERTATION OVERVIEW

Excess sediment and nutrient loading is currently a major water quality issue for freshwater ecosystems and it is likely to have an increasingly significant impact with anticipated changes in climate. This work was a component of a broader project that was largely motivated by the observed increase in the frequency and severity of algal blooms in Lake Champlain, a freshwater lake situated between Vermont, New York, and Canada. The presence of surplus phosphorus promotes the excessive growth of algae, which can result in cyanobacteria blooms that have negative impacts on the quality and value of water resources in Lake Champlain (Lake Champlain Basin Program, 2012), as well as have the potential to impact human health in the basin (Boyer et al., 2004). It is known that a significant portion of phosphorus reaches the lake as sediment-bound phosphorus which is transported from non-point watershed sources. From among the sources of sediment reaching receiving water bodies such as Lake Champlain, a portion originates from overland erosion, particularly from agricultural and urban areas, as well as from the erosion of unpaved roads. It has been more recently determined that in addition to surface and road erosion, streambank erosion and scour can yield large amounts of sediment from within a watershed (DeWolfe, Hession, & Watzin, 2004; Kalma & Ulmer, 2003; Ross et al., 2010).

Increased sediment loading due to streambank erosion can not only contribute large amounts of sediment-bound phosphorus and other nutrients, but can alone negatively impact water quality both in the watershed and further downstream. Accelerated streambank erosion can contribute to disproportional sediment supply to specific areas of a watershed, stream channel instability, land and habitat loss, as well as

have other consequences (US EPA, 2012). In addition, erosion and undercutting of banks and the continued incision of streams can affect infrastructure and flood resiliency of adjacent areas.

It is well known that changing weather patterns will have complex and nonlinear effects on many human and environmental systems, and this study is part of a larger examination of adaptation and resiliency in Vermont to such changes in climate as well as to increased variability in climate drivers. Processes leading to increased sediment mobilization, particularly from streambank erosion, will be impacted by changes in climate. For example, the northeastern United States is expected to experience an increase in temperatures and extreme precipitation, as well as alter precipitation patterns (Betts, 2011; Frumhoff, Melillo, Moser, & Wuebbles, 2007; Groisman et al., 2005; Guilbert et al., 2014; Guilbert, Betts, Rizzo, Beckage, & Bomblies, 2015; Stager & Thill, 2010). These changes will alter flow regimes as well as watershed conditions, leading to potentially significant changes in sediment loading at watershed outlets. Physics-based watershed models can be used as a tool for evaluating the potential impacts of changes in climate and land use on watershed processes affecting streamflow and sediment transport. However, currently no models exist that simulate streambank erosion and failure within a framework suitable for assessing potential changes in climate that are outside the current range of variability.

The primary goals of this work were to develop an improved approach to modeling sediment mobilization and loading within a watershed that includes representation of mechanisms leading to streambank erosion and failure, as well as then to answer questions related to sediment mobilization resulting from anticipated shifts in

precipitation patterns and resulting changes in flow regimes. The improved modeling approach was achieved by fully coupling two existing models: a distributed watershed hydrology model and a bank stability model. This work represents a methodological advance in our ability to mechanistically simulate processes that mobilize suspended sediment within a watershed, particularly with respect to erosion and failure of streambanks, and thereby an improved approximation of how much sediment and nutrients are transported to receiving water bodies such as lakes. This will be particularly valuable for investigating the potential impacts of anthropogenic changes in climate and land use. The long term objectives of developing this coupled approach include investigating the impact of climate change-driven extreme events, which involves climatic conditions that fall outside of the range of prior observations. The physics-based nature of these models provides a useful tool for assessing the impacts of land use and climate changes on the specific generation and transport of sediments within a watershed, because it has the ability to simulate system response to climate drivers that are outside the observed envelope of variability.

The remainder of this dissertation consists of a literature review as well as two peer-reviewed journal articles. Chapter 2 of this dissertation is a comprehensive review of current literature pertaining to the negative effects of suspended sediment loading in freshwater systems, anticipated changes in climate and the potential impacts on sediment and nutrient loading, and the use of modeling tools to quantify and evaluate changes in sediment and nutrient mobilization in the face of climate change. Chapter 3 consists of an article presenting the development of an improved modeling approach for simulating sediment mobilization within a watershed that includes representation of streambank

erosion in a distributed, mechanistic framework. This article also describes the initial application of this improved modeling approach to the Mad River Valley in central Vermont, including calibration and validation efforts. Chapter 4 is a second article that uses the calibrated Mad River model to evaluate changes in flow regimes and sediment mobilization in that watershed, driven by changes in precipitation and temperature that reflect local climate change trends. This last work makes use of the coupled modeling approach to gain insight into the variability we might expect to see in sediment loading as a result of climate change and discusses the potential implications of such changes.

CHAPTER 2: COMPREHESIVE LITERATURE REVIEW

2.1. OVERVIEW OF SUSPENDED SEDIMENT CONTAMINATION

The detrimental impacts of suspended sediments on global freshwater ecosystems are well known (Berry, Rubenstein, & Melzian, 2003; Bilotta & Brazier, 2008; Vörösmarty et al., 2010; Waters, 1995; Wilber & Clarke, 2001). Suspended sediments and nutrients are considered two of the leading causes of water quality impairment in Unites States lakes and reservoirs (Lake Champlain Basin Program, 2012; OW US EPA, 2000, 2002). Similarly the European Environmental Agency (EEA) has acknowledged that non-point pollution contributing to eutrophication and contamination of aquatic resources is a major environmental concern (European Environment Agency, 1995; Stanners, Bourdeau, & Agency, 1995). Excess phosphorus in freshwater ecosystems can promote eutrophication and the dominance of cyanobacteria, leading to serious degradation of aquatic ecosystems and impairment of water usage for drinking, recreation, industry, agriculture, and other uses (Carpenter et al., 1998; V. H. Smith, Tilman, & Nekola, 1999; Val H. Smith, 1998). Suspended sediments directly impact surface water quality by decreasing water clarity and increasing turbidity, increasing scour and decreased lifespan of dams and infrastructure, changing sediment storage capacity, degrading aquatic habitats, and in many other ways (Berry et al., 2003; Bilotta & Brazier, 2008; US EPA, 2000, 2002). In addition to being a contaminant in its own right, suspended sediment is also one of the primary pathways by which nutrients, as well as other binding contaminants, are transported (Nebel & Wright, 1993; A. N. Sharpley et al., 1995; Andrew N. Sharpley et al., 1994; Søndergaard, Jensen, & Jeppesen, 2003; US EPA, 2000, 2002). Excessive phosphorus and nitrogen concentrations can lead to harmful

algal blooms (HABs) making sediment-bound nutrients an additional water quality concern associated with sediment transport (Paerl, Hall, & Calandrino, 2011; Schindler et al., 2008). Many studies have investigated and reviewed the impacts of sediments and nutrients on surface waters, including but not limited to Waters et al. (1995), Carpenter et al. (1998), Smith et al. (1999), Wilber & Clarke (2001), Berry et al. (2003), and Bilotta & Brazier (2008).

Actively eroding stream channels have been observed in many regions where post-glacial alluvial sediments dominate and stream channels have more recently undergone human modifications. In several studies conducted in such regions, authors have found that a significant portion of the total sediment load reaching stream and river outlets can result from bank erosion and failure (Evans, Gibson, & Rossell, 2006; Kronvang, Grant, & Laubel, 1997; Kronvang, Laubel, & Grant, 1997; Laubel, Svendsen, Kronvang, & Larsen, 1999; Sekely, Mulla, & Bauer, 2002; A. Simon, Rinaldi, & Hadish, 1996). Sekely (2002) used topographic surveys and field data to estimate that streambank slumping contributed between 31% and 44% of total annual suspended sediment load at the mouth of the Blue Earth River in Minnesota, which in turn represented between 7% and 10% of the annual total phosphorus load. The results of a study that used a mixing model and uncertainty analysis, and conducted on six watersheds of Cayuga Lake, determined that bank erosion contributed between 8% and 76% of sediment loads(Nagle, Fahey, Ritchie, & Woodbury, 2007). Contributions were particularly high where widespread and actively eroding glaciolacustrine deposits were present along streams.

2.2. SEDIMENT AND NUTRIENT LOADING IN THE LAKE CHAMPLAIN BASIN

Sediment and phosphorus loading is an issue that affects water quality in Lake Champlain, situated in Vermont, New York and Quebec, and is currently a focus of management activities such as the development of new total maximum daily loads (TMDLs) for the lake (Lake Champlain Basin Program, 2015). In the Lake Champlain basin specifically, there is evidence that much of the phosphorus reaching Lake Champlain is originating from watershed sources. Smeltzer et al. (2009) attributed 95% of the total phosphorus load in Lake Champlain to nonpoint sources within the watershed, and Sharpley et al. (1995) indicated that most of the phosphorus originating from land surfaces, particularly cultivated land, is in the form of sediment bound particulate phosphorus. Moreover, a large portion of the sediment-bound phosphorus reaching Lake Champlain originates as agricultural and urban runoff (Lake Champlain Basin Program, 2012; McDowell, Biggs, Sharpley, & Nguyen, 2004), as well as from soil erosion, storm water, and flow off roads. Meals & Budd (1998) estimated 66% of annual nonpoint phosphorus was contributed to Lake Champlain by agricultural land use.

In addition to surface erosion, particularly from agricultural and urban landscapes, streambank erosion and scour can yield large amounts of sediment from within a watershed (DeWolfe et al., 2004; Kalma & Ulmer, 2003; Ross et al., 2010). Findings of a study that used remote sensing techniques, conducted on multiple watersheds in Chittenden County within the Lake Champlain Basin of Vermont, indicated that lateral channel migration contributed between 0% to 26% of the total sediment loading produced by channel processes (Morrissey, Rizzo, Ross, & Alves, 2011). Using a bank stability model to simulate fluvial erosion and geotechnical bank

failure, Langendoen et al. (2012) estimated that streambank erosion contributed 36% of total suspended load entering the Mississquoi Bay of Lake Champlain from the Mississquoi River, which comprises a largely agricultural watershed in Vermont. DeWolfe et al. (2004) found that erosion from streambanks was highly variable among stream reaches within the Lake Champlain Basin, but that this mechanism ranged from the highest to lowest single contributor of nonpoint sediment and phosphorus on a reach basis. Although these authors suggested that overall stream erosion rates (0.26m/yr) were moderate when compared to results for similar watersheds, this represents a potentially large and unquantified source of sediment to Lake Champlain. These contributions have not yet been well defined or quantified from a process-based perspective.

There is still uncertainty surrounding the quantification of streambank erosion and failure and the resulting contributions to sediment and phosphorus loading in the Lake Champlain basin. However, it has been noted that 75% of stream reaches in Vermont are eroding (VT DEC, 2007) and there is agreement that bank erosion and failure is an important source of sediment and phosphorus that needs further investigation (Lake Champlain Basin Program, 2012). In addition, the impacts of stream erosion and scour are increasingly important in the light of climate change, which is showing more frequent and/or higher magnitude flooding events (Guilbert et al., 2015; Hayhoe et al., 2006, 2008). For example, Tropical Storm Irene, which hit Vermont in August of 2011, resulted in intense flooding of at least 10 of 17 major river basins in Vermont, peak flows at nine stream gaging stations that were estimated to have a 1% or less chance of occurring in any year, as well as significant channel enlargement, deposition, and relocation of several river sections (Pealer, 2012). Streambank erosion and failure are

important mechanisms that mobilize sediment from watersheds, and are likely to be particularly sensitive to anticipated changes in climate and land use.

2.3. CLIMATE CHANGE AND SEDIMENT LOADING

Climate is the primary driver of erosional processes in a watershed, in addition to watershed characteristics such as vegetation and soil types and antecedent conditions such as soil moisture. We can therefore expect that changes in climate will have an impact on the mobilization and transport of sediment from watershed sources. Global climate change is well documented and known to be influencing temperature and precipitation in the United States (T.R. Karl, Melillo, & Peterson, 2009; Solomon, Qin, & Manning, 2007). Data from the National Oceanic and Atmospheric Administration (NOAA) and numerous research efforts have provided evidence that over the last century average temperatures have increased, sea levels have risen, the amount of precipitation has changed, and a greater portion of total precipitation is occurring in the form of extreme single day events (Gleason, Lawrimore, Levinson, Karl, & Karoly, 2008; T.R. Karl et al., 2009; OA US EPA, n.d.). In addition, it is expected that the United States will continue seeing an increase in the frequency and magnitude of heavy and extreme precipitation events in addition to warming temperatures (Thomas R. Karl & Knight, 1998; Kenneth E. Kunkel, 2003; Kenneth E. Kunkel, Andsager, & Easterling, 1999).

Of particular interest are local and regional changes that are more likely to have a direct impact on aspects of human life (Hayhoe et al., 2006, 2008). In the northeastern United States, *Kunkel et al.* (2013) found that between 1815-2011 temperatures have risen by 2° F and precipitation has increased by 10%. *Groisman et al.* (2013) showed a 70% increase in precipitation occurring as extreme precipitation events (heaviest 1% of

rainfall) between 1985-2010. Several studies have shown that precipitation in the northeastern United States specifically is increasing and becoming more variable in magnitude (Beckage et al., 2008; Groisman et al., 2005; Guilbert et al., 2015; K.E. Kunkel et al., 2013). For example, *Kunkel et al.* (2013) projected that if emissions continue to increase, temperatures will rise 4.5°-10° F by 2080 and that heavy precipitation as well as seasonal drought risk will also increase. Authors also note variability in these trends for different regions and elevations. In New England as well as in Vermont specifically, authors suggest that trends similar to those cited for the whole United States will continue, including seasonal warming, higher seasonal drought risk, precipitation that increases in magnitude and variability, as well as longer periods of continuous days with precipitation (Betts, 2011; Frumhoff et al., 2007; Guilbert et al., 2015; Stager & Thill, 2010). In addition, authors have described earlier spring ice out dates, decreases in snow depth and in snow to precipitation ratios, higher and earlier spring stream flows, extended growing season, earlier bloom dates, and other alterations in regional climate indicators (Betts, 2011; Guilbert et al., 2014; Hayhoe et al., 2006; G. A Hodgkins, Dudley, & Huntington, 2003; Glenn A. Hodgkins & Dudley, 2006; Huntington, Hodgkins, Keim, & Dudley, 2004).

2.3.1 Implications of Climate Change on Surface Water, Sediment, and Nutrient Fluxes

Changing temperature and precipitation patterns, as well as anthropogenic changes such as increased agriculture and urbanization, will clearly affect surface water, as well as sediment and nutrient fluxes (Vörösmarty et al., 2010; Whitehead, Wilby, Battarbee, Kernan, & Wade, 2009). Based on a review of studies examining the impact of climate change on various factors affecting eutrophication, Whitehead et al. (2009)

concluded that is likely that altered conditions will lead to more frequent and severe algal blooms. Similarly, Moss (2012) also concluded that climate change will significantly influence nutrient processes in lakes and lead to more intense eutrophication. A study conducted on the Connecticut River watershed in New England used SWAT to assess the effects of climate change on watershed processes and determined that the impacts included changes in streamflow and variability of flow, sediment and nutrient loading, well as on variability of flow and pollutant loading (Marshall & Randhir, 2008). Also based on SWAT modeling, El-Khoury et al. (2014) found that both future climate and land use change increased maximum monthly streamflow, as well as nitrate and organic phosphorus loads, while simulations resulted in a decrease in organic nitrogen and nitrite loads.

Although relationships between sediment loading and discharge vary among watersheds (Asselman, 1999; Webb & Walling, 1982; Williams, 1989), authors have also found that high precipitation and/or resulting flow events result in disproportionately higher suspended sediment loading where sediment in not limiting (Gonzalez-Hidalgo, Batalla, Cerdà, & de Luis, 2010; Oeurng, Sauvage, & Sánchez-Pérez, 2010). Ockenden et al. (2016) found that the majority of suspended sediment and total phosphorus (TP) load in two UK catchments was transported during the highest discharge events and that high concentrations of phosphorus also occurred during events that followed dry periods, particularly during summer months. Incorporating anticipated changes in climate, a study conducted in Florida predicted that peak flow and associated sediment load will increase due to more intense and less frequent rainfall events (X. Chen, Alizad, Wang, & Hagen, 2014). Anthropogenic changes to the landscape are accelerating conveyance of

contaminants from land surfaces and reducing retention capacity (such as by removing floodplain access and channelizing streams), which is likely to increase the variability in pulses resulting from extreme storm events (Kaushal et al., 2010). Kaushal et al. also indicated that the occurrence of such contaminant pulses can impair ecological habitat, scour bridges, transport nutrients, metals and other contaminants, and affect reservoirs and drinking water supplies, making them a significant consideration in watershed management.

2.3.2. Modeling Impacts of Climate Change on Sediment and Nutrient Loading

Hydrological models can be used to assess the impacts of climate change on watershed systems and inform resource management and policy decisions targeted at building resiliency. In order to simulate the impacts of climate change however, locally focused models require high resolution meteorological inputs that reflect the anticipated deviations in climate variables, particularly in temperature and precipitation. General circulation models (GCMs) predict large-scale future climate scenarios based on numerical models of earth systems and are a valuable tool for understanding climate change. However, GCMs are not suitable for driving hydrological models due to the large difference in scale between these models, as well as because of the over-simplification of runoff prediction and inability to represent subgrid-scale processes (Fowler, Blenkinsop, & Tebaldi, 2007; Xu, 1999a) (which is critical in simulating watershed response).

Several methods exist for downscaling GCMs to achieve finer spatial resolutions and better represent regional and local scale processes. Fowler et al. (2007) conducted a review of downscaling techniques for driving hydrological models, presented relatively new alternatives for producing climate scenarios, and recommended strategies for

improving the effectiveness of climate and hydrologic modeling with respect to impact assessment. Some studies show that regionally downscaled climate models (RCMs) were able to capture extreme events (for example (Fowler, Ekström, Kilsby, & Jones, 2005; Frei, Schöll, Fukutome, Schmidli, & Vidale, 2006)) and improve estimates of hydrological impacts (Leung et al., 2004). However, these models are strongly affected by bias in the GCM used and do not reflect local trends or variability in precipitation for other regions (Guilbert et al., 2014; Mohammed, Bomblies, & Wemple, 2015). RCMs also introduce additional variability into climate predictions (Fowler et al., 2007). Numerous statistical downscaling techniques produce scenarios that differ significantly in their ability to represent extreme events and local trends or variability. Fowler et al. (2007) presents an overview of dynamic and statistical downscaling methods focused on providing data for driving hydrological models, including their advantages and disadvantages as well as information on newly emerging methods for either approach. The best approach depends on watershed characteristics, GCM biases, questions under investigation, and other considerations.

Statistical methods for generating meteorological time series, known as weather generators (WG's), are an alternative to deterministic climate models. Stochastic weather generators typically predict precipitation occurrence using daily precipitation and a two-state Markov chain dependent on transition factors, and estimate precipitation amount using gamma distributions (Fowler et al., 2007). Other variables are calculated based on their relationships with each other and the occurrence of wet and dry days. Wilks and Wilby (1999) reviewed the history and development of WG methods, including a description of statistical properties of precipitation occurrence and amounts, a brief

presentation of approaches for simulating other meteorological variables, discussion of interannual variability in WG data, as well as an explanation of applications such as climate downscaling and filling in missing data. Researchers have developed WGs with varying success at representing regional or local trends and variability, some with the intention of driving hydrological models (Chen, Brissette, & Leconte, 2010; Forsythe et al., 2014; Ivanov, Bras, & Curtis, 2007; Kilsby et al., 2007; Semenov & Barrow, 1997; Semenov, Brooks, Barrow, & Richardson, 1998).

2.4. OVERVIEW OF HYDROLOGY AND BANK STABILITY MODELS

2.4.1. Hydrology and Watershed Models

Numerous watershed models have been developed to answer questions about the interactions between climate and land-surface hydrology, and can aid water resource management (Singh & Woolhiser, 2002). Similarly, many sediment transport and erosion models exist at the hillslope or watershed scale and can answer questions about how climate and hydrology affect the movement of sediment. Catchment scale models have largely included sediment mobilization by sheet and rill erosion processes, and some include gully erosion. Merritt et al. (2003) as well as Aksoy & Kavvas (2005) reviewed in detail the range of erosion and sediment transport models that include representation of erosion processes. These models include a variety of conceptual, empirical, and physics-based models of varying spatial scales that simulate the generation of sediment as well as the transport of sediment. Some also include representation of pollutant transport. However, few include physics-based representation of rainfall-runoff processes, land surface sediment mobilization, and an in-stream model, much less the inclusion of

streambank erosion as well as mass failure of banks. The SHETRAN model for instance is such a watershed model that includes surface and gully erosion, as well as fluvial in-stream erosion (Bathurst, 2002; Ewen, Parkin, & O'Connell, 2000). SHETRAN has been used to examine the effects of basin and land use characteristics on overall sediment yield (Bathurst, Moretti, El-Hames, Moaven-Hashemi, & Burton, 2005; Birkinshaw & Bathurst, 2006; Lukey, Sheffield, Bathurst, Hiley, & Mathys, 2000). However, no simulation of geotechnical bank failure is included in that model. Models to estimate erosion, point location bank failure, and sediment transport exist, however a mechanistic model that can simulate changing contribution of streambank sediment from erosion as well as geotechnical failure processes to an overall watershed sediment and nutrient load under changing climatic conditions has not yet been published.

DHSVM is a physics-based model that simulates water and energy fluxes at the land surface using a spatially-explicit representation of topography, vegetation and soil properties. The model enables the user to represent modifications to the land surface, such as deforestation and urbanization (Wigmosta et al., 1994; Wigmosta and Lettenmaier, 1999; Wigmosta and Perkins, 2001; Cuo et al., 2008). Topography drives the downslope movement of water, both across the land surface and within the channel network. All of the grid cells are linked hydrologically through the surface and subsurface flow routing. With respect to sediment, current versions of DHSVM include representations of surface erosion, hillslope erosion, mass wasting in the form of landslides and redistribution of mass downslope, as well as erosion of road surfaces (Doten, Bowling, Lanini, Maurer, & Lettenmaier, 2006). The model has been applied to simulate impacts of forest management practices on land surface processes (Storck et al.,

1998; Bowling and Lettenmaier, 2001; Wigmosta and Perkins, 2001; Waichler et al., 2005), as well as to study the interactions between climate change and hydrology (Cuo, Lettenmaier, Alberti, & Richey, 2009; Leung & Wigmosta, 1999; M. S. Wigmosta & Leung, 2001, 2001).

In DHSVM, sediment enters the stream network via debris flows from mass wasting events, overland inflow, and over road inflow. All local inputs are distributed evenly along the stream reach. Sediment entering the channel network is distributed into sediment classes, based on a lognormal distribution and user defined d_{50} and d_{90} particle sizes (Doten et al., 2006). Discharge of sediment is calculated using a linear reservoir routing scheme and was based on work by Wicks and Bathurst (1996). The total sediment transport capacity is computed for both the upstream and downstream flow rates (which have been calculated prior to sediment routing), based on Bagnold's equation for suspended and bed load (Bagnold, 1966; Doten et al., 2006; Graf, 1971). The equation for transport capacity is then substituted into the mass balance equation and solved for downstream sediment outflow rate using a four-point finite difference formulation as described in the work of Wicks and Bathurst (1996).

2.4.2. Bank Stability Models

A range of bank erosion and channel evolution models exist for simulating river banks and channels, but none allow for full coupling to perturbations in the watershed. The Bank Stability and Toe Erosion Model (BSTEM) is a predominant bank stability model that simulates erosion and geotechnical failure of streambanks at a specific location or segment of channel based on limit-equilibrium analysis (Andrew Simon, Curini, Darby, & Langendoen, 2000; Andrew Simon, Langendoen, & Thomas, 2003;

Andrew Simon, Pollen-Bankhead, & Thomas, 2011). Alternatively, the stages of channel evolution described by Schumm et al. (1984) and later modified by Simon (1989, 1994) are the basis of most existing channel evolution models. These changes in morphology are represented as changes in the width and bed elevation of channel segments, where disturbance is first seen in lower channel reaches and then move progressively upstream. Current channel evolution models include numerical models such as those developed by Darby et al. (1996), Nagata et al. (2000), Wang et al. (2010), and Xiao et al. (2016), as well as the Enhanced CCHE2D model (Duan, Wang, & Jia, 2001). The National Sedimentation Laboratory developed the CONservation Channel Evolution and Pollutant Transport System (CONCEPTS), which simulates the evolution of incised streams and has been used to assess long-term impacts of stream stabilization measures and reduction of sediment yields (Langendoen, 2000, 2001; Langendoen, Simon, & Alonso, 2000; Langendoen, Simon, Curini, & Alonso, 1999). CONCEPTS includes unsteady, one-dimensional flow, sediment transport and bed adjustment, bank erosion and channel widening processes, as well as representation of instream hydraulic structures such as bridges and culverts. These models do not typically include watershed processes that influence spatially variable soil characteristics, the effects of vegetation, or variable flow conditions.

BSTEM is a bank stability model that simulates toe erosion rates and failure events along channel reaches. BSTEM is a product of continuing research and development at the U.S. Department of Agriculture, Agricultural Research Service, National Sedimentation Laboratory (NSL). We chose BSTEM (Version 5.4) due to its advanced representation of both hydraulic and geotechnical processes contributing to

bank failure. BSTEM has been used to investigate the impacts of reduced erosion on sediment loading from streambanks and has been modified for iterative use to estimate volumes of sediment originating from stream reaches (Andrew Simon et al., 2011). It has also been applied to simulate long term lateral retreat of streambanks (Midgley, Fox, & Heeren, 2012). BSTEM comprises two components: (1) a toe erosion module that simulates undercutting of banks resulting from fluvial erosion as a function of excess shear stress; and (2) (Andrew Simon et al., 2000)a bank stability module that calculates a Factor of Safety (*FoS*) based on force equilibrium analysis (Andrew Simon et al., 2000).

2.5. GAP IN EXISTING KNOWLEDGE AND MODELING CAPABILITIES

A large number of models exist that attempt to simulate erosion and sediment transport, as well as many that include sediment routing algorithms and in-stream transport of sediment. These models vary in type (empirical, conceptual, physics-based), complexity, assumptions and processes incorporated, temporal and spatial resolutions, data required, scale, as well as other aspects (Merritt, Letcher, & Jakeman, 2003). Erosion and sediment generation includes sheet and rill erosion processes, which are due to overland flow, as well as gully and in-stream erosion. However, most existing models that simulate erosion and sediment generation represent only surface erosion due to overland flow. Bull and Kirkby (1997) review model development into the 1990s that focuses on gully erosion. Another set of models have been developed to simulate in-stream erosion; these typically include representations of streamflow routing, sediment load, changes in channel width and depth, and potentially of changes to curvature. Merritt et al. (2003) describes in detail the range of erosion and sediment transport models that existed at that time. Currently however, models that represent stream bank erosion based

on physical processes are often separate from watershed models that incorporate land surface processes, spatially explicit hydrologic and soil conditions, and the routing of water and sediment through channel networks. No existing models fully couple physics-based watershed functions with the mechanisms driving stream bank erosion as well as geotechnical failure. Fully coupling these models will allow for the representation of interdependencies between spatially explicit soil and vegetation parameters, temporally-dependent conditions such as soil moisture, pore pressures, and stream flow, as well as progressive streambank erosion.

2.6. SUMMARY

There is a significant body of work surrounding suspended sediment and nutrient loading in surface waters, and in particular phosphorus loading in freshwater ecosystems. It has been well established that movement of sediment is a primary pathway by which phosphorus is transported to receiving waters and that a large portion of sediment and nutrients originate from non-point watershed sources. Previous work has used various techniques to quantify sediment contributions from sources such as surface and road erosion, as well as streambank erosion. Physics-based models have been developed as one way for researchers to tease apart the impacts of driving variables like precipitation or land use on watershed responses such as in the generation of runoff and suspended sediment. However, no current models exist that include mechanistic and distributed representation of land surface erosion, road erosion, as well as erosion and geotechnical failure of streambanks.

The number of studies investigating watershed responses to the impacts of climate change is growing rapidly. Again physics-based models allow researchers to

simulate the response of systems to conditions that are outside the currently known range of variability. Researchers have developed multiple methodologies for creating predictions of future climate that can be used to drive hydrologic models, although these products still present challenges and limitations. The ability of extreme events to disproportionately impact sediment and nutrient loads make this a critical topic for risk and impact assessment studies. In the Northeast United States, increasing trends in temperature, precipitation, and extreme precipitation are particularly pronounced. Processes driving high runoff and discharge in watersheds, as well as erosion and suspended sediment transport, are likely to be highly affected by such climate trends. There is therefore a need to advance modeling techniques to include physics-based simulation of streambank erosion and failure, in addition to erosion of land surfaces and roads, to more inclusively represent suspended sediment loading in a watershed, and how these processes will be affected by changes in driving forces like climate.

CHAPTER 3: MODELING SEDIMENT MOBILIZATION USING A DISTRIBUTED HYDROLOGICAL MODEL COUPLED WITH A BANK STABILITY MODEL

3.1. INTRODUCTION

The detrimental impacts of suspended sediments on global freshwater ecosystems are well known (Berry et al., 2003; Bilotta & Brazier, 2008; Vörösmarty et al., 2010; Waters, 1995; Wilber & Clarke, 2001). Suspended sediments and nutrients are considered two of the leading causes of water quality impairment in United States lakes and reservoirs (OW US EPA, 2000, 2002) and similarly the European Environmental Agency (EEA) has acknowledged that non-point pollution contributing to eutrophication and contamination of aquatic resources is a major environmental concern (European Environment Agency, 1995; Stanners et al., 1995). According to the US Environmental Protection Agency (US EPA), suspended sediment directly impacts water clarity, scour, sediment storage, and other aspects of water quality. Suspended sediment can also transport bound nutrients such as phosphorus from cultivated land, and other binding contaminants (Nebel & Wright, 1993; A. N. Sharpley et al., 1995; Andrew N. Sharpley et al., 1994; Søndergaard et al., 2003; US EPA, 2000, 2002). Excessive phosphorus and nitrogen concentrations can lead to harmful algal blooms (HABs) making sediment-bound nutrients an additional water quality concern associated with sediment transport (Paerl et al., 2011; Schindler et al., 2008).

Actively eroding stream channels have been observed in many regions where post-glacial alluvial sediments dominate and stream channels have more recently undergone human modifications. In such regions, a significant portion of the total sediment load reaching stream and river outlets can result from bank erosion and failure

(Evans et al., 2006; Kronvang, Grant, et al., 1997; Kronvang, Laubel, et al., 1997; Laubel et al., 1999; Sekely et al., 2002; A. Simon et al., 1996). Sekely (2002) used topographic surveys and field data to estimate that streambank slumping contributed between 31% and 44% of total annual suspended sediment load at the mouth of the Blue Earth River in Minnesota, which represented between 7% and 10% of the annual total phosphorus load. Using the erosion pin method, Huang (2012) estimated that 67% of the suspended sediment loading in an urbanizing watershed in Missouri resulted from stream bank erosion. The results of a study that used a mixing model and uncertainty analysis, conducted on six watersheds of Cayuga Lake, New York, determined that bank erosion contributed between 8% and 76% of annual sediment loads (Nagle et al., 2007). Contributions of sediment from stream banks were particularly high where widespread and actively eroding glaciolacustrine deposits were present along streams. Several studies in Vermont watersheds, such as those of Simon et al. (2006), DeWolfe et al. (2004), and Morrissey et al. (2011) have also indicated that stream bank erosion, scour, and mass failure can account for anywhere from 30 to 80% of total sediment loading into streams and lakes.

Empirical studies have demonstrated the importance of channel bank erosion on watershed sediment fluxes. In order to better quantify sediment loads from bank erosion, it is helpful to understand the conditions that drive bank erosion and failure processes. Activities such as channel straightening, removal of riparian vegetation, and urban development have also been shown to increase streambank erosion (Andrew Simon & Rinaldi, 2006). Streambanks can also represent a source of legacy phosphorus (Kleinman, Sharpley, Buda, McDowell, & Allen, 2011), particularly when adjacent to agricultural

areas with long histories of fertilizer use. Large precipitation events and flooding that cause bank erosion and collapse can thereby result in pulses of sediment and associated phosphorus into streams and larger waterbodies. In many regions precipitation is becoming more intense (Guilbert et al., 2015; T.R. Karl et al., 2009) and therefore the need to simulate the impacts of changing precipitation climatology on nutrient transport into receiving waters will be of great value in informing management and policy actions. Although the need to represent stream bank contributions to sediment and nutrient budgets at the watershed scale is recognized, thus far mechanistic representation of both bank erosion and geotechnical failure processes in watershed models has remained elusive. Here we present a coupled modeling framework that addresses the prior shortcomings.

A range of bank erosion and channel evolution models exist for simulating river banks and channels, but none allow for full coupling to perturbations in the watershed. The Bank Stability and Toe Erosion Model (BSTEM) is a predominant bank stability model that simulates erosion and geotechnical failure of streambanks at a specific location or segment of channel based on limit-equilibrium analysis (Andrew Simon et al., 2000, 2003, 2011). Alternatively, the stages of channel evolution described by Schumm et al. (1984) and later modified by Simon (1989, 1994) are the basis of most existing channel evolution models. These changes in morphology are represented as changes in the width and bed elevation of channel segments, where disturbance is first seen in lower channel reaches and then move progressively upstream. Current channel evolution models include numerical models such as those developed by *Darby et al.* (1996), *Nagata et al.* (2000), *Wang et al.* (2010), and *Xiao et al.* (2016), as well as the Enhanced

CCHE2D model (Duan et al., 2001). The National Sedimentation Laboratory developed the CONservation Channel Evolution and Pollutant Transport System (CONCEPTS), which simulates the evolution of incised streams and has been used to assess long-term impacts of stream stabilization measures and reduction of sediment yields (Langendoen, 2000, 2001, Langendoen et al., 2000, 1999). CONCEPTS includes unsteady, one-dimensional flow, sediment transport and bed adjustment, bank erosion and channel widening processes, as well as representation of instream hydraulic structures such as bridges and culverts. These models do not typically include watershed processes that influence spatially variable soil characteristics, the effects of vegetation, or variable flow conditions.

Existing watershed models are also limited in their representation of sediment mobilized from the landscape, as to date they mostly incorporate surface erosion due to overland flow and landslide processes, and some include representation of fluvial erosion of stream channels. Catchment scale models have largely included sediment mobilization by sheet and rill erosion processes, and some include gully erosion. Merritt et al. (2003) as well as Aksoy & Kavvas (2005) reviewed in detail the range of erosion and sediment transport models that include representation of erosion processes. These models include a variety of conceptual, empirical, and physics-based models of varying spatial scales that simulate the generation of sediment as well as the transport of sediment. Some also include representation of pollutant transport. However, few include physics-based representation of rainfall-runoff processes, land surface sediment mobilization, and an in-stream model, much less the inclusion of streambank erosion as well as mass failure of banks. The SHETRAN model for instance is such a watershed model that includes

surface and gully erosion, as well as fluvial in-stream erosion (Bathurst, 2002; Ewen et al., 2000). SHETRAN has been used to examine the effects of basin and land use characteristics on overall sediment yield (Bathurst et al., 2005; Birkinshaw & Bathurst, 2006; Lukey et al., 2000). However, no simulation of geotechnical bank failure is included in that model. Models to estimate erosion, point location bank failure, and sediment transport exist, however a mechanistic model that can simulate changing contribution of streambank sediment from erosion as well as geotechnical failure processes to an overall watershed sediment and nutrient load under changing climatic conditions has not yet been published.

Mechanistic hydrologic models are well suited for investigating the nonlinear impacts of changing land use and climate conditions on flow and stream bank erosion. The alternatives—empirical and probabilistic models—may be limited in applicability because the magnitude of a disruption or change can fall outside of the range of previously observed events, and in nonlinear systems past observations may not be adequate for predicting future response. Hence a mechanistic model has better capability to represent sediment mobilization processes resulting from flows that exceed previous observations. The impacts of bank erosion and failure are increasingly important because of the changing climate and land use, and the ensuing potential for more frequent and higher magnitude flooding events. Here we present a coupled model approach to enable the representation of an important sediment source from the landscape and allow for perturbations in the watershed to impact the processes mobilizing sediment from streambanks.

3.2. MODEL DESCRIPTION

To address the need for mechanistic models to represent streambank erosion and failure under changing climate and hydrologic regimes, we coupled two existing models: the Distributed Hydrology, Soil, and Vegetation Model (DHSVM) (Mark S. Wigmosta et al., 1994) and BSTEM (Andrew Simon et al., 2000, 2003, 2011). DHSVM is a mechanistic model that simulates water and energy fluxes at subdaily time steps at the watershed scale. BSTEM is a bank stability model that simulates toe erosion rates and failure events along channel reaches. Both models are described in full detail in associated publications; a brief introduction to the models and discussion of processes related to sediment and the model coupling is provided below. A schematic of the coupled model processes, inputs and outputs is shown in Figure 1.

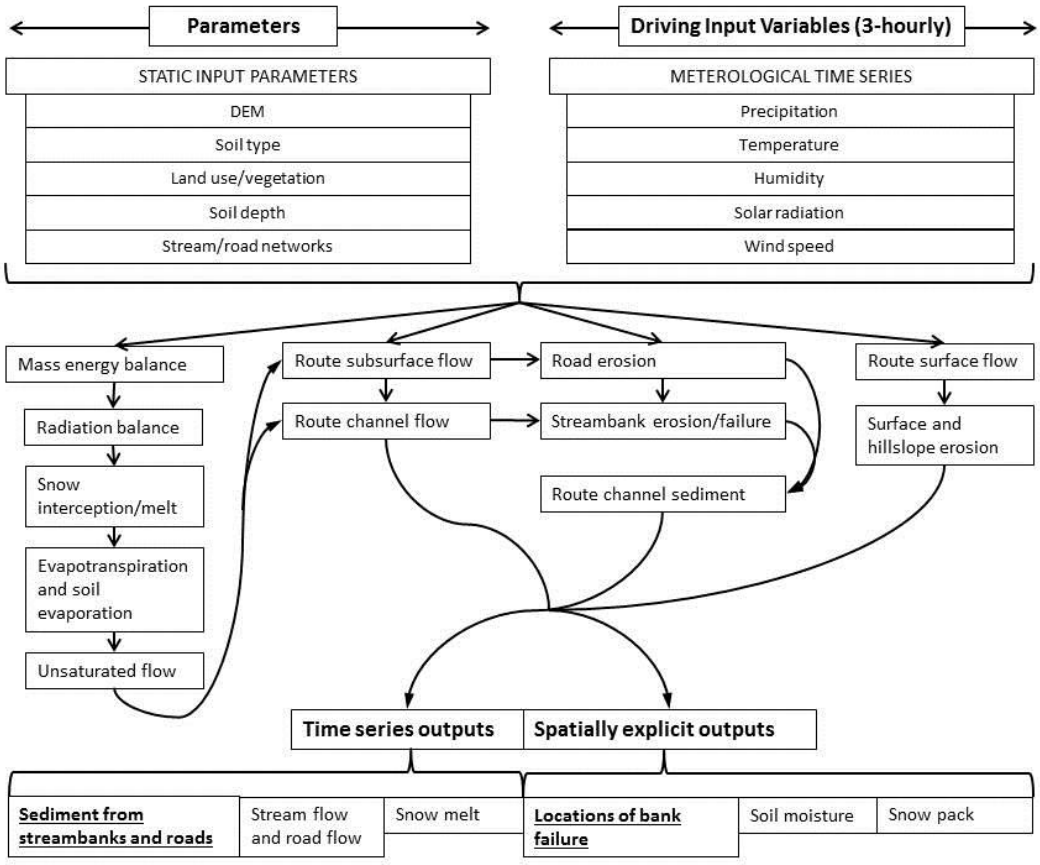

Figure 1. Schematic of coupled model processes, inputs and outputs.

BSTEM is a product of continuing research and development at the U.S. Department of Agriculture, Agricultural Research Service, National Sedimentation Laboratory (NSL). We chose BSTEM (Version 5.4) due to its advanced representation of both hydraulic and geotechnical processes contributing to bank failure. BSTEM has been used to investigate the impacts of reduced erosion on sediment loading from streambanks and has been modified for iterative use to estimate volumes of sediment originating from stream reaches (Andrew Simon et al., 2011). It has also been applied to simulate long term lateral retreat of streambanks (Midgley et al., 2012). BSTEM comprises two components: (1) a toe erosion module that simulates undercutting of banks resulting from

fluvial erosion as a function of excess shear stress (Andrew Simon et al., 2000); and (2) a bank stability module that calculates a Factor of Safety (*FoS*) based on force equilibrium analysis (Andrew Simon et al., 2000).

The toe erosion module simulates undercutting of banks resulting from fluvial erosion as a function of excess shear stress (Andrew Simon et al., 2000). The erosion distance, *E* (cm), is calculated as

$$E = \kappa * \Delta t(\tau_o - \tau_c) * 1e4, \quad (1)$$

where κ is an erodibility coefficient ($cm^3\ N^{-1}\ s^{-1}$), Δt is the time step (s), τ_o is average boundary shear stress (Pa), and τ_c is the critical shear stress (Pa) (Andrew Simon et al., 2011). The soil critical shear stress and erodibility parameters are supplied by the user. Average shear stress is calculated for 23 separate nodes along the bank profile based on the flow segment affecting each node, as opposed to one average shear stress for the entire bank. This is well described and shown in Figure 2 of Simon et al. (2009). In addition, BSTEM corrects the boundary shear stress for the effects of curvature using Crosato's "no-lag kinematic model" (Crosato, 2009):

$$\tau_o = \frac{\gamma_w n^2 (u+U)^2}{R^{\frac{1}{3}}}, \quad (2)$$

where *n* is Manning's roughness coefficient, *u* is the water velocity ($m\ s^{-1}$) averaged over the reach, and *U* is the increase in near-bank velocity due to superelevation ($m\ s^{-1}$), *R* is hydraulic radius (m), and $\gamma_w$is the unit weight of water ($9.81\ kN\ m^{-3}$). Curvature here, as well as radius of curvature, refers to longitudinal curvature such as along a stream reach.

The bank stability module of BSTEM calculates a factor of safety, *FoS*, based on force equilibrium analysis (Andrew Simon et al., 2000). Bank resistance is calculated by a revised Mohr-Coulomb equation that includes the increase in shear strength due to

the increase in matric suction for the portion of the bank above the groundwater table where pore-water pressure is negative (positive matric suction). This revised equation for shear strength (S_r) is

$$S_r = c' + (\sigma - \mu_a)tan\phi' + (\mu_a - \mu_w)tan\phi^b, \quad (3)$$

where c' is effective cohesion (kPa), $(\sigma - \mu_a)$ is the net normal stress on the failure plane (kPa), μ_w is the pore-water pressure on the plane (kPa), ϕ' is the effective friction angle and ϕ^b describes the increase in shear strength due to an increase in matric suction. Blow the water table, under saturated soil conditions, matric suction has no effect on effective cohesion and the shear strength equation becomes,

$$S_r = c' + (\sigma - \mu_w)tan\phi' \quad (4)$$

BSTEM loops through the nodes on the bank and settles on the mostly critical failure plane based on its starting elevation and angle. Once this failure plane is known, the model calculates the resisting and driving forces in order to determine a final *FoS*. If the potential *FoS* is less than 1.3 and greater than 1, the bank is considered conditionally stable (Andrew Simon et al., 2000), where often the within-bank water table elevation is a critical determinant of stability. If the *FoS* is less than or equal to 1, the bank is considered unstable and BSTEM will calculate a new more stable geometry based on the failure plane base and angle.

DHSVM is a physics-based model that simulates water and energy fluxes at the land surface using a spatially-explicit representation of topography, vegetation and soil properties. The model enables the user to represent modifications to the land surface, such as deforestation and urbanization (Cuo et al., 2008; Mark S. Wigmosta & Lettenmaier, 1999; Mark S. Wigmosta & Perkins, 2001; Mark S. Wigmosta et al., 1994).

Topography drives the downslope movement of water, both across the land surface and within the channel network. All of the grid cells are linked hydrologically through the surface and subsurface flow routing. With respect to sediment, current versions of DHSVM include representations of surface erosion, hillslope erosion, mass wasting in the form of landslides and redistribution of mass downslope, as well as erosion of road surfaces (Doten et al., 2006). The model has been applied to simulate impacts of forest management practices on land surface processes (Bowling & Lettenmaier, 2001; Storck et al., 1998; Waichler et al., 2005, 2005; Mark S. Wigmosta & Perkins, 2001), as well as to study the interactions between climate change and hydrology (Cuo et al., 2009; Leung & Wigmosta, 1999; M. S. Wigmosta & Leung, 2001, 2001).

In DHSVM, sediment enters the stream network via debris flows from mass wasting events, overland inflow, and over road inflow. All local inputs are distributed evenly along the stream reach. Sediment entering the channel network is distributed into sediment classes, based on a lognormal distribution and user defined d_{50} and d_{90} particle sizes (Doten et al., 2006). Discharge of sediment is calculated using a linear reservoir routing scheme and was based on work by Wicks and Bathurst (1996). The transport equation for total load, where changes in suspended sediment are small compared to bed material storage, is:

$$\frac{\partial}{\partial t} m_s + \frac{\partial}{\partial x} ACV\rho_s = \rho_s q_s, \tag{5}$$

where m_s is the mass of stored sediment in the bed per meter of channel length (kg/m); ρ_s is particle density of the sediment (kg/m^3); A is the cross-sectional flow area (m^2); C is the total sediment concentration (m^3/m^3); V is the average channel flow velocity (m/s); and q_s is the local volumetric sediment inflow rate to the channel reach per meter length

($m^3/s/m$). The total sediment transport capacity is computed for both the upstream and downstream flow rates (which have been calculated prior to sediment routing), based on Bagnold's equation for suspended and bed load (Bagnold, 1966; Doten et al., 2006; Graf, 1971). The transport capacity is calculated as:

$$Q_s = \frac{TC_c}{g(1-\frac{\rho}{\rho_s})}, \quad (6)$$

where Q_s is the transport capcity in dry mass per unit width (kg/m/s), TC_c is the total sediment transport capacity in immersed weight per unit channel width from Bagnold's equation, g is gravitational acceleration, and ρ is the density of water. This equation is substituted into the mass balance equation and solved for downstream sediment outflow rate using a four-point finite difference formulation as described in the work of Wicks and Bathurst (1996). This gives the main sediment routing equation:

$$(ACV\rho_s)_i^t = \frac{1}{\theta}(\theta(ACV\rho_s)_{i-1}^t - (1-\theta)((ACV\rho_s)_i^{t-1} - (ACV\rho_s)_{i-1}^{t-1}) + \rho_s q_s \Delta x - \frac{\partial}{\partial t} m_s) \quad (7)$$

where θ is a time-weighting factor set to 0.55 and all other terms are as previously stated.

To improve the representation of sediment mobilization in DHSVM, we programmed the BSTEM algorithm, based on Version 5.4 as made available by the National Sedimentation Laboratory, into the DHSVM framework. The BSTEM algorithm is executed after channel routing is performed, between road sediment routing and routing of sediment through the stream network. At each grid cell in which a channel exists, the model first estimates toe erosion as described in the previous section, where flow depth and water table depth are the same as the water table in the corresponding DHSVM grid cell and based on discharge calculated in the flow routing functions of

DHSVM. The bank profile updates if needed to represent changing geometry such as an actively undercutting bank (Figure 2). Once the effects of toe erosion have been implemented, the model executes a *FoS* analysis for each grid cell along the channel network. The *FoS* calculation is an instantaneous estimation of failure probability based on average conditions of the channel and bank material at that point in the simulation after erosion occurs. The algorithm loops over each node on the bank profile, randomly generating angles of potential failure planes and deciding on the most likely starting location for a failure plane. Next the model searches for the most likely failure plane angle between calculated maximum and minimum angles, which are dependent on the minimum angle of the bank and the assigned friction angle of soil. The final *FoS* for that time step and grid cell with a streambank is the *FoS* value of the most likely failure plane, based on searching through potential failure planes beginning at each node on the bank profile. If erosion or mass failure occurs in that grid cell, the mass of sediment is estimated for the portion of the channel within that grid cell and that sediment enters the stream network.

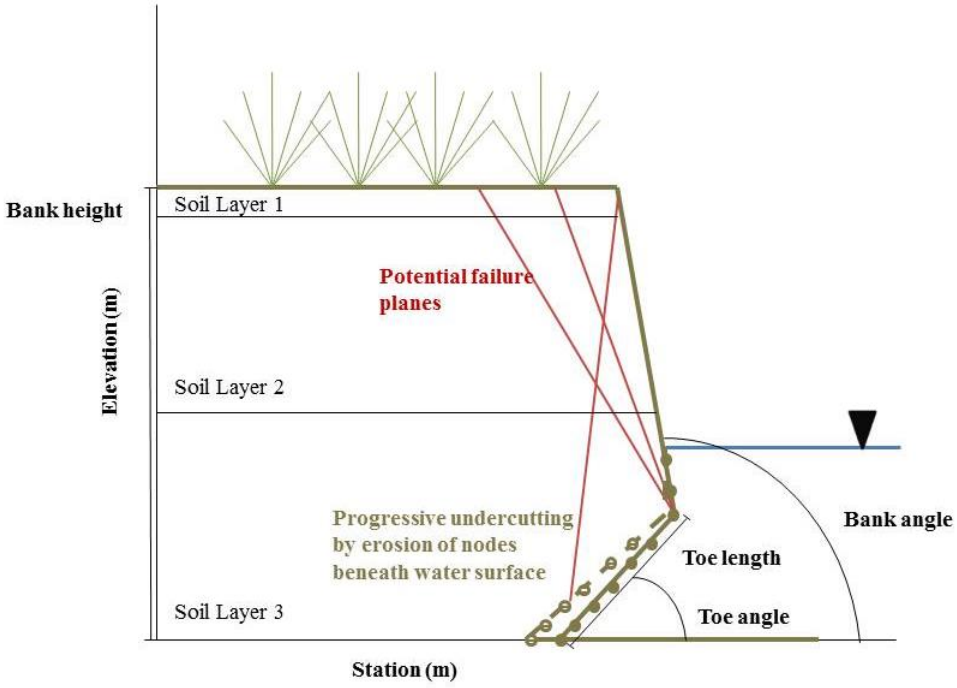

Figure 2. Representation of progressive undercutting, and possible failures planes.

In the coupled model, sediment can thereby enter the stream network not only by overland and road erosion, but also through bank erosion along a channel segment. Eroded and failed sediment combines with other local sediment inflows to the channel segment in the transport equation for total load as

$$\frac{\partial}{\partial t} m_s + \frac{\partial}{\partial x} ACV\rho_s = \rho_s(q_s + q_{sb}), \tag{8}$$

where q_{sb} is the local volumetric sediment inflow rate to the channel reach per meter length ($m^3/s/m$). This sediment is then transported throughout the channel network and potentially to the watershed outlet based on the existing DHSVM routing functions and presented equations.

As sediment is routed downstream through the channel network (Doten et al., 2006), the coupled model tracks the proportion of sediment originating from streambanks

(Figure 3). For each channel segment the ratio of streambank inputs to all other sediment inputs is calculated as

$$R_m^i = \frac{((R_{m-1}^i * U_m^i) + (R_m^{i-1} * \Delta SS_m^{i-1}) + B_m^i)}{(U_m^i + \Delta SS_m^{i-1} + B_m^i + Or_m^i + Ol_m^i + D_m^i)}, \quad (9)$$

where *m* is the channel segment identifier, *i* is the time step, *B* is sediment from streambank erosion/failure, *Ol*is sediment from overland inflow, *Or* is from over road inflow, *D* is debris inflow, *U* is inflow from upstream segment, and Δ*SS* is stored sediment in that channel segment. This results in an estimate of what percentage of total sediment at the watershed outlet, or at any chosen location, originated from streambank erosion and failure.

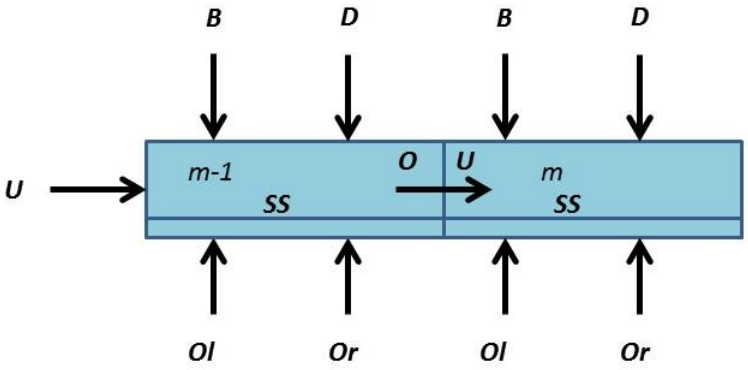

Figure 3. Representation of inputs to each channel segments *m* and *m-1*.

DHSVM input files include a configuration file to assign soil and vegetation parameters based on raster maps of soil and land use types which are prepared using ArcGIS. Where possible, the BSTEM module uses the same parameters as those required by other DHSVM functions (Table 1). For example, soil layers in BSTEM are defined based on the same soil depths set in the DHSVM input file as are certain properties of those soil layers such as porosity. Information calculated dynamically in DHSVM also

provides input data for BSTEM. The BSTEM algorithm activates after subsurface conditions and flow routing are calculated, so water table and flow depth at each time step and in each grid cell are used to inform BSTEM of within-bank water table level and channel flow surface levels, respectively. We modified the configuration files to include additional parameters needed for BSTEM calculations, which were set either by soil, vegetation, or stream class. We also assigned physical attributes of the channels, such as bank angles and bank toe length, based on the channel classes as set in the DHSVM channel network input files. In the case of soil cohesion and friction angle of the soil (which influence both surface erosion from the landscape and BSTEM calculations), DHSVM assigns these parameters to soil types. However, since these parameters were different for streambank soils than for soils further away from streams, these two parameters were separately assigned to bank soils based on channel class. Inputs to the model are described in later sections.

Table 1. Shared and added parameters, relevant to the addition of BSTEM to DHSVM, as well as parameters that were similar in the two models but also assigned in the coupled model based on channel class for bank soils.

Shared variables and parameters	**Added BSTEM parameters**	**Similar, reassigned parameters**
Flow depth (m)	Bank angle (°)	Soil cohesion (kPa)
Water table depth (m)	Bank toe angle (°)	Friction angle (°)
Channel segment width (m)	Bank toe length (m)	Saturated unit weight (kN/m^3)
Channel segment length (m)	Critical shear stress of bank material (kPa)	
Bank height (m)	Critical shear stress of toe material (kPa)	
Manning's n of channel	Particle diameter, d_{50} (mm)	
Soil depth (m)	Internal friction angle (°)	
Soil layer thicknesses (m)	Angle due to matric suction (°)	
	Radius of curvature (m)	

3.3. METHODS AND DATA

3.3.1. Site Description

For initial assessment of our approach, we modeled the Mad River watershed (Figure 4) in central Vermont, a tributary of the Winooski River. The watershed drains approximately 373km^2 and ultimately empties into Lake Champlain, which itself is part of the St. Lawrence basin. The steep valley is bordered by the Green Mountains, which are composed of highly metamorphosed rock with widespread glacial deposits along the valley floors (Field Geology Services, 2007). Elevation ranges from approximately 70 to just over 1200 meters. A mix of surficial geologic deposits exist in the watershed, including glacial tills in the highlands, glaciofluvial deposits along the valley margins, and alluvial fan deposits near tributary and mainstem junctions (Dunn, Springston, & Donahue, 2007a, 2007b; Whalen, 1998). In the lower reaches, erodible glaciolacustrine deposits commonly underlie alluvial deposits, which contribute to the sensitivity of both major tributaries and the mainstem of the Mad River to changes in land use (Barg & Blazewicz, 2003; Dunn et al., 2007a, 2007b; Nagle et al., 2007). Following European settlement, the watershed experienced a period of deforestation and mill dam construction in the 19th century and early 20th century, followed by a period of forest regrowth (Field Geology Services, 2007; Foster & Aber, 2004; Kline & Cahoon, 2010). Although mill dams existed in the watershed and have largely been removed, local geomorphology is more strongly influenced by post-glacial deposits and legacy sediments from deforestation, as well as from significant climate events and changes (Dunn et al., 2007a, 2007b; Walter & Merritts, 2008; Whalen, 1998). More recently, the area has become a

popular destination for vacationers. Additional development has occurred in the form of homes, ski resort facilities, and associated commercial areas.

Human alterations, as well as the geologic setting and occurrence of natural incision processes, have influenced the channel morphology and hydrology of the watershed, making it susceptible to the impacts of floods and extreme precipitation events. Channel incision exacerbates the sediment and phosphorus transport problem by naturally impairing stream channels, translating flood waves downstream instead of dissipating the energy contained in high flows. Bank erosion is therefore an issue of concern in the Mad River watershed, and has been documented in a series of Geomorphic Assessments issued by the Vermont Agency of Natural Resources (VT ANR, 2008a; 2008b; 2008c). Concern over erosion and failure of stream banks arises due to reasons discussed previously. Particularly along the mainstem and main tributaries of the Mad River, undercutting and erosion of banks can be visibly observed. Figure 5 shows an example of undercutting along a section of the Mad River mainstem, near the town of Waitsfield in the center of the watershed.

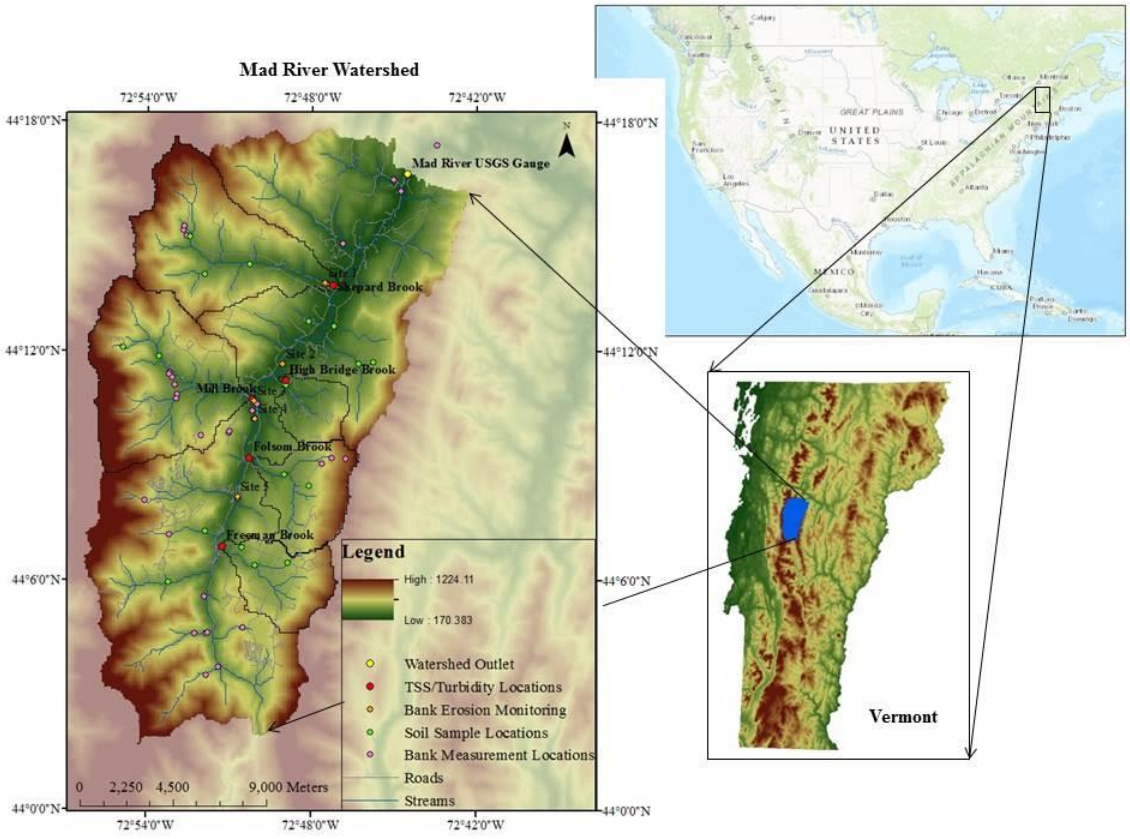

Figure 4. Mad River watershed, Vermont. Map shows the five subbasins included in this study, locations of bank monitoring sites (BST), bank profile measurements, additional soil samples locations (bulk density and grain size analysis), and TSS/turbidity measurements.

A USGS gaging station is located near the outlet of the Mad River watershed in Moretown, Vermont (#04288000) and has been collecting data since 1927. Based on data downloaded from this station, average annual flow (for USGS water years, which extend from October through September) from 1929 through 2015 was 7.7 m^3/s, and ranged from 3.8 m^3/s to 13.8 m^3/s. Peak annual streamflow ranged from 35 m^3/s to 685 m^3/s between the years 1927 and 2015, with the flood of record occurring in August 2011 during Tropical Storm Irene. The 2-year return flow is approximately 169 m^3/s based on

those 86 years of annual flow data (approximately 608400 m^3/hr for comparison to subsequent flow plots).

Figure 5. Photo of undercut and eroding bank along Mad River mainstem channel, near Lareau Farm Inn in Waitsfield, VT.

Five tributaries were included in this study: Mill Brook, Shepard Brook, Freeman Brook, Folsom Brook, and High Bridge Brook (Figure 4). These subbasins represented a range of land use types and elevations that are found in the Mad River watershed. Table 2 presents relevant characteristics of these subbasins, including area, road to stream length ratio, and percent coverage of potentially influential land cover types. These subbasins were selected to make use of previous studies (Wemple, 2013; Hamshaw, 2014), described below, for model validation.

Table 2. Proportional characteristics of subbasins including road to stream length ratio and land cover proportions.

	Mad River watershed	Mill Brook subbasin	Shepard Brook subbasin	Freeman Brook subbasin	Folsom Brook subbasin	High Bridge subbasin
Total area, km^2 (percentage of watershed)	359.0 (100%)	49.3 (13.7%)	44.8 (12.5%)	16.6 (4.6%)	18.5 (5.2%)	9.1 (2.5%)
Road:stream length ratio	1.9	1.8	1.2	15.1	1.6	3.6
Percent agriculture and pasture (%)	4.4	3.8	2.8	15.4	14.7	22.6
Percent urban/residential (%)	5.5	2.9	1.0	4.0	1.9	5.6
Percent roads/ transportation (%)	2.1	3.4	2.5	4.5	2.9	7.6
Percent forest (conifer, deciduous, mixed) (%)	86.5	85.4	91.3	73.5	78.8	62.0

3.3.2. Meteorological Data

Climate variables—primarily precipitation—drive the hydrological processes that can cause stream bank erosion and collapse. DHSVM requires several input variables at a relatively high temporal resolution: precipitation, temperature, humidity, incoming short wave radiation, incoming long wave radiation, and wind speed. We installed a meteorological station to measure local high resolution data near the center of the watershed at an elevation of approximately 208 m.a.s.l. This station began recording 31 July 2013.

In addition to the meteorological station data, we used National Centers for Environmental Protection (NCEP) Reanalysis data provided by the NOAA/OAR/ESRL

PSD, Boulder, Colorado, USA, (http://www.esrl.noaa.gov/psd/). The North American Regional Reanalysis (NARR) data are generated using the high resolution NCEP Eta Model, with a grid resolution of 32 km, along with the Regional Data Assimilation System (RDAS). The resulting product is a high resolution combined model and assimilated time series dataset and was available at a resolution of 8 times daily. We obtained this data for water years 2009 through 2014. In August 2011, Tropical Storm Irene passed through Vermont, resulting in storm total precipitation of 7.5 cm to 12.5 cm across the region. NARR data did not reflect the magnitude of this event in the grid cells covering the Mad River watershed, as measured by Doppler radar. Since one of the primary objectives of this coupled approach is to represent impacts of extreme events, such as what occurred as a result of Tropical Storm Irene, we used local spotter reports of storm totals to replace NARR Reanalysis precipitation for the Tropical Storm Irene event (National Weather Service, 2011). The distribution of rain over the storm period was kept the same as seen in NARR data, but increased in magnitude to equal locally observed rainfall totals over the storm period.

A comparison of NARR data to meteorological station data indicated some notable differences (Figure 6). Non-winter months (April through September) are shown since this is the period where differences in precipitation were most notable. There were differences in both the timing of certain events as well as in event totals, although precipitation totals over the entire time period were similar (0.1905 m verses 0.1988 m in 2013 non-winter months and 0.4864 m verses 0.5105 m in 2014 non-winter months for the meteorological station and NARR data, respectively). It is likely that local convective storms were responsible for a significant portion of precipitation, particularly during

summer months, and that these events were not reflected in NARR Reanalysis results, at least in part due to differences in spatial resolution. NARR data were therefore used to support overall hydrological validation and meteorological station data were used for hydrological calibration as well as to drive the model for the purposes of simulating the response in sediment generation to specific storm events in the Mad River watershed. The model time step for runs using NARR data was 3 hours and the time step for runs using station data was 2 hours.

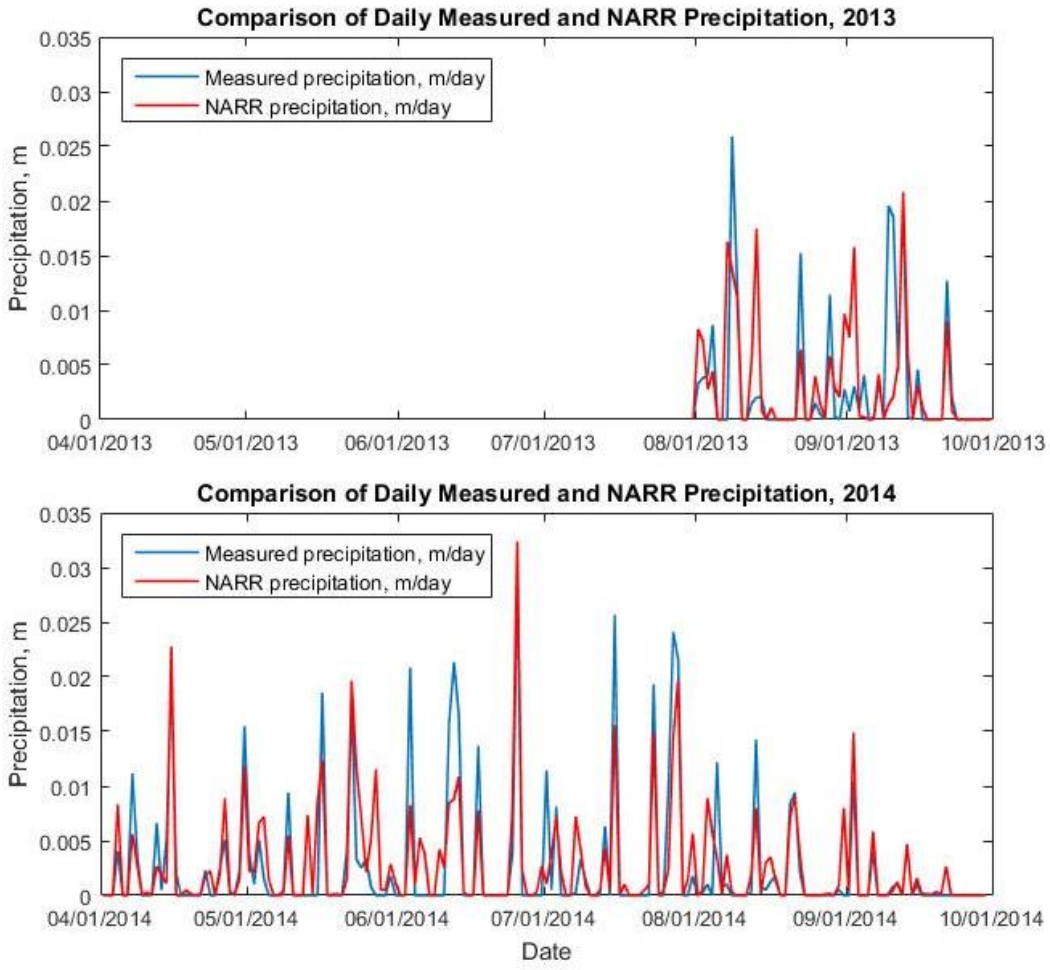

Figure 6. Comparison of precipitation data for 2013 and 2014 non-winter periods for which field data were available.

We also conducted an analysis of all meteorological variables for the time period that measured data were available (31 July 2013 – 30 September 2014). Figure 7 shows plots and corresponding correlation coefficients for daily values of each variable. It appears that there may be some error in measurements made by our radiometer, resulting in a low bias in measured incoming shortwave and particularly longwave radiation. However, we are confident that the impact of this bias on modeled sediment mobilization and loading from erosional processes was minimal. The dominant driving variable of these processes of interest is precipitation. In the case of precipitation, NARR data do not match daily values of precipitation in the chosen watershed during the shown time period particularly well. Temperature also has an important influence on snow melt and soil moisture conditions. Measured and modeled daily temperatures had a high correlation coefficient (0.98) indicating a good fit between measured and NARR values. Although other variables impact watershed processes including evapotranspiration, precipitation and temperature are still the primary variables affecting discharge as well (temperature in the case of melt events). Based on this analysis, it again seems likely that the poor fit of 2013 and 2014 discharge resulted from inadequate precipitation data in those years.

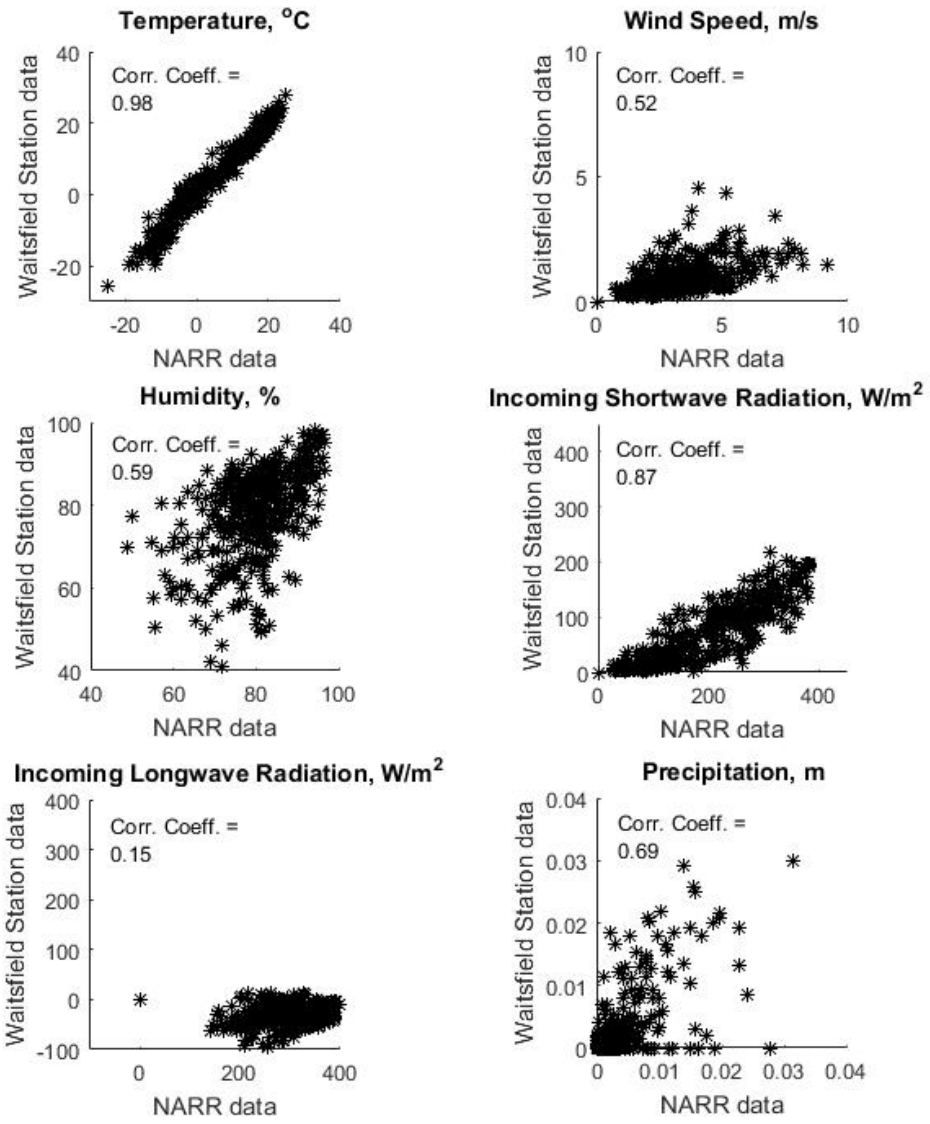

Figure 7. One-to-one plots of NARR versus measured meteorological variables.

3.3.3. Model Inputs and Field Data Collection

DHSVM requires GIS-derived inputs, as well as configuration files containing user-defined parameter values. Wherever possible we used site specific data collected in the field to inform parameter values, and remaining values were assigned based on literature-cited values. We generated topography layers using USGS National Elevation Dataset (NED) 10-meter data, aggregating this to a resolution of 100 meters for the entire

Mad River watershed. We classified soil based on Natural Resources Conservation Service (NRCS) hydrologic soil units and land use based on the 2006 National Land Use Cover Dataset (NLCD). We generated soil depth layers as a function of elevation data and minimum/maximum soil depths, using scripts that accompanied the DHSVM source code downloaded from the University of Washington Land Surface Hydrology Research Group website (http://www.hydro.washington.edu/Lettenmaier/Models/DHSVM/).

DHSVM also requires the input of stream and road networks. We created these based on scripts also provided with the source code, however these scripts were modified to represent local road and stream characteristics. In addition to creating data files containing network and map information, these scripts also assign channel segments to classes so that unique parameters can be defined for each class. In this work, road classes were based on road surface characteristics provided by the Vermont 911 board and obtained from the Vermont Center for Geographic Information. Classes differentiated paved from unpaved roads and were parameterized such that paved roads were not erodible. We classified streams based on contributing area, where streams with contributing areas less than 500,000 m^2 were stream class 1, greater or than 500,000 m^2 and less than 10,000,000 m^2 were stream class 2, greater than 10,000,000 m^2 and less than 20,000,000 m^2 were stream class 3, greater than 20,000,000 m^2 and less than 180,000,000 m^2 were stream class 4, and greater than 18,000,000 m^2 were stream class 5. The resulting stream network mimicked the assignment of Strahler stream order in that small first order streams were assigned to stream class 1 and most of the mainstem reaches were assigned to stream class 5 based on the GIS analysis. Using these contributing area thresholds, part of the mainstem channel at the southern end of the

watershed near the headwaters, was as assigned to stream class 4 (as opposed to Strahler order 5), as were some of the major tributaries. This was in line with observations that these stream sections were narrower, had generally lower banks, and experienced faster flows than the downstream portion of the mainstem channel.

The stream channel network was delineated using ArcGIS and stream classes were assigned based on contributing drainage area. These channel classes are the basis for parameter assignment described in subsequent sections. Parameters describing the bank profile are also set by stream class. In addition, to calculate the volume of sediment mobilized from a stream bank, the erosion rate calculated for any segment is currently applied to half the length of the channel segment present in that cell. Similarly, if a failure occurs, it occurs along half the length of the segment in that cell. Because we used a 100m resolution, and a relatively coarse stream delineation, the application of the erosion rate or failure to the entire length of the channel was expected to overestimate the volume of sediment originating from stream banks. We chose half the channel length based on *Morrissey et al.* (2011), in which authors indicated that streambank erosion affected 47-72% of reach lengths.

Local field data collected between 2012 and 2015 provided information used to set model parameters, as well as to calibrate and validate model results. Field work included erosion monitoring at specific sites, measurements of bank profiles throughout the watershed, soil testing and investigation of bank parameters, as well as grab samples for analysis of total suspended solids (TSS). Several sites were chosen for bank erosion monitoring and further investigation of geotechnical soil properties (yellow circles in Figure 4); these sites were located mostly along the mainstem of the Mad River and were

chosen based on observed and anticipated bank activity, site vegetation and physical characteristics, as well as accessibility. Bank soils at these sites were largely composed of silt loam and sandy loam and considered representative of soils along the mainstem and major tributaries. Vegetation along the mainstem of the Mad River was largely dominated by the invasive Japanese knotweed (*Fallopia japonica*), however sites were chosen to include some variation in vegetation as well. Other vegetation observed at monitored sites included pasture grasses, forested areas, and native perennial species such as Canadian goldenrod (*Solidago Candensis*). We also collected soil samples at 20 locations in the watershed (green circles in Figure 4) for grain-size and bulk density analysis.

We also used suspended sediment data presented by *Hamshaw* (2014) collected at the outlet of the Mad River near Moretown, as well as at the outlets of the five previously mentioned tributaries. Based on high temporal resolution turbidity monitoring and measurements of suspended sediment, Hamshaw developed TSS-turbidity relationships to assist in training an artificial neural network (ANN) for the Mad River watershed. He estimated suspended sediment loads based on the theoretical equation

$$Load = \int_{t_1}^{t_2} Q_t TSS_t dt, \tag{10}$$

where Q_t is the stream discharge at time *t* and TSS_t is the total suspended solid concentration at time *t.* Loads were calculated using turbidity-based estimates of TSS and compared to loads calculated using estimates of TSS based on the traditional sediment rating curve approach (SRC). In this study, we used Hamshaw's turbidity-based estimates of TSS to calculate suspended sediment load at the outlet in the same manner for the simulated time period. Hamshaw used data that spanned from April - November 2013

and from June - November 2014. We also used discrete sample results to assess modeled suspended sediment at the watershed and subbasin outlets (red circles in Figure 4).

3.3.3.1 *Geotechnical Soil Data*

The BSTEM algorithm requires the definition of parameters related to geotechnical properties of soil and additional stability provided by roots or bank protection measures. Critical shear stress and erodibility parameters were set initially based on previously described measurements taken by *Hanson* (1990), *Hanson and Simon* (2001), and *Simon et al.* (2003) using an in situ jet-test device. We conducted borehole shear testing (BST) at the identified streambank monitoring sites (Figure 4) to obtain *in situ* measurements of soil cohesion and friction angle. BST tests were conducted at between one and three feet in all cases except one. This was due to the presence of a gravel layer at almost all sites that hindered auguring to further depths.

Results from the BST indicate relatively little difference in cohesion and friction angle measurements between sites (Table 3). This was not unexpected as most sites comprised relatively similar sandy soils with an underlying gravel layer. We omitted the results obtained at Site 3 because the gravel layer prevented testing at depths greater than 0.5 feet, which we considered too shallow to get accurate readings using the BST device. All sites were along the mainstem of the Mad River, except Site 1, which was located on a major tributary near the outlet of Shepard Brook (Figure 4). We observed no notable differences in soil parameters among sites.

Table 3. Values of BST, DST, and calculated cohesion and friction angle results for identified streambank sites. Negative cohesion values are not uncommon in field testing of sandy soils; these values were interpreted as zero cohesion.

Site Number	Number of samples (n)	Average sample depth, m	BST cohesion, kPa	Friction angle, degrees
1	4	0.38	3.65	35.84
2	3	0.61	4.85	33.86
4	3	0.56	6.96	34.78
5	2	0.76	-3.53 (0*)	34.79 (32.04*)

*Values computed with regression forced through zero cohesion

We assigned cohesion and internal friction angle to bank soils in each grid cell (that contained a stream channel) based on user-defined probability distributions in order to account for normal spatial variability in these parameters. We also explicitly assigned radius of curvature and added cohesion values to each stream segment using probability distributions defined by field-based data. Radius of curvature represents sinuosity, and added cohesion represents the influence of vegetation or bank stability measures to each stream segment. Separate probability distributions were defined for each channel class and values were assigned to each grid cell containing a bank segment during initialization, then held constant for the duration of the model run. Thereby a stream segment randomly assigned a high curvature value would see more progressive undercutting than a straighter stream segment over longer time periods. The parameters assigned probabilistically therefore also remain constant during execution of the BSTEM algorithm in each grid cell. The parameter that represents the increase in soil strength due to an increase in matric suction, ϕ^b, can also be assigned by channel class. For all stream classes in this work ϕ^b was set to 15, based on BSTEM v5.4 suggested values. Internal friction angle and ϕ^b both had a relatively small impact on sediment results.

Field data on bulk density and grain size were collected at 20 sites throughout the watershed (Figure 4) at depths of less than one foot. Bulk density values ranged from 1586 kg/m^{3}to 2067 kg/m^3 and d_{50} ranged from 0.16 mm to 0.83 mm. Again, we found no relationships between these values and channel class or soil type. This is separate from the bulk density values already assigned to the soil layers of each soil type (for land surface soils verses bank soils) in the original DHSVM configuration file. We assigned average d_{50} as well as critical shear stress values by channel class; these were used as calibration parameters as they had the most impact on bank erosion rates. In addition, erodibility (κ) is currently calculated as a function of critical shear stress,

$$\kappa = 0.09 * {\tau_c}^{-1/2}, \quad (11)$$

where τ_c is critical shear stress in Pa (Hanson & Simon, 2001).

Additional BSTEM parameters include radius of curvature of a stream segment and an added cohesion value that represents the influence of vegetation or bank stability measures such rip rap or jute net. To inform radius of curvature distributions, we made approximate measurements of radius of curvature based on GIS delineation of streams. To simulate the presence of vegetation along a stream bank, the cohesion value of bank soil layers can be increased to represent the added cohesion due to roots (*Pollen and Simon,* 2005; *Pollen-Bankhead and Simon,* 2009). Similarly, the cohesion value of the bank toe (or bank soil layers) can be increased to simulate bank protection measures such as the implementation of rip rap or jute net. In the coupled model, the user can similarly adjust root cohesion of vegetation classes assigned to each grid cell or bank cohesion assigned to each stream class. In the application of the model for this work, we assigned bank cohesion values to each stream class based on field work that incorporated cohesion

due to vegetation; however no explicit representation of bank protection measures were included.

3.3.3.2 *Bank Geometry*

BSTEM requires the user input bank geometry either as a series of 23 points that describe the detailed geometry of the bank, or as several measurements that are used to compute a simplified geometry (BSTEM v5.4). For this work, we programmed the second option into DHSVM, so that the user inputs bank height, bank angle, toe length, and toe angle for each channel class in the stream input file. Based on these parameters, BSTEM calculates a simplified bank profile. We made 35 measurements across all stream channel classes of these parameters describing the streambank profiles (pink circles in Figure 4); we used these data to set initial bank profiles for each channel class. As the model progresses and bank erosion or failures occur, the bank angle, toe length, and toe angle can evolve during simulation. The elevation of the bank height remains constant as the flood plain elevation; however individual nodes along the bank profile can decrease in elevation due to failure and erosion. In order to prevent instabilities in the model, the bank profiles are reset at the beginning of the water year. (If allowed to retreat over multiple years without being reset, the x and y positions of banks can become large negative numbers.) However, the mass of progressive erosion and failures are continuously stored and not reset.

3.3.4. Calibration and Validation Methods

To assess the functionality of this coupled modeling approach, we focused first on flow and then results of simulated sediment mobilization in the watershed. We used measured meteorological data from the field station at a 2-hr time step, for the 2014 water

year (01 October 2013 to 01 October 2014), to achieve initial hydrological calibration and compared model flow results to flow data from the USGS gauge at Moretown, Vermont. Although DHSVM has a relatively large number of input parameters, previous studies have indicated that the model is mostly sensitive to a few key parameters (Cuo, Giambelluca, & Ziegler, 2011; Surfleet, Skaugset, & McDonnell, 2010; M. S. Wigmosta, Nijssen, Storck, & Lettenmaier, 2002; Yao & Yang, 2009). Based on these previous studies, we chose lateral conductivity, a factor representing exponential decrease in conductivity with depth, field capacity, and porosity as calibration parameters and we manually modified these within realistic ranges to adjust stream flow. We then ran the model with the same parameter set for several years using NARR data at a 3-hr time step to validate model performance. The model spin-up period was one year for all model runs and was driven by NARR data.

Several measures of fit were chosen to assess model performance with respect to flow. For the initial calibration period, driven by measured meteorological data, we primarily used the Nash-Sutcliffe efficiency (Nash & Sutcliffe, 1970) (E_2). E_2 is a commonly used measure of fit for hydrological models and ranges from -∞ to 1.0, where 1.0 indicates a perfect fit and 0.0 indicates the model results are no better than the mean value of the observed dataset. We further assessed model fit for these multi-year model runs using two additional measures proposed by *Legates and McCabe* (1999) and described by *Waichler et al.* (2005) to incorporate inherent seasonal variability in flow data. These additional measures included the baseline-adjusted first-degree efficiency (E_1'), where the baseline mean was defined as the mean for each month of the year, taken across all years in the simulation period, as well as the baseline-adjusted modified index

of agreement (d_1') (Waichler et al., 2005). E_1' has a range of -∞ to 1.0 and d_1' has ranges from 0 to 1.0. These additional measures of fit are of particular interest in assessing multi-year simulations, but were also calculated for initial runs done with locally measured meteorological data for consistency.

Following calibration/validation of model hydrology, we calibrated sediment generation in the watershed using TSS data from four locations in the watershed. All sediment results presented here were generated using measured meteorological data since this produced better hydrology results and better represented actual conditions in the watershed. Additionally, subsequent results are the average of 10 identically parameterized runs. This was to account for probabilistic variation in explicit parameter definition as well as in failure calculations. Again, we used average bank d_{50} and critical shear stress values as the primary calibration parameters for the streambank sediment module.

We used two independent datasets to assess the ability of our coupled model to estimate sediment fluxes. Data from *Hamshaw* (2014), who used high frequency turbidity sensing and discrete TSS sampling on our five study subbasins to establish high temporal resolution estimates of TSS concentrations and suspended sediment flux were used to evaluate model performance and as validation of our estimates of basin-scale sediment flux. Data from *Wemple* (2013), who used storm based sampling of road-sediment fluxes and a simple GIS-based model for basin-scale estimates, were compared to modeled results of road-generated sediment flux. We first compared modeled suspended sediment loads for the Mad River watershed to those estimated using turbidity-based TSS (Hamshaw, 2014), for the non-winter months of 2013 and 2014. Next we used 2013-2014

discrete TSS measurements (Hamshaw, 2014) at four locations in the watershed (red circles in Figure 4) to examine model performance at discrete times and locations. The locations included the outlet of the Mad River at Moretown and the outlets of three of the subbasins, Mill Brook, Shepard Brook, and Folsom Brook. Too few samples taken at Freeman Brook and High Bridge subbasins coincided with modeled periods, so these were not used for discrete sample comparison. For these four locations radius of curvature values were hardcoded into model initialization functions, instead of assigned based on the stream class probability distribution. Finally, we examined the proportions of sediment mobilized throughout the watershed generated by overland erosion, road erosion, and streambank erosion or failure. We also then examined the proportions of sediment from each of these mechanisms that were present in the stream channels at the Mad River outlet at Moretown, as well as at the outlets of all five subbasins. The goal was to assess whether the relative proportions of sediment changed and whether characteristics of the subbasins, as discussed in the Site Description section, had an impact on simulated sediment.

3.4. CALIBRATION AND VALIDATION OF COUPLED MODEL APPROACH

3.4.1. Flow

Fit was generally good for the runs driven with measured meteorological data (E_2 = 0.76, E_1' = 0.47, d_1' = 0.73) and was considered adequate for runs driven with NARR data (E_2 = 0.67, E_1' = 0.32, d_1' = 0.67) for all four years). The model performed very well for the 2011 and 2012 water years (E_2 = 0.90 and 0.92, E_1' = 0.50 and 0.52, d_1' = 0.92 and 0.94, respectively); however, results for 2013 and 2014 water years did not show such a good fit (Figure 8). Figure 8c shows that the model did not simulate several

discharge peaks, particularly during the summer months of 2013. We expect that these events were driven by local convective storms and that NARR data did not represent small scale weather events such as these local storms. The largest discrepancy in 2014 was the spring melt period. Small changes in temperature can drive these melt processes and NARR temperatures likely did not accurately reflect those small fluctuations in temperatures that impacted snow melt throughout the watershed. This again is likely a result of the NARR data resolution and the ability of those data to represent local weather patterns and the effects on local hydrological processes. These plots also reflect gaps in the measured USGS data, where the gauge was unable to record, most likely due to winter ice conditions.

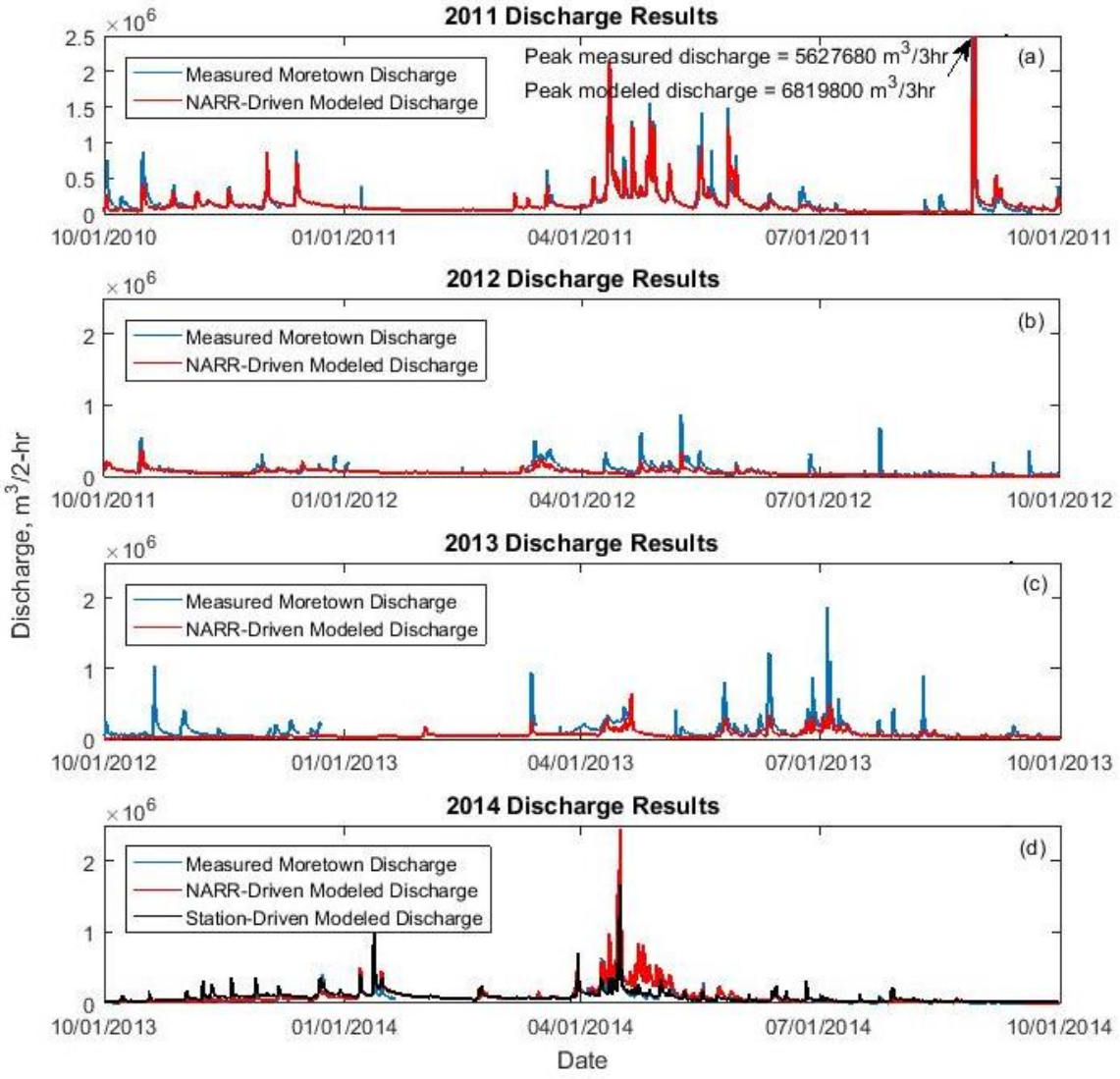

Figure 8. Model and observed flow data for water years 2011-2014.

3.4.2. Sediment

We first examined simulated sediment mobilization with respect to flow and watershed conditions. Figure 9 shows the model discharge at the watershed outlet and total sediment mobilized in the watershed during the 2014 water year (Figure 9b), as well as precipitation during that time period (Figure 9a). Sediment mobilization generally

corresponds with peaks in flow, although as expected, the amount of sediment mobilized is not linearly related to the peak in discharge. The sediment pulses seen in Figure 8b are the result of bank failures. Failures that occurred in January 2014 corresponded with temperatures above freezing, indicating a mid-winter thaw, as well as the occurrence of precipitation. Relatively few failures were seen during the period of high flows resulting from snow melt, likely because no significant precipitation events occurred during that time period. Erosion and failure of streambanks is affected by not only high flows, but also the intensity and persistence of precipitation, as well as antecedent conditions such as soil moisture and vegetation. Smaller amounts of sediment enter channels at lower flow events; this sediment is the result of erosion processes (as opposed to mass failures), from streambanks, as well as overland and road erosion. It should be noted that Figure 9b shows total mobilized sediment entering stream channels, and not sediment output from the watershed. A portion of suspended sediment is deposited before reaching the outlet.

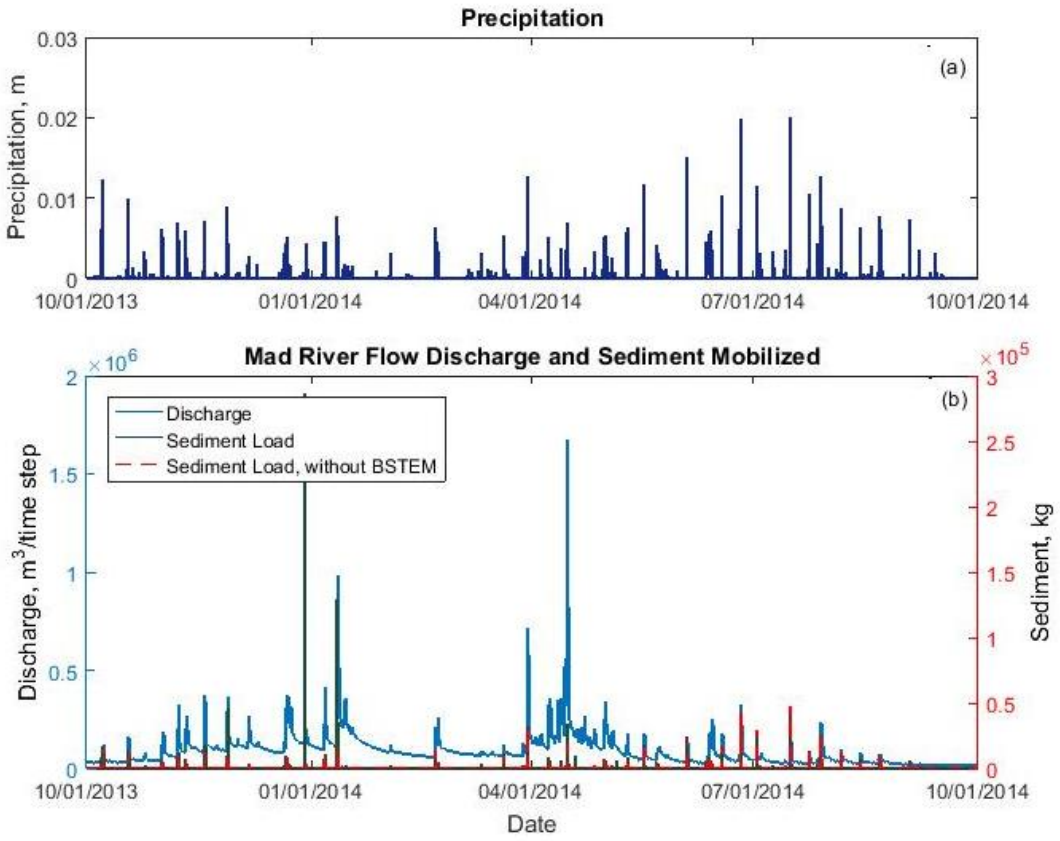

Figure 9. Precipitation inputs (a), as well as discharge and total sediment mobilized within watershed at the Mad River outlet (b).

We compared model predicted suspended sediment concentrations to discrete suspended sediment measurements taken during summer months of 2013 and 2014 at the Mad River outlet and three subbasins (Figure 10). Not enough samples were taken within the modeled time period at Freeman Brook and High Bridge Brook to compare with model results. Although the inclusion of BSTEM does not change suspended sediment concentrations for all events, it does improve the representation of high concentrations associated with higher flow events as well as produce peaks during some small events that otherwise were not present (Figure 10d). For example, in the subwatersheds, the inclusion of BSTEM had the most impact on suspended sediment concentrations during

spring melt (shown in Figure 10b), however no samples were taken during that period. The model simulates relatively well the occurrence of sediment peaks, and in most cases the magnitude of those peaks are comparable. The model generally underpredicts suspended sediment concentration in comparison to samples, particularly at the subbasin outlets. We attribute this to the rapid response of subbasin discharge during flow events and the temporal resolution of the model being too coarse to capture those fluctuations. In many cases, there were multiple TSS samples that showed considerable variation and were taken within a single model time step (2 hours).

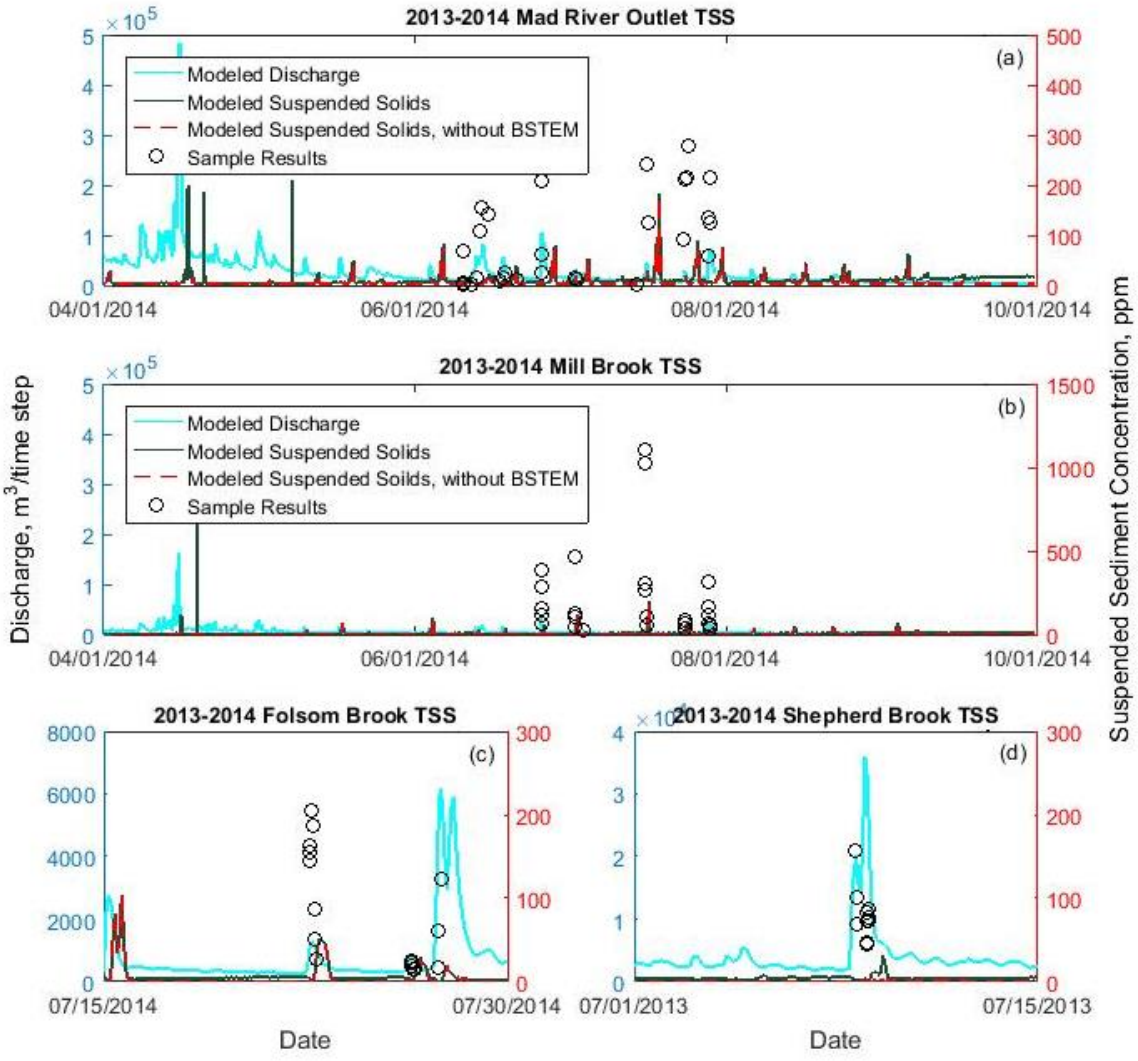

Figure 10. Suspended sediment concentrations at the Mad River and subbasin outlets.

For most events, Figure 10 shows a lag in modeled sediment, particularly at the outlet of the larger watershed (Figure 10a). Few studies have compared DHSVM-modeled sediment concentrations to site specific suspended sediment measurements such as this, though two works have noted similar lags in sediment ranging from -9.5 to 26.5 hours and from one to 37 hours behind discharge peaks (Beeler, 2014; Clement, 2014). *Clement* (2014) suggested that variability in lag times between turbidity and discharge

were related to precipitation pattern, where longer lag times were associated with higher duration, lower intensity events and could indicate the occurrence of a mass failure event. In this application lag times at the watershed outlet were approximately 60 hours (30 time steps), while at the major tributary outlets (Mill Brook, Shepard Brook, Folsom Brook, and High Bridge Brook) the lag time ranged from 8-14 hours (4-7 time steps). At the outlet of Folsom Brook sediment typically lagged only 2 hours (1 time step) behind peak discharge. No discernable pattern of lags was found in the modeled versus measured discharge; peak modeled discharge occurred almost simultaneously with measured peak discharge (± 2 hours/1 time step). We believe the lag observed in modeled suspended sediment is related to the temporal and spatial resolution of the model and the number of model steps required to move sediment from various locations in the watershed to the channel network and then downstream to an outlet segment. In the current model, sediment supply is not limiting, but transport may be limited by estimation of flow conditions over the 2-hr time step. Pulses of sediment from simulated bank failures can be seen immediately following peak discharge in some cases (Figure 10a). These likely occurred within close proximity to the outlet, resulting in less lag time (2-4 hours, 1-2 time steps) than occurred with sediment originating further from outlet points, such as from upland erosion of land or road surfaces or upstream erosion of banks.

We compared cumulative total load, calculated using *Hamshaw's* (2014) turbidity-based TSS data, to cumulative modeled load at the watershed outlet (Figure 11). Modeled load is similar to the field-estimated load for the non-winter months of 2013, although again underestimates loading in 2014. The modeled cumulative sediment load for 1 August 2013 – 25 November 2013 was approximately 1,240,000 kg, which was

lower than the 1,960,000 kg estimated using data from the work of *Hamshaw* (2014). However, the modeled cumulative load with BSTEM inactivated was approximately 667,000 kg for the same period. For 06 June 2014 through 05 December 2014, modeled cumulative load was approximately 345,000 kg and estimated load was 666,000 kg, where the modeled load with BSTEM inactivated was approximately 125,000 kg. The model underestimates suspended sediment loads in comparison to the field-based estimates of loading at the watershed outlet. In particular, the simulated peaks in suspended sediment due to specific precipitation and high flow events are underpredicted while there is some overprediction of suspended sediment concentrations during baseflow conditions. While calibrating this model, we observed a trade-off between simulating elevated baseflow suspended sediment as well as increased numbers of failures and simulating baseflow accurately with fewer failures occurring.

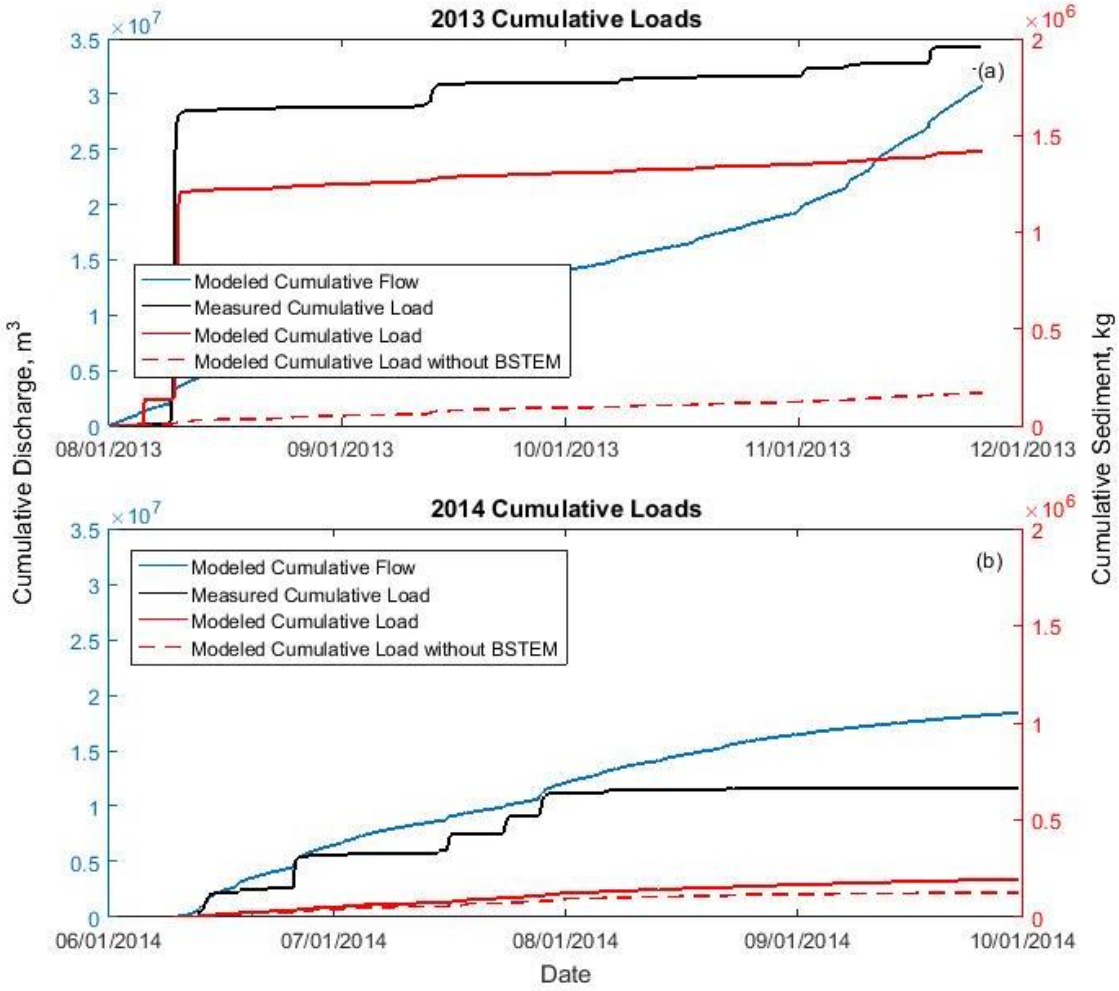

Figure 11. Modeled verses measured cumulative sediment load at outlet of Mad River watershed during modeled non-winter months in 2013 and 2014. Measured sediment load was based on turbidity-estimated TSS (Hamshaw, 2014).

In addition to producing comparative amounts of sediment between estimated and modeled loads, the model also simulates a similar response in sediment mobilized in the watershed. The vertical pulses seen in Figure 11 are indicative of flow events that resulted in increased mobilization of sediment. The observed loads show only small contributions of sediment during periods of low flow. The modeled loads show a similar response overall, with relatively low amounts of sediment being mobilized during low flow periods. In 2014, the model does not capture pulses of sediment that likely occurred

as a result of small precipitation and flow events (Figure 11b). The model can be parameterized to capture more mobilization of sediment at low flows, however this results in a large overestimation of sediment at higher flows. The results of the coupled model do however show improved overall estimation of cumulative sediment as compared to the model with BSTEM inactivated (original DHSVM), particularly in 2013 where more frequent and high magnitude precipitation events occurred than in 2014.

Another goal for simulating sediment was to represent realistic proportions of sediment mobilized by overland erosion, road erosion, and streambank erosion. Few studies have quantified sediment loading resulting from streambank or road erosion in Vermont watersheds. Studies typically report considerable variability in those estimates, particularly with respect to streambank erosion among different reaches (DeWolfe et al., 2004; Langendoen, Simon, Klimetz, Bankhead, & Ursic, 2012; Morrissey et al., 2011; Wemple, 2013). Despite this variability, we used these prior studies as a basis for approximating relative proportions of sediment being generated from overland erosion, streambank erosion, and erosion of roads. The Mad River watershed is largely forested, so overland erosion was expected to be relatively low in comparison to other watersheds where urban and agricultural land uses may dominate. Figure 12 shows total sediment mobilized and entering the stream channel network within the entire watershed by the three mechanisms previously mentioned. On average, streambank erosion and failure generated approximately 62% of total sediment load during the modeled time period, road erosion produced 33%, and overland erosion produced the remaining 5%. For this calibration, the proportion of sediment mobilized by each source only varied within ±4% of the average of these 10 results. Again the behavior of sediment mobilization by

streambank erosion/failure is also apparent in this plot, where cumulative sediment increases in pulses that correspond to precipitation and/or high flow events.

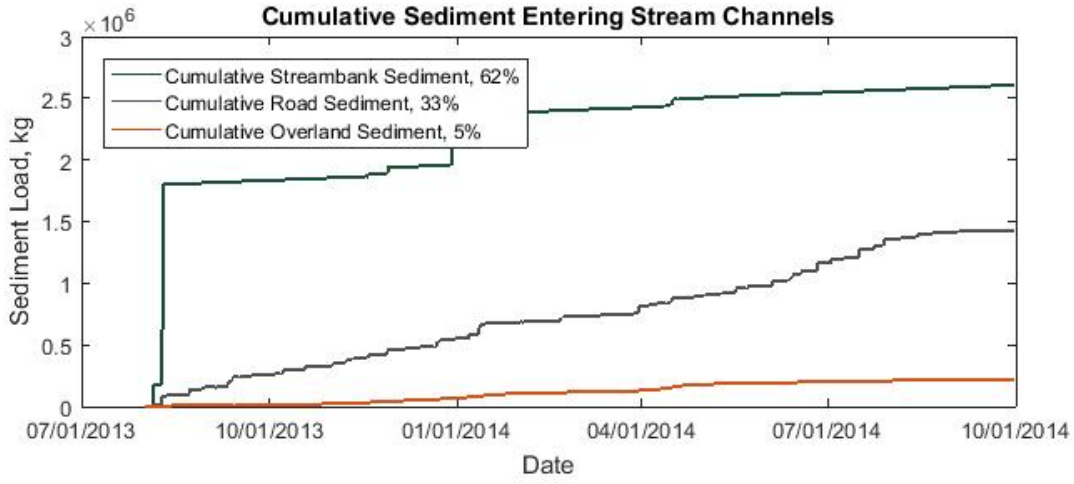

Figure 12. Cumulative proportions of sediment mobilized by overland erosion, road erosion, and streambank erosion and entering stream channel network throughout Mad River watershed.

Further examination of model-generated sediment by these three sources shows that these proportions show logical variability between subbasins. Although we could not output total sediment mobilized throughout each of the subbasins, we could look at the make-up of suspended sediment at the outlet of the subbasins. These results are different from those presented above in that they are impacted by sediment transport processes. Heavier particles are allowed to settle out in stream segments where velocity and stream power decline. Therefore, the relative proportions of sediment in subbasin outlets, and particularly at the outlet of the watershed at Moretown, differ from the original proportions of total sediment mobilized within the watershed. Total cumulative suspended sediment was calculated for these subbasins using the modeled suspended sediment concentration at each outlet, the corresponding outlet discharge, and the tracked

ratio of streambank, road, and overland erosion that is outputted at each time step and each location. Figure 13 shows the cumulative suspended sediment from overland erosion, roads, and streambanks at the outlet of the watershed, as well as at each of the five subbasin outlets. Table 2 lists relative characteristics of these subbasins, such as the road-to-stream length ratios and percent coverage of land cover types. Freeman and High Bridge subbasins have the highest road-to-stream ratios as well as the highest percentage of land use classified as roads, which is reflected in higher proportions of sediment from road erosion in these subbasins (37% and 24%, respectively) than in other watersheds. The largest percentages of sediment from overland erosion at outlet locations occurred in Mill Brook and Shepard Brook, which were also the largest subwatersheds (Table 2) and had the largest ranges of elevation. The contribution of sediment from overland erosion was very negligible in small upland subwatersheds (<1% in Folsom and High Bridge).

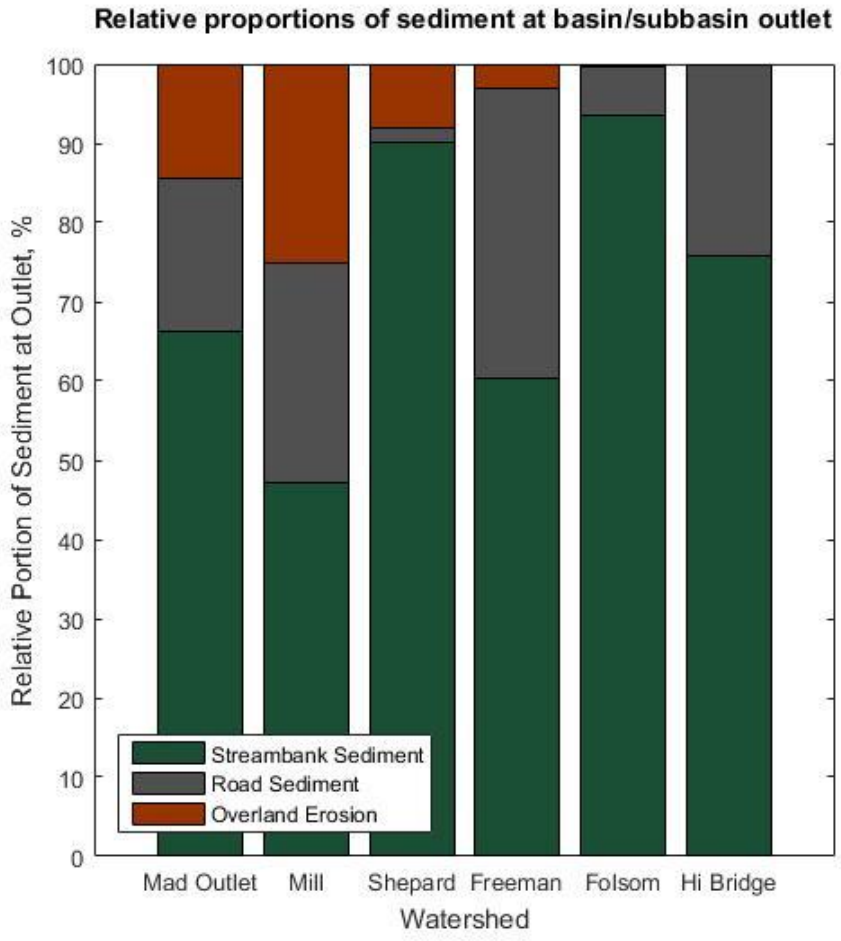

Figure 13. Relative proportions of cumulative suspended sediment at Mad River and subbasin outlets.

3.5. DISCUSSION AND CONCLUSIONS

This work presents a new capability in an existing watershed model for simulation of sediment generation within a spatially explicit environment. By coupling a watershed and bank stability model we can more inclusively represent the processes that mobilize sediment, including the erosion and particularly failure of streambanks, which were previously not present in similar distributed models but represent important sediment mobilization processes in many watersheds. Overall the streambank erosion processes are

captured in the coupled model approach, with some limitations. The results indicate that the coupled model simulates the approximate magnitude and timing of sediment mobilization in the watershed and its subbasins, however generally underestimates suspended sediment concentrations as well as cumulative loading. The ability of the model to simulate peak sediment concentrations is also affected by the spatial and temporal resolution of the model. Measured suspended sediment concentrations varied significantly within a single model time step and this variability is difficult to model unless accurate and high resolution inputs are available to drive the model. However, the coupled model still improved prediction of cumulative loads and in some cases suspended sediment concentrations in association with high flow events, particularly in comparison to the simulation conducted without representation of these processes. The coupled model also logically represents watershed characteristics that would impact erosion processes, such as land use, slope, and vegetation.

Although several sites were monitored for bank erosion and failure, no instances of mass failure occurred during the modeled time period so no comparison or analysis of specific failure events could be made in this work. The 2014 water year was relatively dry with few events that elevated flow other than spring melt. Mid-winter thaws that occurred during January 2014 were reflected in sediment results, where precipitation that occurred during these periods were modeled as rain on snow events. Temperatures above freezing resulted in snow melting, elevated flow conditions, and the occurrence of bank failures as expected. Elevated erosion and small failures also occurred during flows associated with the spring melt and were likely a result of bank undercutting during this period. No significant precipitation coincided with this spring period. Also, no data

related to suspended sediment, erosion, or failures were available during the winter or spring melt period.

Results indicated that there was generally more sediment available than transport capacity to move that sediment during relatively low flow events. This was reflected in similar suspended sediment concentrations predicted by the model at low flows, with and without BSTEM activated. Changes in parameter values that increased available sediment resulted in no changes in the low flow, subbasin sediment concentration values. The years for which we have data on suspended sediment in the watershed were relatively dry, with no significant precipitation or high flow events. It was therefore difficult to assess model performance under conditions where large amounts of sediment would be mobilized by bank failures and high flow conditions would allow transport of that material. The variability in results due to probabilistic parameter assignment was seen primarily in the magnitude of sediment pulse events, where the number of failures showed some variability, but typically occurred within the same few time steps. This was reflected in higher peaks in suspended sediment concentrations at relatively higher flows, however no difference was seen with low flow events. The results presented here indicate the potential for this approach to improve our ability to simulate sediment mobilization and transport under higher flow conditions.

Results indicate that in the Mad River watershed, where the landscape is largely forested and surface erosion is minimal, streambank erosion and failure were major contributors of sediment to streams and receiving waters between 01 August 2013 and 30 September 2014. Land use and watershed characteristics impact the spatially explicit calculation of sediment mobilization from the landscape and stream banks, as well as

sediment transport in the stream network. Differences in the relative proportions of suspended sediment originating from streambank, road, and overland erosion at subbasin outlets are indicative of factors such as land use and channel characteristics impacting the simulation of those processes. Previous studies conducted in Vermont watersheds have large ranges of sediment proportion generated by streambank erosion and failure. For example, Morrissey et al. (2011) estimated that on a reach basis, streambank erosion accounted for 15-80% of total eroded sediment. Langendoen et al. (2012) used BSTEM to estimate sediment loading from streambank erosion in an agricultural watershed in Vermont and found that 36% of total suspended sediment leaving the watershed was from streambank erosion. Specific to the Mad River watershed, Wemple (2013) estimated that unpaved roads contribute 10-27% of the annual sediment yield from the five subbasins used in this study. The coupled model presented here generated suspended sediment loads that agreed well with these field-based estimates. Model results indicated that road sediment contributed 2-37% of sediment seen at these same subbasin outlets.

Additionally, in this study, roads contributed 33% of mobilized sediment that reached stream networks in the watershed, which also compared well to field-based estimates for annual average suspended sediment from roads for the Mad River and Winooski watersheds (17-31%) (Wemple, 2013). However, 19% of suspended sediment at the watershed outlet near Moretown originated as road sediment. It may be that much of the road sediment from upstream subbasins was redeposited in slower stream segments before reaching the outlet of the watershed. This deposition of road sediment is related to the larger particle size of road-sediment. Road sediment particle size was set larger than streambank sediment. It therefore falls into a larger sediment bin size which the model

transports with remaining stream power once smaller sediment has been moved. Overland sediment was parameterized as finer particles, and although overland erosion was only 5% of total sediment mobilized, 14% of sediment seen at the outlet originated from this source, indicating that these particles remained in suspension.

An increase in the number of failures occurring, the amount of sediment mobilized, and thereby suspended sediment concentrations in the stream channels, can be achieved by adjusting relevant parameters such as cohesion, radius of curvature, and critical shear stress. However, this also results in an increase in suspended sediment concentration during baseflow conditions, indicating an overestimation of continuous erosion of banks, and ultimately leading to overestimation of cumulative suspended sediment. This could potentially be addressed by delineating the stream network into smaller segments or using a smaller grid size (grid cells here were 100m by 100m), but maintaining variability among reaches, so that segments where erosion and failures occur frequently, a smaller volume of sediment is being contributed to the overall system. In this work, erosion calculated on any stream segment was applied to half the length of the channel segment contained in that grid cell. This may be relatively accurate if using a small grid cell size, however the coarser the resolution of the model, the less likely this assumption is to realistically represent actual erosion. Alternatively, the model could be modified so that the volume of sediment lost due to the rate of erosion or a mass failure was calculated based on a smaller portion of that stream segment, perhaps as a function of the radius of curvature.

The ratio used to track streambank sediment was calculated based on the influxes to each stream segment and then applied to sediment leaving that segment. This was

considered a valid assumption since those ratios are calculated and tracked for each model sediment bin size. Once sediment is added to a bin size in DHSVM, it is not further differentiated in the model. Sediment from all sources (roads, streams, overland, and debris flow) entering a stream segment are combined, as well as sediment mass stored in that segment, the total transport capacity is calculated and some portion of the total available sediment is moved to the next segment. Remaining sediment that is in excess of the total transport capacity is redeposited in that segment and available for transport at the next time step. No preference is given to transporting already suspended sediment over stored/settled sediment in any segment. In reality however, currently suspended sediment is more likely to be transported than stored sediment and the ratio of streambank sediment to other sediment entering a reach is not necessarily the same as the ratio at the reach outlet. In the current parameterization, a significant portion of road sediment is redeposited before reaching the outlet because of coarser particle size, whereas sediment from overland erosion is more easily transported due to incipient motion on the land surface favoring fines. Streambank soils are represented mostly as silty loams and loamy sands, which are between road and overland sediment particle sizes. The high proportions of streambank soils seen in these results are also affected by the locations chosen for model comparison. Most simulated streambank erosion and failure occurs along the lower portion of the main stem and to some extent along major tributaries of the Mad River, so these sediments are transported shorter distances to locations where model results are compared to field data.

This application of DHSVM represents a scaling up of the use of this hydrological model from small headwater watersheds to larger watersheds where bank erosion may

play a bigger role. With some exceptions, much of the work using DHSVM has been conducted on watersheds of less than 50km^2 (for example, Wigmosta and Lettenmaier, 1999; Bowling and Lettenmaier, 2001; Waichler et al., 2005, 2005; Doten et al., 2006; Surfleet et al., 2010; Du et al., 2014). In larger watersheds, particularly those where the landscape has been modified in ways that increase stream channel instability (such as deforestation, agriculture, and urban development), simulation of the processes contributing to bank erosion and failure will generate a more complete picture of how sediment is mobilized and transported. The influence of local meteorological data, particularly precipitation, is also clear in the application of this modeling approach. Particularly in larger watersheds and watersheds with large ranges in elevation, the impact of local storms and spatial variability in rainfall may have an important impact on sediment mobilization processes. The model time step used in this work (2-hr) was chosen based on the limited availability of higher resolution data for all variable needed to drive the hydrology model. Inclusion of high spatial resolution precipitation data could improve model performance, particularly with respect to water table conditions and lag times.

This approach could be further improved to better represent the physical conditions and processes contributing to sediment mobilization, in particular from bank erosion and failure. For example, more recent versions of BSTEM incorporate the occurrence and impact of tension cracks on bank stability. In Vermont, tension cracks are not commonly observed and so were not incorporated in this work. However, in other regions, this may have a more pronounced impact on bank stability and further work could enhance the model by incorporating those processes. Additionally, BSTEM

includes a RIP ROOT module (Pollen & Simon, 2005), that calculates the specific additional cohesion due to roots on bank stability forces. Additional work could enhance the ability to simulate specific bank vegetation or bank stability measures in a spatially explicit format.

Bedrock outcroppings in the Mad River Valley constrict the river and cause ponding during heavy precipitation events. Slower velocities lead to sediment deposition and bank erosion where flow is diverted. Sediment in tributaries as well as the mainstem is then periodically flushed out by large events. This ponding effect is difficult to model, but could potentially be achieved by manual delineation and description of the stream network. This was not attempted for this work, but may be an avenue for future research. Using a stream network that more accurately describes explicit changes in widths and slopes of stream segments should allow the model to produce more accurate estimates of stream power, which could potentially be investigated as an indicator of erosional hot spots similar to how Gartner et al. (2015) identified hot spots using a logistic regression model based on channel slope, curvature, and length of upstream segment.

The importance of simulating streambank failures is partly because sediment can be a water quality issue in its own right, but also because bound phosphorus can contribute significantly to nutrification problems in receiving water bodies, such as Lake Champlain which suffers excess nutrient loads that lead to eutrophication and harmful algal blooms. Ishee et al. (2015) suggested that landscape position (floodplain, low slope vs. upland soil) may be useful in identifying streambank erosion sites where soils are more likely to have higher total phosphorus (TP) concentrations (Ishee, Ross, Garvey, Bourgault, & Ford, 2015). However, although TP is often used as an index of P loading,

these authors also suggested, based on lower concentrations of Morgan Modified P (MM P) and degree of phosphorus saturation (DPS), that eroding streambank soils may actually act as phosphorus sinks, contrary to prior conclusions. This suggests that more work is needed to qualify streambank erosion based on bioavailable phosphorus measures in order to assess the impact on nutrient loading.

The presented coupled model advances mechanistic representation of suspended sediment within a watershed. Such modeling ability is valuable for simulating the potential impacts of climate and land use changes on sediment and nutrient budgets as precipitation driving flood events continues to become more extreme. Because we expect higher intensity precipitation events would likely have a larger impact on streambank erosion and failure, this coupling may be particularly beneficial for simulating extreme event and climate change scenarios. The ability to more inclusively simulate the processes that mobilize sediment from a watershed has important implications for water quality assessment and related policy issues (such as climate adaptation). The physics-based nature of this coupled modeling approach will be particularly well suited for assessing the potential impacts of future shifts in climate and land use on water quality and land management.

CHAPTER 4: IMPACTS OF CLIMATE CHANGE ON SEDIMENT MOBILIZATION AND TRANSPORT

4.1 INTRODUCTION

Changing weather patterns will have complex and nonlinear effects on many human and environmental systems, including on processes governing the mobilization and transport of sediment within watersheds. Authors have found significant increases in the frequency of extreme precipitation events in the United States (Guilbert et al., 2015; Thomas R. Karl & Knight, 1998; Kenneth E. Kunkel, 2003; Kenneth E. Kunkel et al., 1999). Although relationships between sediment loading and discharge vary among watersheds (Asselman, 1999; Hamshaw, 2014; Webb & Walling, 1982; Williams, 1989), authors have found that extreme precipitation and/or resulting flow events result in disproportionately higher suspended sediment loading in transport limited systems (Gonzalez-Hidalgo et al., 2010; Oeurng et al., 2010). Increased sediment yields resulting from such events can exceed the capacity of existing infrastructure, as well as result in the increased transport of sediment-bound nutrients to larger water bodies. One of the mechanisms by which sediment is mobilized, particularly in response to high precipitation and flow events, is through streambank erosion and failure. These processes, though widely observed, have not heretofore been widely included in watershed models for assessments in the context of climate change and increasing extremes. Increased sediment loading due specifically to streambank erosion can not only contribute large amounts of sediment-bound phosphorus and other nutrients, but can also negatively impact water quality both in the watershed and further downstream. Accelerated streambank erosion can contribute to disproportionate sediment supply to specific areas

of a watershed, stream channel instability, land and habitat loss, water quality degradation, as well as other consequences (US EPA, 2012). In addition, erosion and undercutting of banks and the continued incision of streams can affect the flood resiliency of adjacent areas. Therefore, ability to model the combination of conditions (watershed state and precipitation) that give rise to huge loadings under changing extremes would advance understanding of response of streams, watersheds, and receiving water bodies to changing precipitation. This includes heavy rainfall and high flows from snowmelt driven by variability in temperature.

Computational techniques have been increasingly used to understand the physical processes and mechanisms responsible for observable changes in the environment. One of the advantages of developing physics-based modeling approaches is the capability of simulating scenarios that are outside the range of those previously observed. Stryker et al. (under review) coupled the Distributed Hydrology Soil Vegetation Model (DHSVM) (Wigmosta et al., 1994) and the Bank Stability and Toe Erosion Model (BSTEM) (Andrew Simon et al., 2000, 2003, 2011) in order to better represent the mechanistic processes governing streambank erosion and failure within a distributed watershed model. DHSVM is a distributed watershed model that simulates water and energy fluxes at sub-daily time steps (Wigmosta et al., 1994). DHSVM has been used extensively to evaluate impacts of environmental change as well as anthropogenic land use change, such as from urbanization and deforestation, on watershed hydrology (Bowling, Storck, & Lettenmaier, 2000; Cuo et al., 2009; Lanini, Clark, & Lettenmaier, 2009; Leung & Wigmosta, 1999; Safeeq & Fares, 2012; Whitaker, Alila, Beckers, & Toews, 2002). This model also incorporates the mobilization of sediment due to overland and road erosion in

response to precipitation, and the transport of sediment across the land surface and within the stream network (Doten et al., 2006). BSTEM was chosen for its advanced, physics-based representation of both hydraulic and geotechnical processes that play a role in bank failure. It consists of two components: a toe erosion module to simulate undercutting of banks by streamflow and a bank stability module to assess the likelihood of failure and the most likely failure plane. The representation of bank undercutting, resulting from fluvial erosion as a function of excess shear stress, is critical to accurate simulation of bank stability (Simon et al., 2000), particularly for examining changing flow regimes. In addition, BSTEM simulates the physical characteristics of soils, including negative pore pressures that can develop in unsaturated soil conditions. Since warmer temperatures are likely to affect soil moisture balances, the ability to simulate the role of these processes on bank stability is also significant. This improved modeling approach is thereby suitable for investigating the impact of climate change scenarios and the occurrence of extreme events on the hydrology and sediment mobilization at the small (10^0-10^1 km^2) and meso (10^1-10^2 km^2) scale watersheds.

In order to simulate the impacts of climate change however, such models require specific meteorological inputs that reflect the anticipated deviations in climate variables, particularly temperature and precipitation. Several studies have shown that precipitation in the United States, and in the Northeast region specifically, is increasing and becoming more variable in magnitude (Groisman et al., 2005; Guilbert et al., 2015; Kunkel et al., 2013; Kunkel, 2003; Kunkel et al., 1999). Kunkel et al. (2013) also projected that temperatures in this region will continue to increase between 4 and 10° F by 2080 at current emission rates, and that heavy precipitation as well as drought risk will continue

to increase. Similarly, Groisman et al. (2013) found a 70% increase in precipitation occurring as extreme precipitation events (heaviest 1% of rainfall) between 1985 and 2010. Regional or local trends are critical for investigating impacts of climate change on human life and ecosystem response (Hayhoe et al., 2006, 2008; Katz & Brown, 1992). Researchers have also noted that global climate models (GCMs), including the Coupled Model Intercomparison Project phase 5 (CMIP5) that has been used for regional downscaling efforts, do not reflect these local trends and variability in precipitation (Guilbert et al., 2014; Mohammed et al., 2015) in some regions.

Another challenge to simulating the impacts of climate change at the watershed scale is the temporal resolution of most climate projection data. Authors such as Xu (1999a; 1999b), Xu et al. (2005), and Prudhomme et al. (2002) noted that GCM products are not adequate for driving hydrological models, in part because they perform poorly at subdaily and even daily time steps. Particularly in mountainous watersheds, storm events often pass within a day, leading to high temporal variability in water and sediment fluxes not captured in models operating on daily time steps. Researchers have developed a number of approaches to address the inappropriate spatial and temporal scale of GCMs, including regional climate models, hypothetical scenarios, and both dynamic and statistical downscaling techniques (Xu, 1999b). Alternative methods to GCMs, such as statistical weather generators (WGs), may be better suited for the prediction of future temperature and precipitation data for specific regions. Although these techniques have been applied to watershed modelling, these approaches also have limitations and key challenges still exist in using existing climate data products to simulate impacts of future trends in settings like this.

We apply a physically-based watershed model to the investigation of climate-change induced increases in extreme-event magnitude and frequency to flow and sediment production dynamics in a meso-scale, high-gradient watershed. Our application is set in a region where changes in extreme precipitation is well documented and is at a watershed scale that encompasses high-gradient headwater forested streams and agricultural floodplains. Post-glacial alluvial sediments dominate the landscape and its history includes significant anthropogenic changes in land use (such as deforestation) and to stream channels (such as mill dams and channelization), making it susceptible to impacts of high precipitation and flow events (Barg & Blazewicz, 2003; Dunn et al., 2007a, 2007b; Nagle et al., 2007; Walter & Merritts, 2008; Whalen, 1998). Again, subdaily simulation is critical for capturing the dynamic processes in such watersheds and understanding the influences of changes precipitation and temperature.

The novelty of this work is in using the improved DHSVM-BSTEM model, with the ability to simulate sediment contributions from streambank erosion processes, to demonstrate the response to climate change and particularly to the observed increases in extreme precipitation. In the context of this paper, extreme precipitation events are characterized as daily flows that exceed the 95^{th} percentile. This work goes beyond using downscaled GCM output to also using temperature and precipitation data created with a statistical WG that captures local trends and variability in precipitation to drive model runs. The primary goal of this study is to assess the hydrological and sediment related impacts of climate change scenarios, including those with the occurrence of representative extreme events. The secondary purpose of this study is to assess the improved ability of these climate products to reflect the non-stationary shifts in climate

that are occurring specifically in a Vermont watershed through the resulting alterations in hydrologic and sediment-related processes.

4.2 METHODS

This study examines hydrological and sediment related results produced by the coupled DHSVM-BSTEM model (Stryker et al., under review) and driven by two sets of meteorological inputs. These authors demonstrated the ability of this coupled model to plausibly represent sediment mobilization from watershed sources, particularly in response to larger precipitation and flow events. The calibrated DHSVM-BSTEM model of the Mad River watershed is described in detail by Stryker et al. (under review) and is used in this work to assess potential changes in hydrology and sediment mobilization, driven by changes in temperature and precipitation. All spatial input files and parameter values are as described by that study.

The Mad River watershed ultimately drains to Lake Champlain, a freshwater lake situated between Vermont, New York, and Canada. Lake Champlain has experienced an increase in frequency of summer blooms (Watzin, Fuller, Bronson, Gorney, & Schuster, 2010), which is in agreement with expected impacts of climate change for many freshwater lakes (El-Khoury et al., 2015; B. Moss, 2012; Whitehead et al., 2009). Data indicate that precipitation trends in Vermont are similar to those found for the northeastern United States, where precipitation is likely to continue increasing in magnitude and variability (Betts, 2011; Frumhoff et al., 2007; Guilbert et al., 2015; Stager & Thill, 2010). In addition to experiencing climate trends representative of the northeastern United States, this watershed is also representative of northern New England watersheds that have steep headwaters draining to floodplains with a history of

deforestation for agriculture. Peak flows in this region typically occur in the spring, where snow melt has a significant impact on flow magnitude in addition to spring precipitation. Tropical Storm Irene, which landed in Vermont in August of 2011 following a heavy spring rainfall, is an example of an extreme event that caused significant impacts to the Lake Champlain Basin. This event caused extreme tributary flooding, intense lateral erosion of streambanks, long term changes to river channels and valley morphology, and significant damage to bridges, stormwater infrastructure, and private property (Lake Champlain Basin Program, 2013; Pealer, 2012). This event also resulted in large pulses of potentially nutrient-laden sediments to Lake Champlain, demonstrating the need for a better understanding of how changes in precipitation will influence sediment fluxes from the landscape.

4.2.1 Climate Data

Using the calibrated DHSVM-BSTEM model for the Mad River watershed, model runs were conducted for the water years (01 Oct – 30 Sept) 2020, 2030, 2040, 2050, 2060, 2070, 2080, 2090, and 2099. Each of these water years was preceded by a 10 month spin-up period (01 Jan – 30 Sep). Two sets of climate temperature and precipitation data were used to drive the model.

The first set of this data was developed by Winter et al. (2016) and based on the output of global climate model (GCM) simulations. Winter et al. used simulations from phase 5 of the Coupled Model Intercomparison Project (CMIP5) multimodel ensemble downscaled to an intermediate resolution using bias corrected with constructed analogs (BCCA) (Brekke, Thrasher, Maurer, & Pruitt, 2013) as the basis for further downscaling. The BCCA ensemble included 20 GCMs run as part of CMIP5 under two representative

concentration pathways (RCPs) (R. H. Moss et al., 2010). This data set was further downscaled specifically for a mountainous region in the Northeast that included our study area by using empirical relationships between elevation and daily maximum and minimum surface temperature and precipitation from local station data (Winter, Beckage, Bucini, Horton, & Clemins, 2016). The result was a 30″ product of maximum and minimum surface temperature, as well as precipitation, available at a daily time step for 1950-2099. For this work we chose four locally downscaled GCM scenarios for RCP 8.5, (which represents the 90th percentile of the reference emissions range and is similarly representative of greenhouse gas and particle emissions resulting in greater than 8.5 W/m^2 of radiative forcing in 2100 (R. H. Moss et al., 2010)). We chose a relatively warm scenario, a cool scenario (2nd coolest of RCP8.5), a relatively wet scenario, and a relatively dry scenario. These scenarios are meant to represent an envelope of variability for future climate trajectories.

The second set of data were developed by White et al. (in press) using a statistical WG. White et al. generated meteorological time maximum and minimum daily temperature and daily precipitation using a Markov-chain Monte Carlo approach with non-stationary precipitation and extreme precipitation distributions. This method incorporated the trends noted by Guilbert et al. (2015) so the result was a precipitation time series that adequately reflects the changing probability of extreme events and allows for increasing variance and skewness in the precipitation distribution looking into the future. These data were available for the years 2011- 2050. For this work we randomly chose 100 realizations from the time series produced by White et al. (in press) for the water years 2020, 2030, 2040, and 2050 to drive the watershed model.

Although simulated runoff and streamflow are most affected by temperature and precipitation, DHSVM requires additional meteorological inputs including humidity, wind speed, incoming longwave radiation, and incoming shortwave radiation. These variables affect energy and carbon fluxes, vegetation processes, and other model processes. Our statistically downscaled GCM and WG scenarios are limited to temperature and precipitation, so for the additional variables we used National Centers for Environmental Protection (NCEP) Reanalysis data provided by the NOAA/OAR/ESRL PSD, Boulder, Colorado, USA, (http://www.esrl.noaa.gov/psd/) to complete the meteorological inputs for the coupled hydrology bank stability model. The North American Regional Reanalysis (NARR) data are high resolution combined model and assimilated time series datasets, available at a resolution of 8 times daily. NARR data was used for wind speed, humidity, incoming longwave radiation, and incoming shortwave radiation for the period 01 Jan 2012 through 30 Sept 2013 in all model runs. We conducted an investigation of these additional NARR variables (wind speed, humidity, incoming longwave radiation, and incoming shortwave radiation) for this baseline period with respect to the 2000-2014 water years (Figure 14). The baseline period was not anomalous in comparison and was therefore considered appropriate for completing necessary inputs and accompanying future predictions of precipitation and temperature.

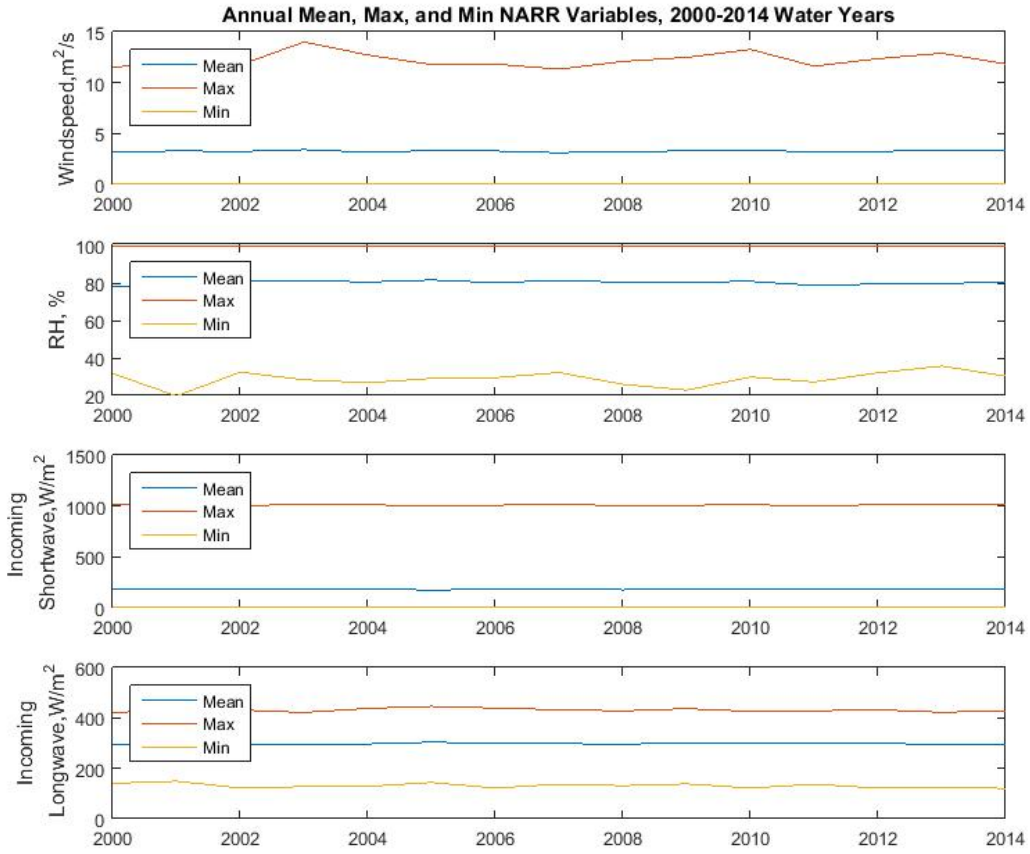

Figure 14. Long-term comparison of NARR variables.

Climate inputs included both deterministically downscaled GCM-based scenarios (4 scenarios for 9 different years) as well as WG-derived scenarios, which were assessed as an ensemble (100 realizations of temperature and precipitation for each of 4 different years). Due to the long run times, continuous long term periods were not simulated and we looked at the results of single water years in 10 year increments. We assessed baseline results as the average of 85 realizations of statistically generated precipitation and temperature for the water year 2012 in order to isolate the impacts of future temperature and precipitation predictions on watershed discharge and sediment. The statistics describing precipitation for the 2012 WG realizations were very similar to those for observed 2011 data and therefore considered representative of a baseline scenario. The

meteorological input files for these baseline realizations were then completed with the same NARR 2012 water year variables as future scenario runs.

4.2.2 Sub-daily Model Inputs

The coupled watershed model operates most reliability at higher temporal resolutions, particularly for the purpose of simulating dynamic hydrologic and sediment in mountain settings such as our study site. Therefore it was necessary to generate subdaily inputs based on the daily data from *Winter et al.* (2016) and *White et al.* (in press). *Chow and Levermore* (2007) described several methods for creating hourly temperature from daily maximum and minimum temperatures (T_{max} and T_{min}, respectively), as well as an improved method using average daily temperature. In this work we used the sin (14R-1) method for linked days as described by *Chow and Levermore,* where T_{max} was set to occur at 2pm and T_{min} to occur one hour before sunrise. Hourly temperature was calculated as

$$T(t) = \left(\frac{Temp_{next}+Temp_{prev}}{2}\right) - \left[\left(\frac{Temp_{next}-Temp_{prev}}{2}\right) \times \cos\left(\frac{\pi(t-t_{prev})}{(t_{next}-t_{prev})}\right)\right], \qquad (12)$$

where $Temp_{next}$ is the next known temperature value (either T_{max} or T_{min}); and $Temp_{prev}$ is the next known temperature value (either T_{max} or T_{min}); t_{next} is the time for the next known temperature value, and t_{prev} is the time for the previous known temperature value, and t is the time. Sunrise and sunset times were calculated according to the latitude of the study site based on standard formula described in *Scharmer and Greif* (2000).

Sub-daily precipitation inputs were generated from daily GCM and WG data by matching predicted storms to existing storms and partitioning the rainfall similarly through the duration of the storm. Quality controlled historical hourly precipitation data from the Burlington International Airport weather station in Burlington Vermont were

downloaded from NOAA's National Climatic Data Center (NCDC: http://www.ncdc.noaa.gov). These data span the period 01 May 1948 through 30 Nov 2011. We pulled statistics on historical precipitation events from this dataset, including the total duration and depth of each storm (in days), as well as the percentage of the total depth that fell in each day and hour of the event. For each future precipitation scenario (at daily resolution), we found the location (in the time series) and magnitude of all non-zero values, to identify individual precipitation events. For each precipitation event, we found daily statistics including duration, depth, and percentage of rainfall that fell in each day of an event. For a one-day event, we sampled a one-day historical precipitation event of the same depth from the Burlington data. If no equal depth was found, we averaged five storms with the closest total depths. For a two-day event, we sampled an existing storm that matched the total depth and the percentage of rain that fell in each day. If we found no exact depth match, we averaged the 10 storms with the closest depths. If we found no equal percentages, we averaged the five storms with the most similar distribution of rainfall. If the storm persisted for longer than two days, we searched the historical record for a matching event. If we identified no suitable precipitation event, then we used a combination of shorter duration precipitation events to generate a suitable event. To accomplish this, we sampled the longest existing storm that matched the depth of equal duration during the daily predicted storm first, then sampled other existing storms of similar depth to fill in the time remaining in the predicted storm. Once we matched each precipitation event with a historical event or combination of historical events, we added or subtracted tenths of millimeters of precipitation from random locations within the event to match the total storm depth from the future precipitation events.

4.3 RESULTS

Temperature and precipitation scenarios had clear influences on simulated hydrologic processes, including snow accumulation and melt, discharge, and sediment mobilization. Modeled climate trends show differences deriving from the GCM and WG data; we present these, followed by resulting differences in flow and lastly sediment. We particularly investigate results representative of changes in extreme flow and sediment yield, where for this work 'extreme' indicates those results exceeding the 95th percentile.

4.3.1 Climate Trends

Temperature and precipitation scenarios had clear influences on simulated hydrologic processes. In particular, this data do not reflect the likelihood of increasing extreme events and variability in precipitation patterns. Annual precipitation shows an increasing trend in WG-driven runs (Figure 15), as well as a slight trend in the 95th percentile of daily precipitation over the period of 2020 through 2050. Annual precipitation and extreme precipitation totals in WG realizations are also higher overall than predicted by GCMs for all years simulated (values vary approximately between .035-.045 m in WG realizations and .01-.02 m in GCM scenarios). These trends are not present in any of the GCM scenarios used here. An increasing trend in maximum storm depth is reflected in WG realizations, although these realizations do not reflect longer storm durations. GCM scenarios have a higher number of wet days, although it has been acknowledged that in part due to the coarse spatial resolution, GCMs tend to overpredict the number of days experiencing rainfall, with rainfall intensity being lower than stations within the GCM grid cell (Wehner, Smith, Bala, & Duffy, 2010). In contrast, GCM scenarios do represent expected trends in temperature, whereas WG realizations do not.

Maximum, minimum, and mean temperatures clearly increase over the 2020 through 2099 period in GCM data. Figures showing the 95th percentile (extreme) precipitation, annual number of wet days, maximum storm depth, maximum storm duration, as well as maximum and minimum temperatures between WG realizations and GCM scenarios are included in Appendix I.

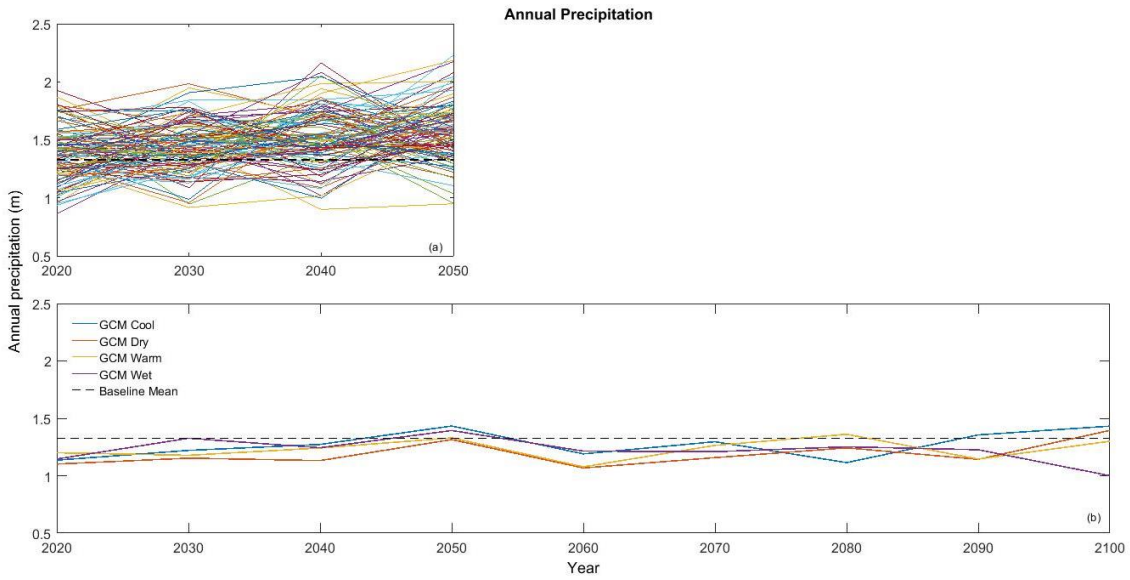

Figure 15. Annual precipitation in climate change scenarios, where panel (a) shows WG realization totals in comparison to the baseline mean and panel (b) showed GCM scenarios in comparison to the same baseline mean.

4.3.2 Stream Flow

GCM-driven runs show a trend of earlier spring melt and lower cumulative snow water equivalent totals (Figure 16). The spring day in which total simulated snow water equivalent was <0.1cm occurred 17 days earlier in the 2099 'warm' GCM simulation than in the corresponding 2020 'warm' GCM simulation. In WG-driven runs, this date was within 5 days of the baseline average of May 3rd, and we saw no trend

between 2020 and 2050 WG-driven simulations. The cumulative amount of snow water equivalent over the winter season (total for the watershed) decreased from 2020 to 2099 in all 4 GCM-driven scenarios, from an average cumulative total of approximately 125 m in 2020 to approximately 34 m in 2099. Snow water equivalent increased in WG-driven runs, from an average cumulative total of approximately 88 m in 2020 to 111 m in 2050.

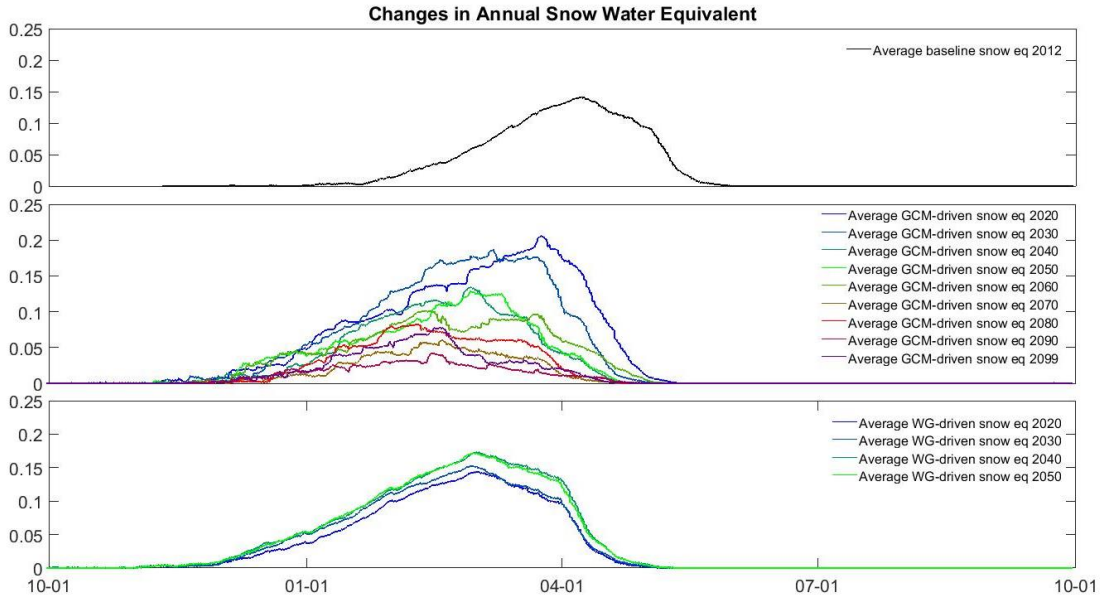

Figure 16. Snow water equivalent in climate change runs, where average of the GCM scenarios and average of WG realizations are shown in comparison to baseline results.

Precipitation trends, or lack thereof, were also apparent in simulated discharge. The WG-driven runs produced a trend in cumulative discharge that reflected the increase in annual precipitation for the modeled watershed (Figure 17). Cumulative discharge in WG-driven runs increases between 2020 and 2050 runs, while GCM-driven runs reflect no clear pattern over time. However, warming temperatures have a clear impact on spring melt processes reflected in discharge occurring particularly during the spring where snow melt contributes to high flows. For instance, the 'wet' GCM 2099 simulation resulted in

higher discharge throughout the winter period and a less significant increase in cumulative discharge during the typical melt period around April. Spring flows were highest in 2030, as well as high in 2020 GCM scenarios; this was due to rapid warming and resulting snow melt.

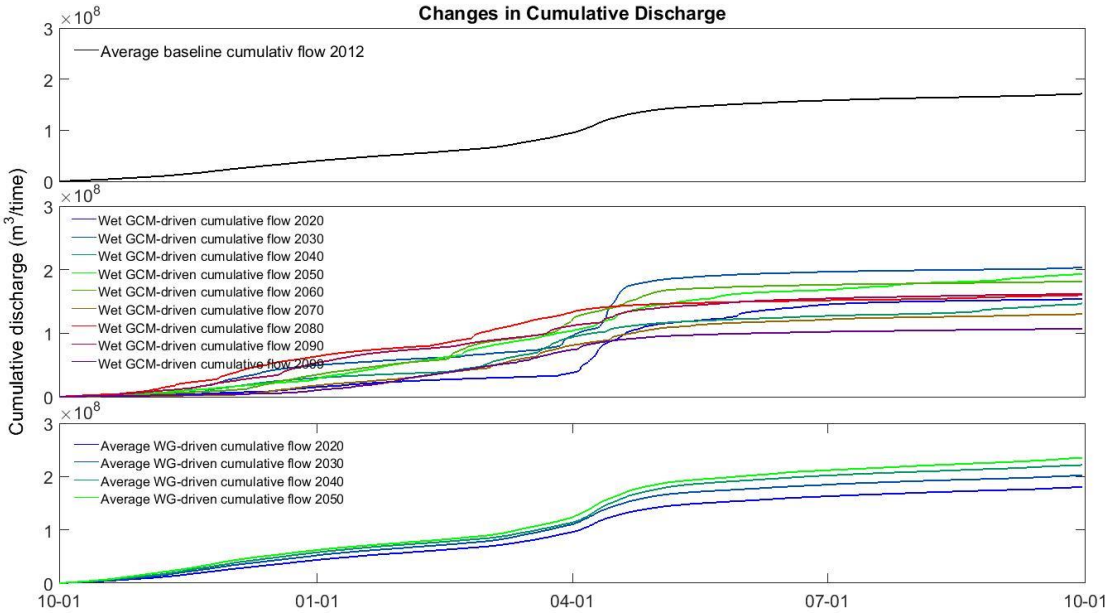

Figure 17. Cumulative discharge in climate change runs, where results of 'wet' GCM scenario and average of WG realizations are shown.

As expected, WG realizations produced higher peak flows and more extreme flows than all GCM scenarios. Average peak flows were higher in WG-driven runs and show an increasing trend between 2020 and 2050 (Figure 18).We saw no clear trend over time in GCM simulations. In Figure 18 we show average peak flows from across the GCM scenarios, WG realizations, as well as the average of baseline scenarios. Peak flows from GCM scenarios were generally similar or less than peak flows seen in baseline simulations. In GCM-driven simulations, peak flow was highest in 2060 and was also high in 2013; these peaks were the result of rapid snow melt in the spring and not a result

of an extreme precipitation event. In addition we also show the max and minimum peak flows in each year for the different sets of runs (error bars in Figure 18). WG-driven realizations resulted in more variability in peak flow events than GCM-driven scenarios. The maximum peak flows are also highest in WG-driven runs, although no trend was evident in these maximum values.

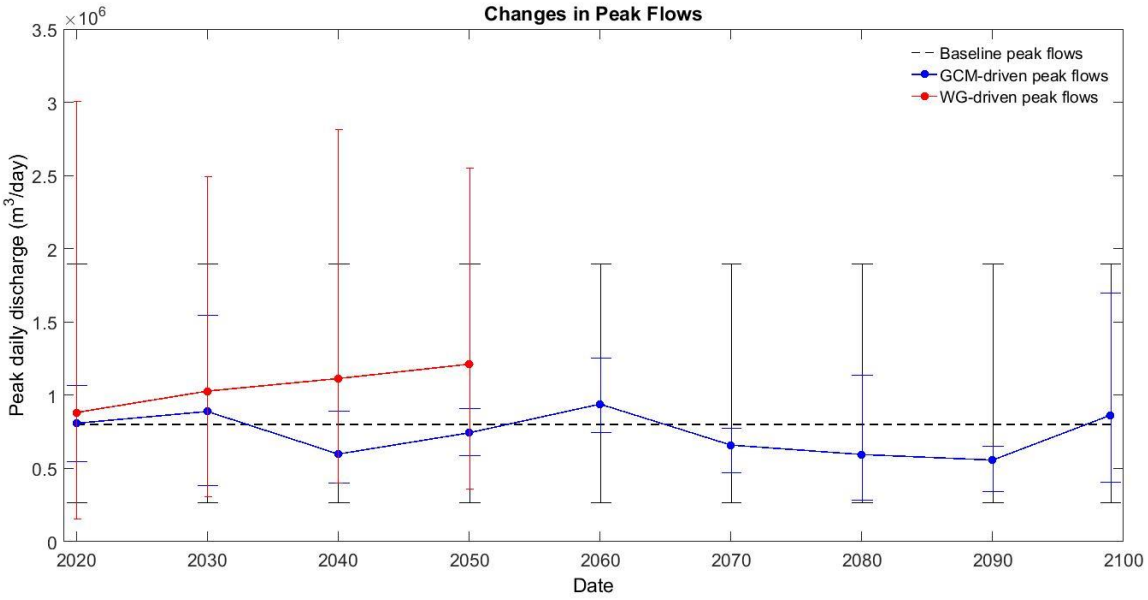

Figure 18. Peak flows in climate change simulations, including error bars indicating maximum and minimum peak flows for each year.

WG-driven runs showed a clear increase over time in flows exceeding the 95th percentile of baseline daily discharge (Figure 19), where GCM-driven runs again showed no obvious trend, and actually decreased between 2050 and 2090. The error bars shown in Figure 19 also indicate the maximum and minimum number of these 'extreme' events for each year simulated in the different sets of runs. Similarly to the case with peak flows, these indicate that WG-driven runs produce higher maximum flows caused by extreme events in some realizations. GCM scenarios lack representation of high flows caused by

extreme precipitation events. The error bars also indicate higher variability in extreme flows.

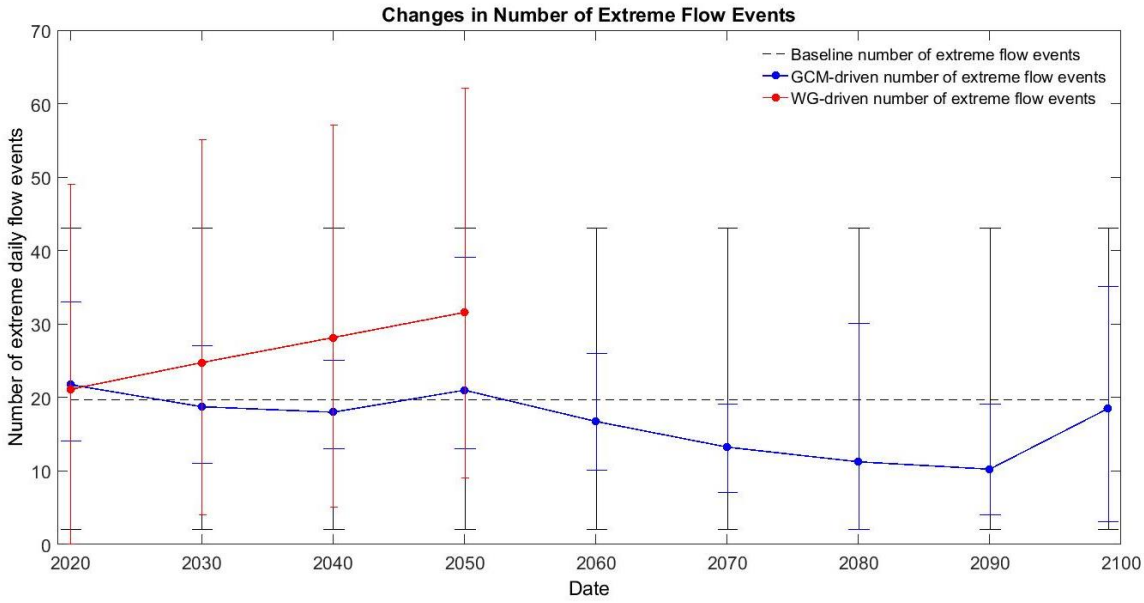

Figure 19. Number of 'extreme' flow events in climate change simulations, including error bars indicating maximum and minimum number of extreme events for each year.

4.3.3 Sediment Transport Trends

Sediment loading in the simulated watershed reflected overall trends in the driving meteorological data as well as modeled discharge. WG-driven runs produced average cumulative sediment loads that were higher than the average baseline cumulative load for all years, and GCM-driven runs produced average cumulative loads lower than the baseline average for most years. No clear trend was seen in GCM-driven runs between 2020 and 2099. As with flow results, cumulative sediment yield was highest in 2030, followed 2020. 2099 did produce the 3rd highest cumulative load of the years modeled. A large increase in cumulative sediment typically occurs in the spring, as a result of spring melt and the associated high flows. This increase was less defined or

occurred earlier in later years of GCM-driven runs, for example 2099 in the 'wet' GCM scenario (Figure 20). As with discharge, WG-driven runs showed increasing cumulative loads from 2020 through 2050. The model also produced steeper increases in cumulative loads during the summer and fall periods in 2020 and 2030 of the GCM-driven simulations, indicating more sediment mobilization following very high flows in the spring.

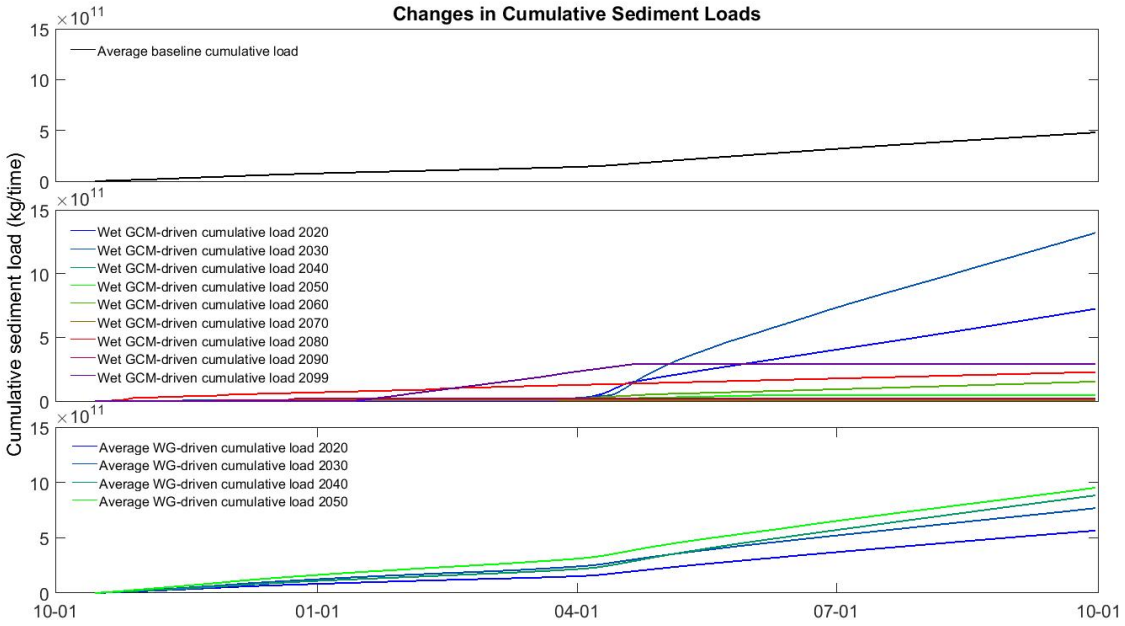

Figure 20. Cumulative sediment loading in climate change simulations, where the results of the 'wet' GCM scenario and the average of WG realizations are shown in comparison to baseline results.

Peak sediment loads were higher in WG-driven runs than in GCM-driven scenarios and baseline realizations. Figure 21 shows average daily peak sediment flux across the 4 GCM runs, as well as the peak sediment flux from across all WG and baseline realization. Similar to peak flow, the maximum and minimum peak loads are indicated by the error bars for each set of runs and each year (Figure 21). The average peak flux in the WG realizations shows an upward trend across the years simulated.

Maximum peak fluxes from WG realizations are also significantly higher than those maximums produced by GCM-driven runs, as is overall variability in peak yields (Figure 21). Alternatively, peak sediment yields generated by the GCM scenarios are generally lower than baseline average peak sediment loads. These also show no increasing or decreasing trend over time.

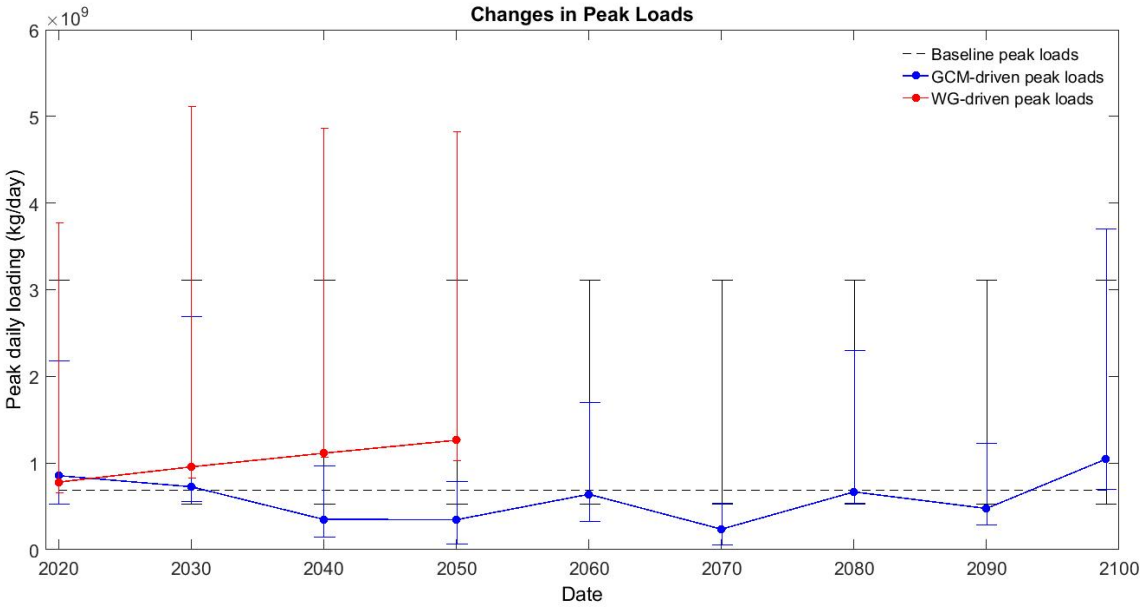

Figure 21. Peak sediment loads in climate change simulations, including error bars indicating maximum and minimum peak daily loads for each year.

The number of 'extreme' sediment yielding events follows a similar trend as 'extreme' flow events. An increasing trend in number of 'extreme' events is evident in WG-driven runs but not in GCM-driven runs. Sediment yields generated by WG realizations also reflect significant variability in comparison to yields generated by GCM scenarios. WG-driven runs also again show the ability to produce conditions leading to years with high numbers of 'extreme' daily sediment loads. WG-driven runs again also show higher variability in the number of days resulting in 'extreme' sediment loads.

Generally GCM-driven runs again produced relatively low numbers of ‘extreme’ daily sediment yields in comparison to baseline and WG-driven runs. There was also significantly lower variability in the GCM-driven sediment yields. The highest number of days with ‘extreme’ sediment yield occurred in 2030 in GCM-driven scenarios, as a result of very high spring flow.

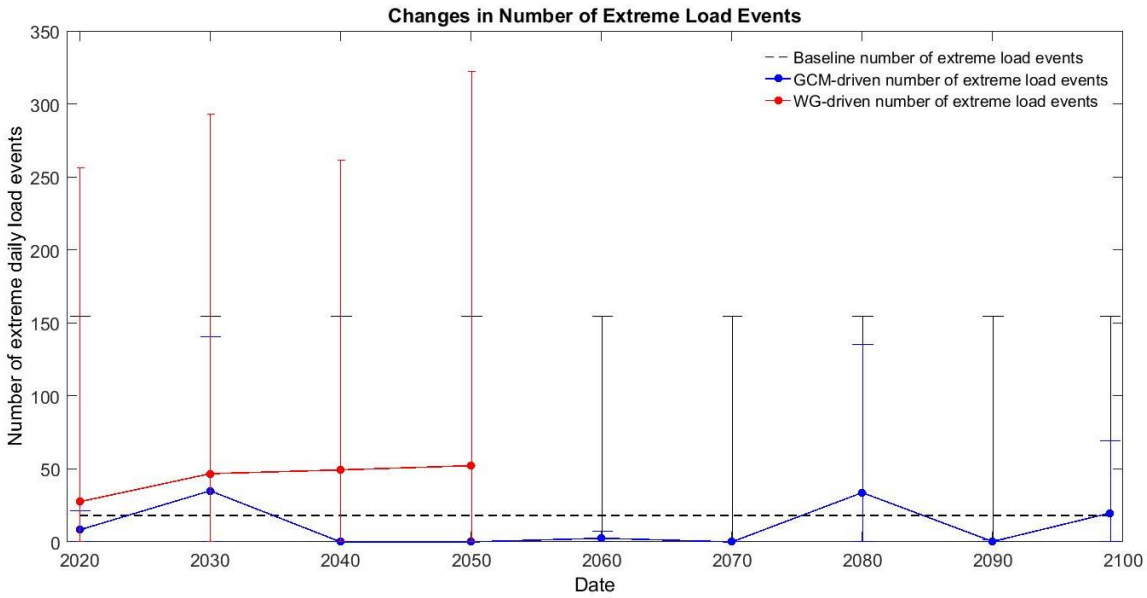

Figure 22. Number of extreme daily sediment loads in climate change simulations, including error bars indicating maximum and minimum extreme loads for each year.

4.4 DISCUSSION

Although the potential impacts of climate change on discharge and sediment mobilization in a watershed are highly variable, it is evident that local trends in precipitation and temperature will have important effects. This study shows the simulated watershed response to increasing precipitation as well as to increasing temperatures. Increasing precipitation in the WG-driven runs caused increases in discharge and sediment loading in simulations using these realizations as driving data. This occurred as

higher snow totals during the winter, higher flows in the spring, and an increase in more extreme precipitation and resulting flow events that caused higher erosion throughout the simulation period. No overall increase in discharge occurred because of increasing temperatures in the GCM-driven runs, although changes in the timing and magnitude of spring melt did occur. The model predicted lower cumulative sediment loading in future years when driven by GCM scenarios, due both to lower flows in spring and fewer extreme precipitation and flow events throughout the summer months.

One limitation to this study was the inability to represent the combined influence of local trends in both temperature and precipitation simultaneously. GCM's, even when regionally downscaled, do not adequately reflect local precipitation trends that are apparent in existing data for our region (Guilbert et al., 2015; Mohammed et al., 2015). Stochastic WG's are typically targeted to generate precipitation realizations, where other variables may be calculated based on their relationships with each other and the occurrence of wet and dry days (Fowler et al., 2007). Neither of these techniques is targeted at developing climate projection data that incorporate trends in both temperature and precipitation at a temporal and spatial scale suitable for driving hydrological models for impact assessment, particularly in small and meso-scale mountainous watersheds. Researchers have developed WGs with varying success at representing regional or local trends and variability (Forsythe et al., 2014; Kilsby et al., 2007; Semenov & Barrow, 1997). We expect that using driving data with representation of both increasing temperatures and precipitation would show more variability in the relative contribution of sediment sources. Increasing temperatures and longer storm durations contributing to wetter antecedent conditions might produce more erosion of land surfaces, where extreme

precipitation events are likely to particularly increase sediment mobilization from erosion of roads and streambanks. Continued efforts in developing WGs should focus on developing an approach that can be tailored to specific regions and represent observed trends as well as variability in multiple climate variables. Additionally, approaches targeted at regional dynamic models should be specifically adapted for simulation of smaller scale weather processes.

This study highlights the need for higher resolution meteorological data that reflects local trends in climate, a regionally-variable deficiency in GCMs. The results presented here clearly show that both temperature and precipitation have a significant influence on discharge and sediment mobilization in a watershed. However, we expect that the combined influence of increasing temperature and increasing precipitation (particularly longer duration and higher intensity precipitation) would produce even higher estimates of sediment loading. For instance, more mid-winter thaws combined with higher precipitation events could results in high flows and periods of erosion during the winter that are currently not represented. Earlier spring snow melt could also result in earlier erosion and incision of banks, making areas more susceptible to spring precipitation events. Representing the trend of increasing storm duration, and the tendency towards longer wet and dry periods, would also affect discharge and loading estimates. Both higher temperatures and longer storm durations would contribute to wetter conditions in the watershed, producing antecedent conditions where soils are more saturated and the watershed is more vulnerable to any precipitation event, even if not extreme in nature. Contrasting model results from the WG versus GCM-driven model runs show that failure to capture changes in extreme precipitation in future climate

scenarios translates to underestimation of the influence of increasing snowpack, higher peak discharges, and greater sediment yields.

Variability in micrometeorological variables not included in our downscaled climate inputs (windspeed, humidity, incoming shortwave and longwave radiation) can be expected to influence a set of ecosystem processes (such as carbon and energy cycling, root uptake by plants, soil moisture, and others) that will impact water and sediment fluxes from watersheds. More comprehensive climate change simulations of these complex ecosystem interactions will require new methods to downscale these micrometeorological variables to subdaily timesteps. High resolution, distributed watershed modeling can help tease apart the specific processes that might be altered as a result of climate change. In this work we focused specifically on the effects of temperature and precipitation, while the effects of these other meteorological variables were not explored in this work. Similarly, processes other than erosion may also be contributing to sediment output in the model, such as soil thawing and the effects of vegetation; these are not considered here.

This work adds to the body of research that shows the influences of climate change on watershed processes that determine discharge and sediment loading, both of which are critical watershed management issues. There is significant value in high resolution modeling of these processes so as to help understand potential changes that critically affect water quality of streams and rivers as well as receiving water bodies. However, such modeling requires high resolution meteorological data that represent expected changes in local climate, particularly in both temperature and precipitation. This work uses a new approach to simulating distributed bank erosion and failure within a

watershed model to explicitly investigate the impacts of climate change on sediment fluxes. We conclude that local increases in temperature and precipitation are likely to increase sediment loading in the modeled watershed, as a result of changes in snow melt process, an overall increase in wetter conditions, as well as in response to more extreme precipitation and flow events. The interaction of these influences is likely to create the most significant instances of bank erosion and sediment loading that would impact ecological systems, infrastructure, water quality, and other aspects of watershed health and sustainability.

CHAPTER 5: CONCLUSIONS

The results of the research presented in this dissertation add to the body of evidence indicating that streambank erosion and failure can mobilize significant amounts of sediment and demonstrate that considering these processes is critical for inclusive representation of suspended sediment loading in a watershed. Knowledge of the relative contributions of sediment from watershed sources would be helpful in allocating resources aimed at reducing non-point sediment and nutrient loading. For example, although some research has shown that erosion of unpaved roads can mobilize relatively large amounts of sediment in specific areas (such as in upland subbasins), this work indicates that on a watershed scale, the contribution of road erosion is less than that of streambank erosion towards total suspended sediment loading at the outlet of the watershed. This approach could help more appropriately target funding and implementation of practices targeted at reducing watershed suspended sediment.

This physics-based, distributed model with representation of streambank erosion and failure is also suitable for other types of investigations that may be of value in watershed management. This model could be re-applied for identifying areas within a watershed prone to erosion or bank failure, further targeting restoration and/or mitigation practices. It could also be used to assess the impacts of land use changes on surface, road, and streambank erosion, as well as on the relative contributions of each source. Such an application may help inform land use management and zoning decisions. The model could also be run at higher temporal and/or spatial scales based on the questions the user intends to answer. For example, watershed response to specific storm events could be investigated by using site specific, high resolution meteorological data.

The examination of the climate change impacts conducted as part of this work is also consistent with other studies in that it shows important changes in discharge and suspended sediment from a watershed. Local increases in temperature can be expected to alter snow melt processes and flow regimes. Local increases in precipitation and extreme events can be expected to generate larger amounts and concentrations of suspended sediment. However, this work also illustrated a deficiency in our ability to represent the impacts of climate change at this scale. There is a lack of meteorological data representing expected changes in both temperature and precipitation, and in particular changes in the occurrence and magnitude of extreme events. As other studies have also shown, the inability of GCMs to represent extreme events is clear in this work. GCMs should not be used to drive models for assessing the impacts of extreme events, which are a critical element of climate change.

Part of the motivation of this work was the increased frequency and magnitude of algal blooms seen in Lake Champlain, and the interdisciplinary approach to building resiliency and adaptive capability. Although this study focuses on sediment transport, previous research has established that a significant portion of phosphorus reaching the lake is transported as sediment-bound phosphorus. Therefore, the implications of this work are also relevant in our understanding of how phosphorus reaches receiving waters from watershed sources. This research is in agreement with other studies that indicate climate change will alter hydrological processes such that conditions favoring eutrophication will increase. Again this has implications for watershed management including reduction of phosphorus inputs and maintenance of a healthy Lake Champlain.

This research provides insight into the relative contributions of suspended sediment from a watershed, and how they might be affected by climate change. Although other researchers have made the link between sediment and phosphorus transport, more work is needed to mechanistically simulate phosphorus and other nutrient transport as a function of watershed processes. The ability of the coupled model approach presented here to be used for investigating nutrient transport from watershed sources could be improved by fully coupling chemical transport equations. Representation of nutrients in the watershed might include adsorbed nutrients on sediment and field soil, as well as soluble nutrients in runoff and soil. Representation of field soil nutrient conditions would be particularly important for determining how to target reduction practices. For example, despite the findings of this work that streambank sediment was the major component of sediment seen at the outlet of the watershed, sediment from overland erosion of agricultural areas may contain considerably higher phosphorus levels. Overall contributions of phosphorus from agricultural soils may be similar or higher than streambank soils even with larger contributions of streambank sediments, particularly in watersheds with higher agricultural land use.

Future work might also refine or improve upon the coupled model approach presented here. In the current implementation of the coupled DHSVM-BSTEM model, only planar and cantilever failures were included. Although in Vermont tension cracks and other types of failures are not often observed, these may be important mechanisms for other watersheds and regions where the model could be applied. This approach also includes a detailed representation of the bank profile in all locations (23 2-dimensional nodes are generated from inputs to describe bank geometry), which allows preferential

erosion of the bank toe. However, in some cases, particularly after prolonged erosion but without conditions that induce failure, the model can form bank profiles that would be physically unrealistic. Resetting of the bank to some stable profile under certain conditions might improve estimates of the volumes of sediment lost to erosion. In the current version, when a bank fails, it is reset to the original bank profile, which may also be more incised and prone to further erosion (based on initial parameterization of the stream bank classes), which may be resulting in an overestimation of streambank suspended sediment under particularly wet conditions. This may also be improved by resetting the bank to a more stable profile, as opposed to the initial profile.

The physics-based nature of this coupled modeling approach is particularly well suited for assessing the potential impacts of future shifts in climate and land use on water quality and land management issues. Increased variability in precipitation patterns will alter hydrologic flow regimes, which will impact land use decisions, both of which will impact the physical processes that mobilize sediment from a landscape. The ability to represent the interconnectedness of these processes will improve our understanding of how changes in these mechanisms will affect water quality in streams as well as receiving waters such as Lake Champlain. With an improved understanding of the contributions of suspended sediment from different sources in a watershed, monitoring and management efforts can more appropriately distribute resources and target practices that will have the most impact. Such an approach provides researchers with a platform for continued improvements in spatially explicit modeling of sediment mobilization and transport processes, as well as can provide information to policy makers and land owners to improve Vermont's resiliency to climate and land use change.

REFERENCES

Aksoy, H., & Kavvas, M. L. (2005). A review of hillslope and watershed scale erosion and sediment transport models. *CATENA*, *64*(2–3), 247–271. https://doi.org/10.1016/j.catena.2005.08.008

Asselman, N. E. M. (1999). Suspended sediment dynamics in a large drainage basin: the River Rhine. *Hydrological Processes*, *13*(10), 1437–1450. https://doi.org/10.1002/(SICI)1099-1085(199907)13:10<1437::AID-HYP821>3.0.CO;2-J

Bagnold, R. A. (1966). An approach of sediment transport model from general physics. *U.S. Geological Survey Professional Paper*, *422*(J).

Barg, L., & Blazewicz, M. (2003). *Assessment of Fluvial Geomorphology in Relation to Erosion and Landslides in the Mad River Watershed in Central Vermont* (Prepared for Vermont Geological Survey).

Bathurst, J. C. (2002). Physically-based erosion and sediment yield modelling: the SHETRAN concept. In *Modelling erosion, sediment transport and sediment yield* (p. 47).

Bathurst, J. C., Moretti, G., El-Hames, A., Moaven-Hashemi, A., & Burton, A. (2005). Scenario modelling of basin-scale, shallow landslide sediment yield, Valsassina, Italian Southern Alps. *Natural Hazards and Earth System Science*, *5*(2), 189–202.

Beckage, B., Osborne, B., Gavin, D. G., Pucko, C., Siccama, T., & Perkins, T. (2008). A rapid upward shift of a forest ecotone during 40 years of warming in the Green Mountains of Vermont. *Proceedings of the National Academy of Sciences*, *105*(11), 4197–4202. https://doi.org/10.1073/pnas.0708921105

Beeler, K. B. (2014). *Sediment and phosphorus inputs from perennial streams to Lake Whatcom, northwestern Washington State* (M.S.). Western Washington University, Bellingham, WA.

Berry, W., Rubenstein, N., & Melzian, B. (2003). *The biological effects of suspended and bedded sediment (SABS) in aquatic systems: a review* (United States Environmental Protection Agency Internal Report No. 102).

Betts, A. (2011). *Climate change in Vermont* (Climate Change Adaptation White Paper Series). Climate Change Team, Vermont Agency of Natural Resources. Retrieved from http://www.anr.state.vt.us/anr/climatechange/Pubs/VTCCAdaptClimateChangeVTBetts.pdf

Bilotta, G. S., & Brazier, R. E. (2008). Understanding the influence of suspended solids on water quality and aquatic biota. *Water Research*, *42*(12), 2849–2861. https://doi.org/10.1016/j.watres.2008.03.018

Birkinshaw, S. J., & Bathurst, J. C. (2006). Model study of the relationship between sediment yield and river basin area. *Earth Surface Processes and Landforms*, *31*(6), 750–761. https://doi.org/10.1002/esp.1291

Bowling, L. C., & Lettenmaier, D. P. (2001). The Effects of Forest Roads and Harvest on Catchment Hydrology in a Mountainous Maritime Environment. In M. S. Wigmosta & S. J. Burges (Eds.), *Land Use and Watersheds: Human Influence on Hydrology and Geomorphology in Urban and Forest Areas* (pp. 145–164). American Geophysical Union. Retrieved from http://onlinelibrary.wiley.com/doi/10.1029/WS002p0145/summary

Bowling, L. C., Storck, P., & Lettenmaier, D. P. (2000). Hydrologic effects of logging in western Washington, United States. *Water Resources Research*, *36*(11), 3223–3240. https://doi.org/10.1029/2000WR900138

Boyer, G. L., Watzin, M. C., Shambaugh, A. D., Satchwell, M. F., Rosen, B. H., & Mihuc, T. (2004). The Occurrence of Cyanobacterial Toxins in Lake Champlain. In T. O. Manley, P. L. Manley, & T. B. Mihuc (Eds.), *Lake Champlain: Partnerships and Research in the New Millennium* (pp. 241–257). Springer US. Retrieved from http://link.springer.com/chapter/10.1007/978-1-4757-4080-6_13

Brekke, L., Thrasher, B., Maurer, E. P., & Pruitt, T. (2013). *Downscaled CMIP3 and CMIP5 climate projections: Release of downscaled CMIP5 climate projections, comparison with preceding information, and summary of user needs* (USBR Tech. Memo) (p. 104). Retrieved from http://gdo-dcp.ucllnl.org/downscaled_cmip_projections/techmemo/downscaled_climate.pdf

Carpenter, S. R., Caraco, N. F., Correll, D. L., Howarth, R. W., Sharpley, A. N., & Smith, V. H. (1998). Nonpoint Pollution of Surface Waters with Phosphorus and Nitrogen. *Ecological Applications*, *8*, 559–568. https://doi.org/10.1890/1051-0761(1998)008(0559:NPOSWW)2.0.CO;2

Chen, J., Brissette, F. P., & Leconte, R. (2010). A daily stochastic weather generator for preserving low-frequency of climate variability. *Journal of Hydrology*, *388*(3–4), 480–490. https://doi.org/10.1016/j.jhydrol.2010.05.032

Chen, X., Alizad, K., Wang, D., & Hagen, S. C. (2014). Climate Change Impact on Runoff and Sediment Loads to the Apalachicola River at Seasonal and Event Scales. *Journal of Coastal Research*, 35–42. https://doi.org/10.2112/SI68-005.1

Clement, C. R. (2014). *Estimating sediment yield from the Swift Creek landslide, Whatcom County, Washington State* (M.S.). Western Washington University, Bellingham, WA. Retrieved from WWU Masters Thesis Collection, Paper 360.

Crosato, A. (2009). Physical explanations of variations in river meander migration rates from model comparison. *Earth Surface Processes and Landforms*, *34*(15), 2078–2086. https://doi.org/10.1002/esp.1898

Cuo, L., Giambelluca, T. W., & Ziegler, A. D. (2011). Lumped parameter sensitivity analysis of a distributed hydrological model within tropical and temperate catchments. *Hydrological Processes*, *25*(15), 2405–2421. https://doi.org/10.1002/hyp.8017

Cuo, L., Lettenmaier, D. P., Alberti, M., & Richey, J. E. (2009). Effects of a century of land cover and climate change on the hydrology of the Puget Sound basin. *Hydrological Processes*, *23*(6), 907–933. https://doi.org/10.1002/hyp.7228

Cuo, L., Lettenmaier, D. P., Mattheussen, B. V., Storck, P., & Wiley, M. (2008). Hydrologic prediction for urban watersheds with the Distributed Hydrology–Soil–Vegetation Model. *Hydrological Processes*, *22*(21), 4205–4213. https://doi.org/10.1002/hyp.7023

DeWolfe, M., Hession, W., & Watzin, M. (2004). Sediment and phosphorus loads from streambank erosion in Vermont, USA. *Critical Transitions in Water and Environmental Resources Management*, *436*, 1–10.

Doten, C. O., Bowling, L. C., Lanini, J. S., Maurer, E. P., & Lettenmaier, D. P. (2006). A spatially distributed model for the dynamic prediction of sediment erosion and transport in mountainous forested watersheds. *Water Resources Research*, *42*(4), n/a–n/a. https://doi.org/10.1029/2004WR003829

Du, E., Link, T. E., Gravelle, J. A., & Hubbart, J. A. (2014). Validation and sensitivity test of the distributed hydrology soil-vegetation model (DHSVM) in a forested mountain watershed. *Hydrological Processes*, *28*(26), 6196–6210. https://doi.org/10.1002/hyp.10110

Duan, J. G., Wang, S. S. Y., & Jia, Y. (2001). The applications of the enhanced CCHE2D model to study the alluvial channel migration processes. *Journal of Hydraulic Research*, *39*(5), 469–480. https://doi.org/10.1080/00221686.2001.9628272

Dunn, R. K., Springston, G. E., & Donahue, N. (2007a). Surficial Geologic Map of the Mad River Watershed, Vermont (Northern Sheet). Vermont Geological Survey.

Dunn, R. K., Springston, G. E., & Donahue, N. (2007b). Surficial Geology Map of the Mad River Watershed, Vermont (Southern Sheet). Vermont Geological Survey.

El-Khoury, A., Seidou, O., Lapen, D. R., Que, Z., Mohammadian, M., Sunohara, M., & Bahram, D. (2015). Combined impacts of future climate and land use changes on discharge, nitrogen and phosphorus loads for a Canadian river basin. *Journal of Environmental Management*, *151*, 76–86. https://doi.org/10.1016/j.jenvman.2014.12.012

European Environment Agency. (1995). *European Rivers and Lakes - Assessment of their Environmental State* (EEA Environmental Monographs No. 1) (p. 122). European Environment Agency. Retrieved from http://www.eea.europa.eu/publications/87-90198-01-8

Evans, D. J., Gibson, C. E., & Rossell, R. S. (2006). Sediment loads and sources in heavily modified Irish catchments: A move towards informed management strategies. *Geomorphology*, *79*(1–2), 93–113. https://doi.org/10.1016/j.geomorph.2005.09.018

Ewen, J., Parkin, G., & O'Connell, P. E. (2000). SHETRAN: Distributed River Basin Flow and Transport Modeling System. *Journal of Hydrologic Engineering*, *5*(3), 250–258. https://doi.org/10.1061/(ASCE)1084-0699(2000)5:3(250)

Field Geology Services. (2007). *Fluvial Geomorphology Assessment of the Mad River Watershed, Vermont* (Mad River Geomorphic Assessment). Vermont Agency of Natural Resources (VT ANR).

Forsythe, N., Fowler, H. J., Blenkinsop, S., Burton, A., Kilsby, C. G., Archer, D. R., … Hashmi, M. Z. (2014). Application of a stochastic weather generator to assess climate change impacts in a semi-arid climate: The Upper Indus Basin. *Journal of Hydrology*, *517*, 1019–1034. https://doi.org/10.1016/j.jhydrol.2014.06.031

Foster, D. R., & Aber, J. D. (Eds.). (2004). *Forests in Time: The Environmental Consequences of 1000 Years of Change in New England*. New Haven, CT: Yale University Press.

Fowler, H. J., Blenkinsop, S., & Tebaldi, C. (2007). Linking climate change modelling to impacts studies: recent advances in downscaling techniques for hydrological modelling. *International Journal of Climatology*, *27*(12), 1547–1578. https://doi.org/10.1002/joc.1556

Fowler, H. J., Ekström, M., Kilsby, C. G., & Jones, P. D. (2005). New estimates of future changes in extreme rainfall across the UK using regional climate model integrations. 1. Assessment of control climate. *Journal of Hydrology*, *300*(1–4), 212–233. https://doi.org/10.1016/j.jhydrol.2004.06.017

Frei, C., Schöll, R., Fukutome, S., Schmidli, J., & Vidale, P. L. (2006). Future change of precipitation extremes in Europe: Intercomparison of scenarios from regional climate models. *Journal of Geophysical Research: Atmospheres*, *111*(D6), D06105. https://doi.org/10.1029/2005JD005965

Frumhoff, P. C., Melillo, J. M., Moser, S. C., & Wuebbles, D. J. (2007). *Confronting climate change in the U.S. Northeast: Science, impacts, and solutions* (Synthesis report of the Northeast Climate Impacts Assessment (NECIA)). Cambridge, MA: Union of Concerned Scientists (UCS).

Gartner, J.E., Santi, P.M., & Cannon, S.H. (2015). Predicting locations of post-fire debris-flow erorion in the San Gabriel Mountains of southern California. *Natural Hazards,77*(2), 1305-1321.

Gleason, K. L., Lawrimore, J. H., Levinson, D. H., Karl, T. R., & Karoly, D. J. (2008). A Revised U.S. Climate Extremes Index. *Journal of Climate*, *21*(10), 2124–2137. https://doi.org/10.1175/2007JCLI1883.1

Gonzalez-Hidalgo, J. C., Batalla, R. J., Cerdà, A., & de Luis, M. (2010). Contribution of the largest events to suspended sediment transport across the USA. *Land Degradation & Development*, *21*(2), 83–91. https://doi.org/10.1002/ldr.897

Graf, W. (1971). *Hydraulics of Sediment Transport*. New York: McGraw-Hill.

Groisman, P. Y., Knight, R. W., Easterling, D. R., Karl, T. R., Hegerl, G. C., & Razuvaev, V. N. (2005). Trends in intense precipitation in the climate record. *Journal of Climate*, *18*(9), 1326–1350. https://doi.org/10.1175/JCLI3339.1

Guilbert, J., Beckage, B., Winter, J. M., Horton, R. M., Perkins, T., & Bomblies, A. (2014). Impacts of projected climate change over the Lake Champlain Basin in Vermont. *Journal of Applied Meteorology and Climatology*, *53*(8), 1861–1875. https://doi.org/10.1175/JAMC-D-13-0338.1

Guilbert, J., Betts, A. K., Rizzo, D. M., Beckage, B., & Bomblies, A. (2015). Characterization of increased persistence and intensity of precipitation in the northeastern United States. *Geophysical Research Letters*, *42*(6), 2015GL063124. https://doi.org/10.1002/2015GL063124

Hamshaw, S. (2014). *Suspended sediment prediction using artificial neural networks and local hydrometeorological data*. University of Vermont, Burlington VT.

Hanson, G. J., & Simon, A. (2001). Erodibility of cohesive streambeds in the loess area of the midwestern USA. *Hydrological Processes*, *15*(1), 23–38. https://doi.org/10.1002/hyp.149

Hayhoe, K., Wake, C., Anderson, B., Liang, X.-Z., Maurer, E., Zhu, J., … Wuebbles, D. (2008). Regional climate change projections for the Northeast USA. *Mitigation and Adaptation Strategies for Global Change*, *13*(5–6), 425–436.

Hayhoe, K., Wake, C. P., Huntington, T. G., Luo, L., Schwartz, M. D., Sheffield, J., … Wolfe, D. (2006). Past and future changes in climate and hydrological indicators in the US Northeast. *Climate Dynamics*, *28*(4), 381–407. https://doi.org/10.1007/s00382-006-0187-8

Hodgkins, G. A., & Dudley, R. W. (2006). Changes in late-winter snowpack depth, water equivalent, and density in Maine, 1926–2004. *Hydrological Processes*, *20*(4), 741–751. https://doi.org/10.1002/hyp.6111

Hodgkins, G. A., Dudley, R. W., & Huntington, T. G. (2003). Changes in the timing of high river flows in New England over the 20th Century. *Journal of Hydrology*, *278*(1–4), 244–252. https://doi.org/10.1016/S0022-1694(03)00155-0

Huang, D. (2012). *Quantifying stream bank erosion and deposition rates in a central U.S. urban watershed* (Thesis). University of Missouri--Columbia. Retrieved from https://mospace.umsystem.edu/xmlui/handle/10355/15264

Huntington, T. G., Hodgkins, G. A., Keim, B. D., & Dudley, R. W. (2004). Changes in the Proportion of Precipitation Occurring as Snow in New England (1949–2000). *Journal of Climate*, *17*(13), 2626–2636. https://doi.org/10.1175/1520-0442(2004)017<2626:CITPOP>2.0.CO;2

Ishee, E. R., Ross, D. S., Garvey, K. M., Bourgault, R. R., & Ford, C. R. (2015). Phosphorus characterization and contribution from eroding streambank soils of Vermont's Lake Champlain Basin. *Journal of Environment Quality*, *44*(6), 1745–1753. https://doi.org/10.2134/jeq2015.02.0108

Ivanov, V. Y., Bras, R. L., & Curtis, D. C. (2007). A weather generator for hydrological, ecological, and agricultural applications. *Water Resources Research*, *43*(10).

Kalma, D., & Ulmer, R. (2003). *Estimating desorbed phosphorus and sediment loading by streambank erosion, Boquet River (Essex County, NY).* (p. 76). Elizabethtown, NY: Boquet River Association.

Karl, T. R., & Knight, R. W. (1998). Secular trends of precipitation amount, frequency, and intensity in the United States. *Bulletin of the American Meteorological Society*, *79*(2), 231–241. https://doi.org/10.1175/1520-0477(1998)079<0231:STOPAF>2.0.CO;2

Karl, T. R., Melillo, J. M., & Peterson, T. C. (2009). *Global Climate Change Impacts in the United States.* (U.S. National Climate Assessment). Cambridge University Press, New York, NY, USA: United States Global Change Research Program.

Katz, R. W., & Brown, B. G. (1992). Extreme events in a changing climate: Variability is more important than averages. *Climatic Change*, *21*(3), 289–302. https://doi.org/10.1007/BF00139728

Kaushal, S. S., Pace, M. L., Groffman, P. M., Band, L. E., Belt, K. T., Meyer, P. M., & Welty, C. (2010). Land Use and Climate Variability Amplify Contaminant Pulses. *Eos, Transactions American Geophysical Union*, *91*(25), 221–222. https://doi.org/10.1029/2010EO250001

Kilsby, C. G., Jones, P. D., Burton, A., Ford, A. C., Fowler, H. J., Harpham, C., … Wilby, R. L. (2007). A daily weather generator for use in climate change studies. *Environmental Modelling & Software*, *22*(12), 1705–1719. https://doi.org/10.1016/j.envsoft.2007.02.005

Kleinman, P., Sharpley, A., Buda, A., McDowell, R., & Allen, A. (2011). Soil controls of phosphorus in runoff: Management barriers and opportunities. *Canadian Journal of Soil Science*, *91*(3), 329–338.

Kline, M., & Cahoon, B. (2010). Protecting river corridors in Vermont. *Journal of the American Water Resources Association*, 1–10. https://doi.org/10.1111/j.1752-1688.2010.00417.x

Kronvang, B., Grant, R., & Laubel, A. L. (1997). Sediment and phosphorus export from a lowland catchment: Quantification of sources. *Water, Air, and Soil Pollution*, *99*(1–4), 465–476.

Kronvang, B., Laubel, A., & Grant, R. (1997). Suspended sediment and particulate phosphorus transport and delivery pathways in an arable catchment, Gelbaek Stream, Denmark. *Hydrological Processes*, *11*(6), 627–642. https://doi.org/10.1002/(SICI)1099-1085(199705)11:6<627::AID-HYP481>3.0.CO;2-E

Kunkel, K. E. (2003). North American trends in extreme precipitation. *Natural Hazards*, *29*(2), 291–305. https://doi.org/10.1023/A:1023694115864

Kunkel, K. E., Andsager, K., & Easterling, D. R. (1999). Long-term trends in extreme precipitation events over the conterminous United States and Canada. *Journal of Climate*, *12*(8), 2515–2527. https://doi.org/10.1175/1520-0442(1999)012<2515:LTTIEP>2.0.CO;2

Kunkel, K. E., Stevens, L. E., Stevens, S. E., Sun, L., Janssen, E., Wuebbles, D., … Dobson, J. G. (2013). *Regional Climate Trends and Scenarios for the U.S. National Climate Assessment: Part 1. Climate of the Northeast U.S.* (NOAA Technical Report NESDIS No. 142–1) (p. 87). Washington D.C.: National Oceanic and Atmospheric Administration, National Environmental Satellite, Data, and Information Service. Retrieved from file:///F:/Zotero/storage/KVBB874D/NOAA_NESDIS_Tech_Report_142-1-Climate_of_the_Northeast_U.S_1.html

Lake Champlain Basin Program. (2012). *State of the Lake and Ecosystem Indicators Report*. Lake Champlain Basin Program.

Lake Champlain Basin Program. (2013). *Flood Resilience in the Lake Champlain Basin and Upper Richelieu River*.

Lake Champlain Basin Program. (2015). *State of the Lake and Ecosystem Indicators Report*. Lake Champlain Basin Program.

Langendoen, E. J. (2000). *CONCEPTS - Conservational channel evolution and pollutant transport system: Stream corridor version 1.0* (No. Research Report No. 16). Oxford, MS: US Department of Agriculture, Agricultural Research Service, National Sedimentation Laboratory.

Langendoen, E. J. (2001). CONCEPTS - A process-based modeling tool to evaluate stream-corridor restoration designs. Presented at the Proceeding 2001 Wetland Engineering & River Restoration Conference, Reno, NV: D. F. Hayes, ed., ASCE, Reston, VA.

Langendoen, E. J., Simon, A., & Alonso, C. V. (2000). Modeling channel instabilities and mitigation strategies in eastern Nebraska. Presented at the Proceedings 2000 Joint Conference on Water Resources Engineering and Water Resources Planning & Management, Minneapolis, MN: R. H. Hotchkiss and M. Glade, eds., ASCE, Reston, VA.

Langendoen, E. J., Simon, A., Curini, A., & Alonso, C. V. (1999). Field validation of an improved process-based model for streambank stability analysis. In *Proceedings*. Seattle, WA: R. Walton and R. E. Nece, eds., ASCE, Reston, VA.

Langendoen, E. J., Simon, A., Klimetz, L., Bankhead, N., & Ursic, M. E. (2012). *Quantifying sediment loadings from streambank erosion in selected agricultural watersheds draining to Lake Champlain* (USDA National Sedimentation Laboratory Technical Report No. 79).

Lanini, J. S., Clark, E. A., & Lettenmaier, D. P. (2009). Effects of fire-precipitation timing and regime on post-fire sediment delivery in Pacific Northwest forests. *Geophysical Research Letters*, *36*(1), L01402. https://doi.org/10.1029/2008GL034588

Laubel, A., Svendsen, L. M., Kronvang, B., & Larsen, S. E. (1999). Bank erosion in a Danish lowland stream system. *Hydrobiologica*, *410*, 279–285.

Leung, L. R., Qian, Y., Bian, X., Washington, W. M., Han, J., & Roads, J. O. (2004). Mid-Century Ensemble Regional Climate Change Scenarios for the Western United States. *Climatic Change*, *62*(1–3), 75–113. https://doi.org/10.1023/B:CLIM.0000013692.50640.55

Leung, L. R., & Wigmosta, M. S. (1999). Potential Climate Change Impacts on Mountain Watersheds in the Pacific Northwest1. *JAWRA Journal of the American Water Resources Association*, *35*(6), 1463–1471. https://doi.org/10.1111/j.1752-1688.1999.tb04230.x

Lukey, B. T., Sheffield, J., Bathurst, J. C., Hiley, R. A., & Mathys, N. (2000). Test of the SHETRAN technology for modelling the impact of reforestation on badlands runoff and sediment yield at Draix, France. *Journal of Hydrology*, *235*(1–2), 44–62. https://doi.org/10.1016/S0022-1694(00)00260-2

Marshall, E., & Randhir, T. (2008). Effect of climate change on watershed system: a regional analysis. *Climatic Change*, *89*(3–4), 263–280. https://doi.org/10.1007/s10584-007-9389-2

McDowell, R. W., Biggs, B. J. F., Sharpley, A. N., & Nguyen, L. (2004). Connecting phosphorus loss from agricultural landscapes to surface water quality. *Chemistry & Ecology*, *20*(1), 1–40.

Merritt, W. S., Letcher, R. A., & Jakeman, A. J. (2003). A review of erosion and sediment transport models. *Environmental Modelling & Software*, *18*(8–9), 761–799. https://doi.org/10.1016/S1364-8152(03)00078-1

Midgley, T. L., Fox, G. A., & Heeren, D. M. (2012). Evaluation of the bank stability and toe erosion model (BSTEM) for predicting lateral retreat on composite streambanks. *Geomorphology*, *145–146*, 107–114. https://doi.org/10.1016/j.geomorph.2011.12.044

Mohammed, I. N., Bomblies, A., & Wemple, B. C. (2015). The use of CMIP5 data to simulate climate change impacts on flow regime within the Lake Champlain Basin. *Journal of Hydrology: Regional Studies*, *3*, 160–186. https://doi.org/10.1016/j.ejrh.2015.01.002

Morrissey, L. A., Rizzo, D. M., Ross, D. S., & Alves, C. (2011). *Quantifying sediment loading due to stream bank erosion in impaired and attainment watersheds in Chittenden County, VT using advanced GIS and remote sensing technologies* (No. Report as of FY2010 for 2009VT44B). USGS. Retrieved from http://water.usgs.gov/wrri/10grants/progress/2009VT44B.pdf

Moss, B. (2012). Cogs in the endless machine: Lakes, climate change and nutrient cycles: A review. *Science of The Total Environment*, *434*, 130–142. https://doi.org/10.1016/j.scitotenv.2011.07.069

Moss, R. H., Edmonds, J. A., Hibbard, K. A., Manning, M. R., Rose, S. K., van Vuuren, D. P., … Wilbanks, T. J. (2010). The next generation of scenarios for climate change research and assessment. *Nature*, *463*(7282), 747–756. https://doi.org/10.1038/nature08823

Nagata, N., Hosoda, T., & Muramoto, Y. (2000). Numerical Analysis of River Channel Processes with Bank Erosion. *Journal of Hydraulic Engineering*, *126*(4), 243–252. https://doi.org/10.1061/(ASCE)0733-9429(2000)126:4(243)

Nagle, G. N., Fahey, T. J., Ritchie, J. C., & Woodbury, P. B. (2007). Variations in sediment sources and yields in the Finger Lakes and Catskills regions of New York. *Hydrological Processes*, *21*(6), 828–838. https://doi.org/10.1002/hyp.6611

Nash, J. E., & Sutcliffe, J. V. (1970). River flow forecasting through conceptual models part I - A discussion of principles. *Journal of Hydrology*, *10*(3), 282–290.

National Weather Service. (2011). *Public Information Statement* (Spotter Reports). Burlington VT.

Nebel, B. J., & Wright, R. T. (1993). Impacts of Sediments on Streams and Rivers. In *Environmental Science: The Way the World Works* (pp. 281–283). Prentice Hall, Inc.

Ockenden, M. C., Deasy, C. E., Benskin, C. M. H., Beven, K. J., Burke, S., Collins, A. L., … Haygarth, P. M. (2016). Changing climate and nutrient transfers: Evidence from high temporal resolution concentration-flow dynamics in headwater catchments. *Science of The Total Environment*, *548–549*, 325–339. https://doi.org/10.1016/j.scitotenv.2015.12.086

Oeurng, C., Sauvage, S., & Sánchez-Pérez, J.-M. (2010). Dynamics of suspended sediment transport and yield in a large agricultural catchment, southwest France. *Earth Surface Processes and Landforms*, *35*(11), 1289–1301. https://doi.org/10.1002/esp.1971

Paerl, H. W., Hall, N. S., & Calandrino, E. S. (2011). Controlling harmful cyanobacterial blooms in a world experiencing anthropogenic and climatic-induced change. *Science of The Total Environment*, *409*(10), 1739–1745. https://doi.org/10.1016/j.scitotenv.2011.02.001

Pealer, S. (2012, January 4). Lessons from Irene: Building resiliency as we rebuild. Vermont Agency of Natural Resources. Retrieved from http://www.anr.state.vt.us/anr/climatechange/Pubs/Irene_Facts.pdf

Pollen, N., & Simon, A. (2005). Estimating the mechanical effects of riparian vegetation on stream bank stability using a fiber bundle model. *Water Resources Research*, *41*(7), W07025. https://doi.org/10.1029/2004WR003801

Prudhomme, C., Reynard, N., & Crooks, S. (2002). Downscaling of global climate models for flood frequency analysis: where are we now? *Hydrological Processes*, *16*(6), 1137–1150. https://doi.org/10.1002/hyp.1054

Ross, D. S., Morrissey, L. A., Alves, C., Gourley, S. H., Rizzo, D. M., & Villars, T. (2010). *Esitmating soil phosphorus concentrations along erodible stream corridors in Chittenden County, Vermont* (Progress Report No. 2009VT45B).

Safeeq, M., & Fares, A. (2012). Hydrologic response of a Hawaiian watershed to future climate change scenarios. *Hydrological Processes*, *26*(18), 2745–2764. https://doi.org/10.1002/hyp.8328

Schindler, D. W., Hecky, R. E., Findlay, D. L., Stainton, M. P., Parker, B. R., Paterson, M. J., … Kasian, S. E. M. (2008). Eutrophication of lakes cannot be controlled by reducing nitrogen input: Results of a 37-year whole-ecosystem experiment. *Proceedings of the National Academy of Sciences*, *105*(32), 11254–11258. https://doi.org/10.1073/pnas.0805108105

Schumm, S. A., Harvey, M. D., & Watson, C. C. (1984). *Incised Channels: Morphology, Dynamics, and Control*. Water Resources Publications.

Sekely, A. C., Mulla, D. J., & Bauer, D. W. (2002). Streambank slumping and its contribution to the phosphorus and suspended sediment loads of the blue earth river, minnesota. *Journal of Soil and Water Conservation*, *57*(5), 243–250.

Semenov, M. A., & Barrow, E. M. (1997). USE OF A STOCHASTIC WEATHER GENERATOR IN THE DEVELOPMENT OF CLIMATE CHANGE SCENARIOS. *Climatic Change*, *35*(4), 397–414. https://doi.org/10.1023/A:1005342632279

Semenov, M. A., Brooks, R. J., Barrow, E. M., & Richardson, C. W. (1998). Comparison of the WGEN and LARS-WG stochastic weather generators for diverse climates. *Climate Research*, *10*(2), 95–107. https://doi.org/10.3354/cr010095

Sharpley, A. N., Chapra, S. C., Wedepohl, R., Sims, J. T., Daniel, T. C., & Reddy, K. R. (1994). Managing agricultural phosphorus for protection of surface waters: Issues and options. *Journal of Environment Quality*, *23*(3), 437. https://doi.org/10.2134/jeq1994.00472425002300030006x

Sharpley, A. N., Hedley, M. J., Sibbesen, E., Hillbricht-Ilkowska, A., House, W. A., & Rryskowski, L. (1995). Phosphorus transfers from terrestrial to aquatic ecosystems. In *Phosphorus in the Global Environment* (pp. 171–199). SCOPE and the United National Environment Program.

Simon, A., Curini, A., Darby, S. E., & Langendoen, E. J. (2000). Bank and near-bank processes in an incised channel. *Geomorphology*, *35*(3–4), 193–217.

Simon, A., Langendoen, E. J., & Thomas, R. (2003). Incorporating Bank-Toe Erosion by Hydraulic Shear into a Bank-Stability Model: Missouri River, Eastern Montana. Retrieved from http://www.tucson.ars.ag.gov/icrw/Proceedings/Simon.pdf

Simon, A., Pollen-Bankhead, N., & Thomas, R. E. (2011). Development and Application of a Deterministic Bank Stability and Toe Erosion Model for Stream Restoration. In A. Simon, S. J. Bennett, & J. M. Castro (Eds.), *Stream Restoration in Dynamic Fluvial Systems* (pp. 453–474). American Geophysical Union. Retrieved from http://onlinelibrary.wiley.com/doi/10.1029/2010GM001006/summary

Simon, A., & Rinaldi, M. (2006). Disturbance, stream incision, and channel evolution: The roles of excess transport capacity and boundary materials in controlling channel response. *Geomorphology*, *79*(3–4), 361–383. https://doi.org/10.1016/j.geomorph.2006.06.037

Simon, A., Rinaldi, M., & Hadish, G. (1996). Channel evolution in the loess area of the midwestern United States. In *Proceedings* (Vol. 3, pp. 86–93). Las Vegas.

Singh, V. P., & Woolhiser, D. A. (2002). Mathematical Modeling of Watershed Hydrology. *Journal of Hydrologic Engineering*, *7*(4), 270–292. https://doi.org/10.1061/(ASCE)1084-0699(2002)7:4(270)

Smeltzer, E., Dunlap, F., & Simoneau, M. (2009). *Lake Champlain Phosphorus Concentrations and Loading Rates, 1990-2008* (Lake Champlain Basin Program Technical Report No. 57). Grand Isle, VT.

Smeltzer, E., Shambaugh, A. d., & Stangel, P. (2012). Environmental change in Lake Champlain revealed by long-term monitoring. *Journal of Great Lakes Research*, *38, Supplement 1*, 6–18. https://doi.org/10.1016/j.jglr.2012.01.002

Smith, V. H. (1998). Cultural Eutrophication of Inland, Estuarine, and Coastal Waters. In M. L. Pace & P. M. Groffman (Eds.), *Successes, Limitations, and Frontiers in Ecosystem Science* (pp. 7–49). Springer New York. Retrieved from http://link.springer.com/chapter/10.1007/978-1-4612-1724-4_2

Smith, V. H., Tilman, G. D., & Nekola, J. C. (1999). Eutrophication: impacts of excess nutrient inputs on freshwater, marine, and terrestrial ecosystems. *Environmental Pollution*, *100*(1–3), 179–196. https://doi.org/10.1016/S0269-7491(99)00091-3

Solomon, S., Qin, D., & Manning, M. (2007). *Climate Change 2007- The Physical Science Basis: Working Group I Contribution to the Fourth Assessment Report of the IPCC* (1st ed.). Intergovernmental Panel on Climate Change.

Søndergaard, M., Jensen, J. P., & Jeppesen, E. (2003). Role of sediment and internal loading of phosphorus in shallow lakes. *Hydrobiologia*, *506–509*(1–3), 135–145. https://doi.org/10.1023/B:HYDR.0000008611.12704.dd

Stager, J. C., & Thill, M. (2010). *Climate change in the Champlain Basin: What natural resource managers can expect and do*. The Nature Conservancy.

Stanners, D., Bourdeau, P., & Agency, E. E. (1995). Europe's environment: the Dobrís assessment. Retrieved August 19, 2016, from http://bases.bireme.br/cgi-bin/wxislind.exe/iah/online/?IsisScript=iah/iah.xis&src=google&base=REPIDISCA&lang=p&nextAction=lnk&exprSearch=56027&indexSearch=ID

Storck, P., Bowling, L., Wetherbee, P., & Lettenmaier, D. (1998). Application of a GIS-based distributed hydrology model for prediction of forest harvest effects on peak stream flow in the Pacific Northwest. *Hydrological Processes*, *12*(6), 889–904. https://doi.org/10.1002/(SICI)1099-1085(199805)12:6<889::AID-HYP661>3.0.CO;2-P

Surfleet, C. G., Skaugset, A. E., & McDonnell, J. J. (2010). Uncertainty assessment of forest road modeling with the Distributed Hydrology Soil Vegetation Model (DHSVM). *Canadian Journal of Forest Research*, *40*(7), 1397–1409. https://doi.org/10.1139/X10-079

US EPA. (2000). 1998 National Water Quality Inventory Report to Congress (Data and Tools). Retrieved December 18, 2015, from http://www.epa.gov/waterdata/1998-national-water-quality-inventory-report-congress

US EPA. (2002). 2000 National Water Quality Inventory. Retrieved January 22, 2014, from http://water.epa.gov/lawsregs/guidance/cwa/305b/2000report_index.cfm

US EPA. (2012). Channel Processes: Streambank Erosion. Retrieved July 6, 2015, from http://water.epa.gov/scitech/datait/tools/warsss/streamero.cfm

US EPA. (n.d.). Climate Change Indicators: Heavy Precipitation (Reports and Assessments). Retrieved December 2, 2016, from https://www.epa.gov/climate-indicators/climate-change-indicators-heavy-precipitation

Vörösmarty, C. J., McIntyre, P. B., Gessner, M. O., Dudgeon, D., Prusevich, A., Green, P., Davies, P. M. (2010). Global threats to human water security and river biodiversity. *Nature*, *467*(7315), 555–561. https://doi.org/10.1038/nature09440

VT DEC. (2007). *Data shows floodplains are key to stream stability and Lake Champlain*. Vermont Department of Environmental Conservation, River Management Section. Retrieved from www.vtwaterquality.org/rivers/docs/rv_FloodplainsKey.pdf

Waichler, S. R., Wemple, B. C., & Wigmosta, M. S. (2005). Simulation of water balance and forest treatment effects at the H.J. Andrews experimental forest. *Hydrological Processes*, *19*, 3177–3199.

Walter, R. C., & Merritts, D. J. (2008). Natural Streams and the Legacy of Water-Powered Mills. *Science*, *319*(5861), 299–304. https://doi.org/10.1126/science.1151716

Waters, T. F. (1995). *Sediment in streams - Sources, biological effects and control* (American Fisheries Society Monograph 7). Bethesda, MD: American Fisheries Society.

Watzin, M. C., Fuller, S., Bronson, L., Gorney, R., & Schuster, L. (2010). *Monitoring and Evaluation of Cyanobacteria in Lake Champlain* (Technical Report No. 61) (p. 24). Grand Isle, VT: Lake Champlain Basin Program and Vermont Agency of Natural Resources.

Webb, B. W., & Walling, D. E. (1982). The magnitude and frequency characteristics of fluvial transport in a devon drainage basin and some geomorphological implications. *CATENA*, *9*(1), 9–23. https://doi.org/10.1016/S0341-8162(82)80002-7

Wehner, M. F., Smith, R. L., Bala, G., & Duffy, P. (2010). The effect of horizontal resolution on simulation of very extreme US precipitation events in a global atmosphere model. *Climate Dynamics*, *34*(2–3), 241–247. https://doi.org/10.1007/s00382-009-0656-y

Wemple, B. (2013). *Assessing the Effects of Unpaved Roads on Lake Champlain Water Quality* (Technical Report No. No. 74). Retrieved from

http://www.lcbp.org/2013/08/assessing-the-effects-of-unpaved-roads-on-lake-champlain-water-quality-report-released/

Whalen, T. N. (1998). *Post-glacial fluvial terraces in the Winooski Drainage Basin, Vermont* (M.S. Thesis). University of Vermont, Burlington VT.

Whitaker, A., Alila, Y., Beckers, J., & Toews, D. (2002). Evaluating peak flow sensitivity to clear-cutting in different elevation bands of a snowmelt-dominated mountainous catchment. *Water Resources Research*, *38*(9), 1172. https://doi.org/10.1029/2001WR000514

Whitehead, P. G., Wilby, R. L., Battarbee, R. W., Kernan, M., & Wade, J. (2009). A review of the potential impacts of climate change on surface water quality. *Hydrological Sciences Journal*, *54*(1), 101–123. https://doi.org/10.623/hysj.54.1.101

Wicks, J. M., & Bathurst, J. C. (1996). SHESED: a physically based, distributed erosion and sediment yield component for the SHE hydrological modelling system. *Journal of Hydrology*, *175*(1–4), 213–238. https://doi.org/10.1016/S0022-1694(96)80012-6

Wigmosta, M. S., & Lettenmaier, D. P. (1999). A comparison of simplified methods for routing topographically driven subsurface flow. *Water Resources Research*, *35*(1), 255–264. https://doi.org/10.1029/1998WR900017

Wigmosta, M. S., & Leung, L. R. (2001). Potential impacts of climate change on streamflow and flooding in forested basins. In *The Influence of Environmental Change on Geomorphological Hazards in Forested Areas*. R.C. Sidle and M. Chigira, eds., Centre for Agriculture and Biosciences International.

Wigmosta, M. S., Nijssen, B., Storck, P., & Lettenmaier, D. P. (2002). The Distributed Hydrology Soil Vegetation Model. In *Mathematical Models of Small Watershed Hydrology and Applications* (pp. 7–42). CO: Water Resources Publications.

Wigmosta, M. S., & Perkins, W. A. (2001). Simulating the Effects of Forest Roads on Watershed Hydrology. In rk S. Wigmosta & S. J. Burges (Eds.), *Land Use and Watersheds: Human Influence on Hydrology and Geomorphology in Urban and Forest Areas* (pp. 127–143). American Geophysical Union. Retrieved from http://onlinelibrary.wiley.com/doi/10.1029/WS002p0127/summary

Wigmosta, M. S., Vail, L. W., & Lettenmaier, D. P. (1994). A distributed hydrology-vegetation model for complex terrain. *Water Resources Research*, *30*(6), 1665–1679. https://doi.org/10.1029/94WR00436

Wilber, D. H., & Clarke, D. G. (2001). Biological Effects of Suspended Sediments: A Review of Suspended Sediment Impacts on Fish and Shellfish with Relation to Dredging Activities in Estuaries. *North American Journal of Fisheries*

Management, *21*(4), 855–875. https://doi.org/10.1577/1548-8675(2001)021<0855:BEOSSA>2.0.CO;2

Wilks, D. S., & Wilby, R. L. (1999). The weather generation game: a review of stochastic weather models. *Progress in Physical Geography*, *23*(3), 329–357. https://doi.org/10.1177/030913339902300302

Williams, G. P. (1989). Sediment concentration versus water discharge during single hydrologic events in rivers. *Journal of Hydrology*, *111*(1), 89–106. https://doi.org/10.1016/0022-1694(89)90254-0

Winter, J. M., Beckage, B., Bucini, G., Horton, R. M., & Clemins, P. J. (2016). Development and evaluation of high-resolution climate simulations over the mountainous Northeastern United States. *Journal of Hydrometeorology*, *17*(3), 881–896. https://doi.org/10/1175/JHM-D-15-0052.1

Xiao, Y., Zhou, G., & Yang, S. (n.d.). 2D numerical modelling of meandering channel formation. *Journal of Earth System Science,* 1–17.

Xu, C. (1999a). Climate Change and Hydrologic Models: A Review of Existing Gaps and Recent Research Developments. *Water Resources Management*, *13*(5), 369–382. https://doi.org/10.1023/A:1008190900459

Xu, C. (1999b). From GCMs to river flow: a review of downscaling methods and hydrologic modelling approaches. *Progress in Physical Geography*, *23*(2), 229–249. https://doi.org/10.1177/030913339902300204

Yao, C., & Yang, Z. (2009). Parameters optimization on DHSVM model based on a genetic algorithm. *Frontiers of Earth Science in China*, *3*(3), 374–380. https://doi.org/10.1007/s11707-009-0040-6

APPENDIX I

This document contains figures that present further detail or additional analysis on data described in the main body of this paper. Data used to generate these figures is described in the main body, but comes from either General Circulation Model (GCM) scenarios, weather generator realizations, or is a result of simulation runs conducted using this data to drive the model. Figure A1 was generated to support the method chosen for completing input data for baseline 2012 scenarios. Figures A2-A7 support analysis of driving meteorological inputs for climate change analysis.

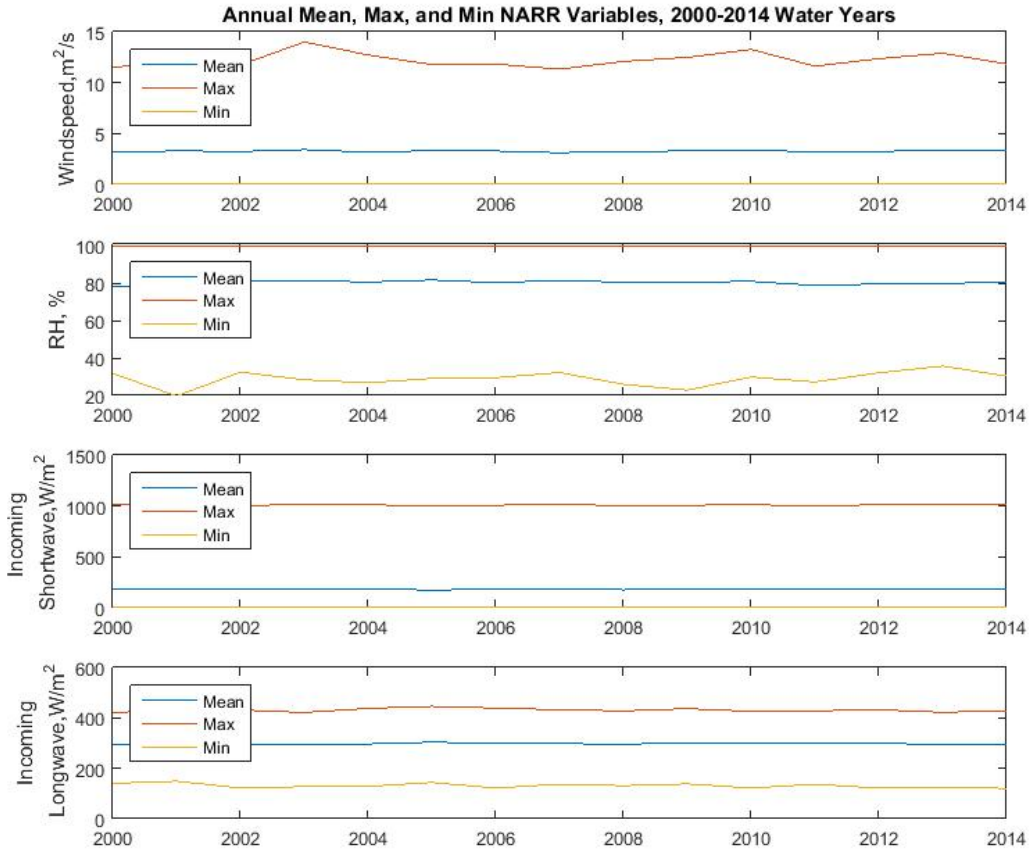

Figure A1. Long-term (15 year) comparison of NARR variables to support using 2012 data to complete meterological input files.

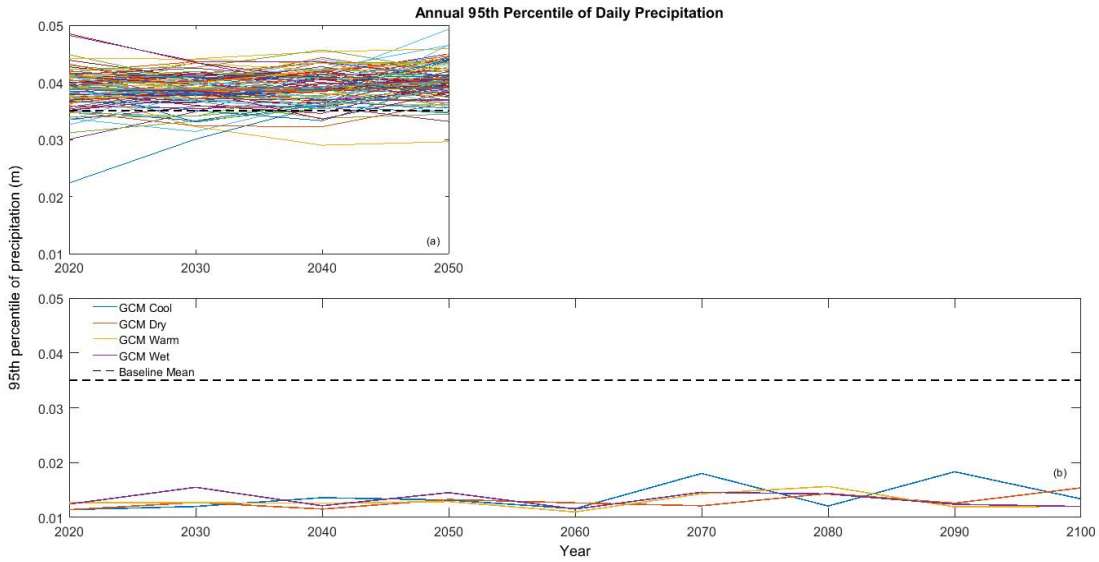

Figure A2. Annual 95th percentile of precipitation in climate change scenarios.

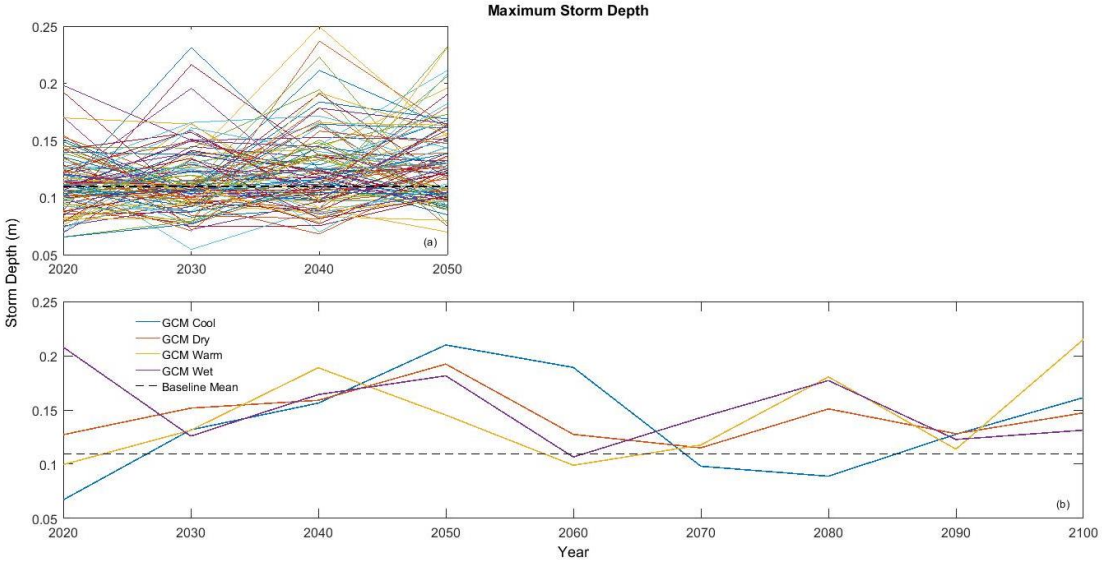

Figure A3. Maximum storm depth in climate change scenarios.

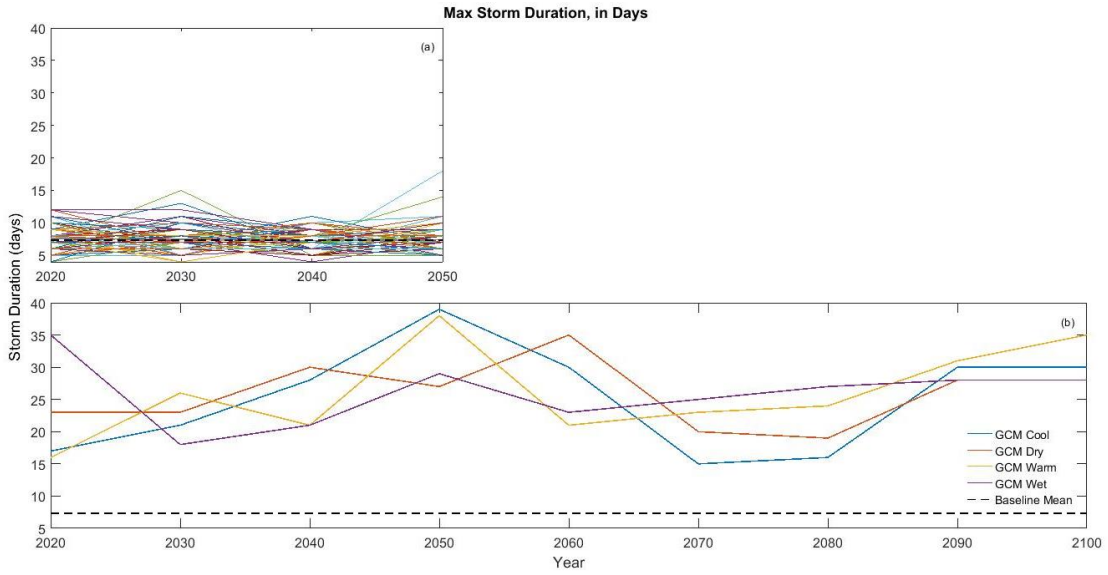

Figure A4. Maximum storm duration in climate change scenarios.

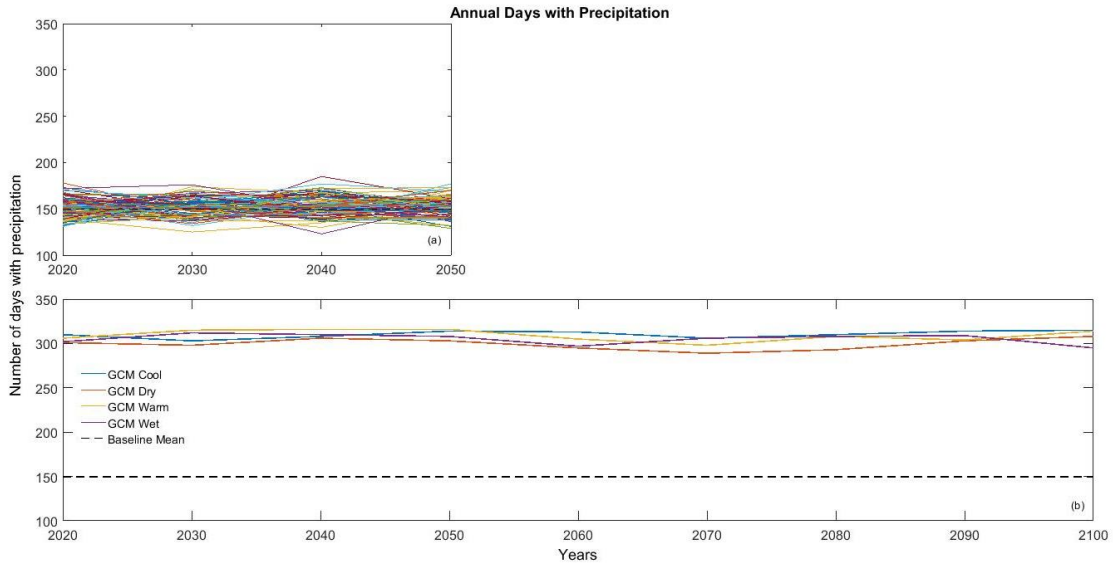

Figure A5. Annual days with precipitation in climate change scenarios.

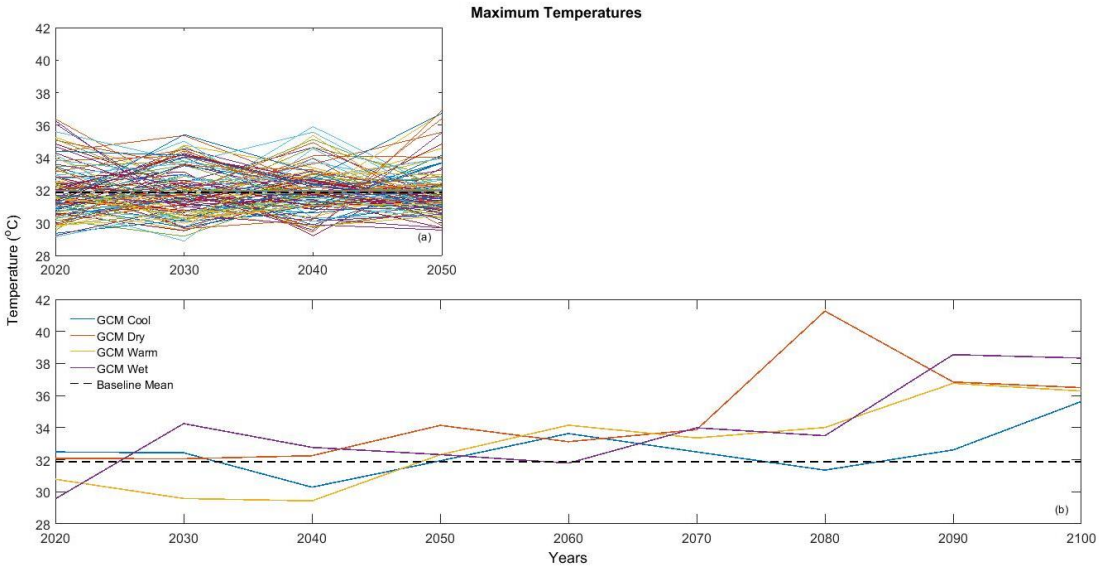

Figure A6. Maximum temperatures in climate change scenarios.

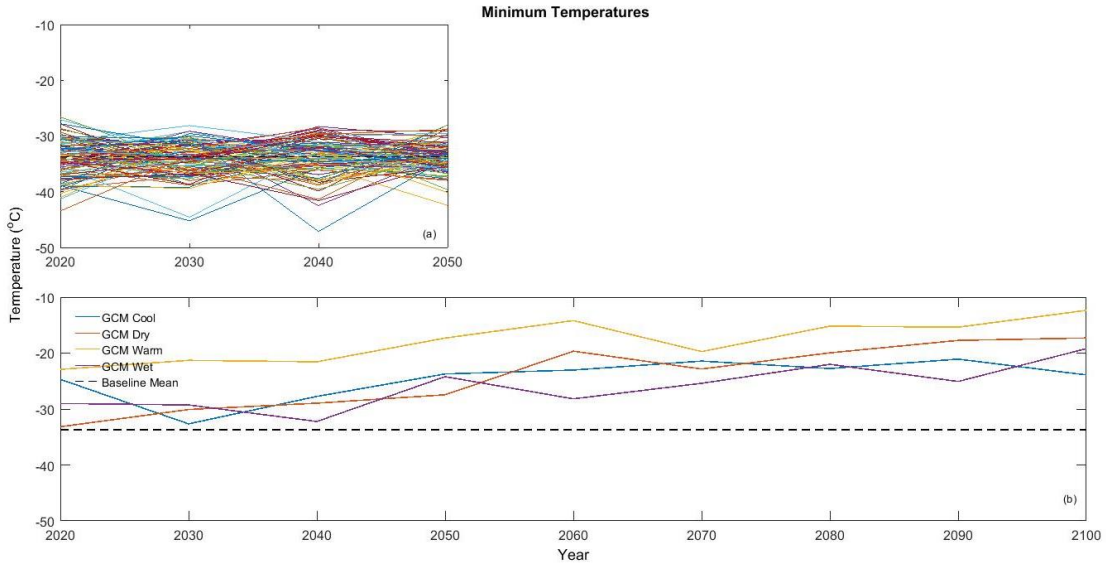

Figure A7. Minimum temperatures in climate change scenarios.

APPENDIX II

DHSVM-BSTEM Input Files

```
################################################################################
# DHSVM INPUT FILE FORMAT
################################################################################
# The file is organized in sections (...), which contain key = entry pairs.
# The file is free format, in that correct reading of the file is not dependent
# on spaces and/or the order of the key-entry pairs within a section.
# The keys are not case-sensitive, but the entries are, because filenames on a
# UNIX platform are case-sensitive.
# Comments are preceded by a '#', and run from the occurrence of '#' till the
# end of the line. You can comment out an entire line (like in this
# header), or you can place a comment after an entry.
# It is important to place the key-entry pair in the correct section, since it
# will not be found if it is in another section.
# The easiest way to make the input file is to fill out this default template.
# Since DHSVM will only use the keys that it requires you do not have to worry
# about empty entries for keys that are not needed. For example, if you are
# running the model in point mode, you do not have to fill out the routing
# section.  If you have already filled it out you can leave it, since DHSVM will
# not use the information.  This allows easy switching between point and basin
# mode.
# For more information about the specific entries see the DHSVM web page


################################################################################
# OPTIONS SECTION
################################################################################
(OPTIONS)                       # Model Options
Format            = BIN         # BIN, BYTESWAP or NETCDF
Extent            = BASIN       # POINT or BASIN
Gradient          = TOPOGRAPHY          # TOPOGRAPHY or WATERTABLE
Flow Routing      = NETWORK       # UNIT_HYDROGRAPH or NETWORK
Sensible Heat Flux  = FALSE       # TRUE or FALSE
Sediment          = TRUE                # TRUE or FALSE
Sediment Input File  = ../configfiles/INPUT_WGbaseline.MWME32.mad     # path for sediment
configuration file
Overland Routing    = KINEMATIC       # CONVENTIONAL or KINEMATIC
Infiltration                = STATIC                # Static or Dynamic
Interpolation     = NEAREST       # NEAREST or INVDIST or VARCRESS
MM5               = FALSE               # TRUE or FALSE
QPF               = FALSE         # TRUE or FALSE
PRISM             = FALSE         # TRUE or FALSE
PRISM data path     = ../PRISM/PRISM            # path for PRISM files
PRISM data extension = bin          # file extension for PRISM files
Canopy radiation attenuation mode = FIXED # FIXED or VARIABLE
Shading           = FALSE           # TRUE or FALSE
Shading data path   =
Shading data extension = hourly.bin     # file extension for shading files
Skyview data path   =
Snotel            = FALSE         # TRUE or FALSE
Outside           = TRUE            # TRUE or FALSE
Rhoverride        = FALSE         # TRUE or FALSE
```

```
Precipitation Source = STATION          # STATION or RADAR
Wind Source         = STATION           # STATION or MODEL
Temperature lapse rate   = CONSTANT      # CONSTANT or VARIABLE
Precipitation lapse rate = CONSTANT      # CONSTANT, MAP, or VARIABLE
Cressman radius      = 10               # in model pixels
Cressman stations    =  1               # number of stations

##############################################################################
# MODEL AREA SECTION
##############################################################################
(AREA)                          # Model area
Coordinate System    = USER_DEFINED             # UTM or USER_DEFINED
Extreme North        = 199735.160592       # Coordinate for northern edge of grid
Extreme West         = 464956.633708        # Coordinate for western edge of grid
Center Latitude      = 44.5           # Central parallel of basin
Center Longitude     = -72.5          # Central meridian of basin
Time Zone Meridian   = -75            # Time zone meridian for area
Number of Rows       = 299              # Number of rows
Number of Columns    = 188              # Number of columns
Grid spacing         = 100              # Grid resolution in m
Point North          =                 # North coordinate for point model if Extent = POINT
Point East           =                 # East coordinate for point modelif Extent = POINT

##############################################################################
# TIME SECTION
##############################################################################
(TIME)                          # Model period
Time Step           = 3               # Model time step (hours)
Model Start          = 09/01/2011-21      # Model start time (MM/DD/YYYY-HH)
Model End            = 09/30/2012-21      # Model end time (MM/DD/YYYY-HH)

##############################################################################
# CONSTANTS SECTION
##############################################################################
(CONSTANTS)                     # Model constants
Ground Roughness     = 0.02             # Roughness of soil surface (m)
Snow Roughness       = 0.01            # Roughness of snow surface (m)
Rain Threshold       = -2.0            # Minimum temperature at which rain occurs (C)
Snow Threshold       = 0.0             # Maximum temperature at which snow occurs (C)
Snow Water Capacity  = 0.04             # Snow liquid water holding capacity (fraction)
Reference Height     = 22.0            # Reference height (m)
Rain LAI Multiplier  = 0.0003           # LAI Multiplier for rain interception
Snow LAI Multiplier  = 0.005           # LAI Mulitplier for snow interception
Min Intercepted Snow = 0.005            # Intercepted snow that can only be melted (m)
Outside Basin Value  = 0               # Value in mask that indicates outside the basin
Temperature Lapse Rate   = -0.006       # Temperature lapse rate (C/m)
Precipitation Lapse Rate = 0.0006              # Precipitation lapse rate (m/m)
##############################################################################
# TERRAIN INFORMATION SECTION
##############################################################################
(TERRAIN)                       # Terrain information
DEM File            = ../input/more_dem100m.bin
Basin Mask File      = ../input/more_msk100.bin

##############################################################################
# ROUTING SECTION
```

```
##########################################################################
(ROUTING)                       # Routing information. This section is
                            # only relevant if the Extent = BASIN

################ STREAM NETWORK ##################################################
# The following three fields are only used if Flow Routing = NETWORK

Stream Map File      =  ../input/stream.map.dat
Stream Network File  =  ../input/stream.network.dat
Stream Class File    =  ../input/stream.class.E14.dat

################ ROAD NETWORK ####################################################
# The following three fields are only used if Flow Routing = NETWORK and there
# is a road network


Road Map File        =  ../input/road.map.dat              # path for road map file
Road Network File    =  ../input/road.network.dat              # path for road network file
Road Class File      =  ../input/road.class.redo42.dat         # path for road network file

################ UNIT HYDROGRAPH #################################################
# The following two fields are only used if Flow Routing = UNIT_HYDROGRAPH

Travel Time File     =                # path for travel time file
Unit Hydrograph File =                   # path for unit hydrograph file

##########################################################################
# METEOROLOGY SECTION
##########################################################################
(METEOROLOGY)                       # Meteorological stations
Number of Stations = 1              # Number of meteorological stations

Station Name 1 = WeatherGenerator_gridpoint
North Coordinate 1 = 173639.089
East Coordinate 1 = 475034.832
Elevation 1 = 765.51
Station File 1 = ../metfiles_baseline/MadMet_weathgen_f49_2012.txt

#Station Name 1 = Center_GCM_gridpoint
#North Coordinate 1 = 175536.156
#East Coordinate 1 = 470338.468
#Elevation 1 = 477.087
#Station File 1 = ../metfiles/MadMet_coolrcp8.5_wy2020.txt

Station Name 2 = Reanalysis_South
North Coordinate 2 = 184742.826
East Coordinate 2 = 473638.025
Elevation 2 = 244.78
Station File 2 = ../metfiles/MadMet_South_2010-14w.txt

Station Name 3 = 3way
North Coordinate 3 = 176603.51
East Coordinate 3 = 474353.99
Elevation 3 = 427.91
Station File 3 = ../metfiles/3wayMet_2010-13w.txt
```

```
Station Name 4 = BraggHill
North Coordinate 4 = 188194.75
East Coordinate 4 = 471916.27
Elevation 4 = 433.10
Station File 4 = ../metfiles/BraggHillMet_2010-13w.txt

Station Name 5 = Randell
North Coordinate 5 = 193150.57
East Coordinate 5 = 472857.93
Elevation 5 = 297.47
Station File 5 = ../metfiles/RandellMet_2010-13w.txt

Station Name 6 = SharpShooter
North Coordinate 6 = 194731.055
East Coordinate 6 = 471532.924
Elevation 6 = 424.98
Station File 6 = ../metfiles/SharpshooterMet_2010-13w.txt

Station Name 7 = SkiValley
North Coordinate 7 = 185695.444
East Coordinate 7 = 476877.115
Elevation 7 = 449.69
Station File 7 = ../metfiles/SkiValleyMet_2010-13w.txt
################ MM5 ##################################################################
# The following block only needs to be filled out if MM5 = TRUE.  In that case
# This is the ONLY block that needs to be filled out

MM5 Start            =              # Start of MM5 file (MM/DD/YYYY-HH),
MM5 Rows             =
MM5 Cols             =
MM5 Extreme North    =
MM5 Extreme West     =
MM5 DY               =

# MM5 met files
MM5 Temperature File  =
MM5 Humidity File     =
MM5 Wind Speed File   =
MM5 Shortwave File    =
MM5 Longwave File     =
MM5 Pressure File     =
MM5 Precipitation File =
MM5 Terrain File      =
MM5 Temp Lapse File   =

# For each soil layer make a key-entry pair as below (n = 1, ..,
# Number of Soil Layers)

MM5 Soil Temperature File 0 =
MM5 Soil Temperature File 1 =
MM5 Soil Temperature File 2 =

################ RADAR ################################################################
# The following block only needs to be filled out if Precipitation Source =
# RADAR.
Radar Start          =
```

```
Radar File            =
Radar Extreme North    =
Radar Extreme West     =
Radar Number of Rows   =
Radar Number of Columns =
Radar Grid Spacing     =

################ Wind ############################################################
# The following block only needs to be filled out if Wind Source = MODEL
Number of Wind Maps    =
Wind File Basename     =
Wind Map Met Stations  =

################ Precipitation lapse rate ########################################
# The following block only needs to be filled out if Precipitation lapse rate
# = MAP
Precipitation lapse rate =

##########################################################################################
# SOILS INFORMATION SECTION
##########################################################################################
(SOILS)                              # Soil information
Soil Map File               = ../input/more_soil100.bin
Soil Depth File    = ../input/more_sdep.bin

Number of Soil Types = 5

################################### SOIL 1, right now same as A#########################
#Soil Description       1 = HydroA
#Lateral Conductivity   1 = 1.458e-04
#Exponential Decrease   1 = 3.0
#Maximum Infiltration   1 = 1.1e-06
#Capillary Drive        1 = 0.2
#Surface Albedo         1 = 0.21
#Number of Soil Layers  1 = 3
#Porosity               1 = .48 .42 .38
#Pore Size Distribution 1 = .35 .35 .36
#Bubbling Pressure      1 = .059 .068 .075
#Field Capacity         1 = .36 .33 .37
#Wilting Point          1 = .06 .04 .045
#Bulk Density           1 = 1370. 1520. 1630.
#Vertical Conductivity  1 = 5.293e-05 5.99e-05 5.99e-05
#Thermal Conductivity   1 = 7.11 6.92 8.01
#Thermal Capacity       1 = 1.4e6 1.4e6 1.4e6
#Mannings n             1 = 0.02

Soil Description       1 = Water
Lateral Conductivity   1 = 5.0e-05
Exponential Decrease   1 = 3.0
Maximum Infiltration   1 = 5.0e-05
Capillary Drive        1 = 0.41
Surface Albedo         1 = 0.1
Number of Soil Layers  1 = 3
Porosity               1 = .4 .4 .4
Pore Size Distribution 1 = .08 .08 .08
Bubbling Pressure      1 = .37 .37 .37
```

Field Capacity 1 = .36 .36 .36
Wilting Point 1 = .27 .27 .27
Bulk Density 1 = 1400. 1400. 1400.
Vertical Conductivity 1 = 1.0e-05 1.0e-05 1.0e-05
Thermal Conductivity 1 = 7.11 6.92 8.01
Thermal Capacity 1 = 1.4e6 1.4e6 1.4e6
Mannings n 1 = 0.001

################################## SOIL 2 - LOAMY SAND
#####################################
Soil Description 2 = HydroA
Lateral Conductivity 2 = 6.458e-03
Exponential Decrease 2 = 3.15
Maximum Infiltration 2 = 6.02e-03
Capillary Drive 2 = 0.2
Surface Albedo 2 = 0.21
Number of Soil Layers 2 = 3
Porosity 2 = .4 .4 .4
Pore Size Distribution 2 = .69 .65 .65
Bubbling Pressure 2 = .073 .075 .077
Field Capacity 2 = .15 .15 .15
Wilting Point 2 = .04 .045 .045
Bulk Density 2 = 1450. 1500. 1550.
Vertical Conductivity 2 = 1.54e-04 1.0e-04 1.0e-04
Thermal Conductivity 2 = 7.11 6.92 8.01
Thermal Capacity 2 = 1.4e6 1.4e6 1.4e6
Mannings n 2 = 0.15

################################## SOIL 3-SILT LOAM/LOAM
#####################################
Soil Description 3 = HydroB
Lateral Conductivity 3 = 1.098e-03
Exponential Decrease 3 = 3.15
Maximum Infiltration 3 = 1.02e-03
Capillary Drive 3 = 0.2
Surface Albedo 3 = 0.23
Number of Soil Layers 3 = 3
Porosity 3 = .37 .37 .37
Pore Size Distribution 3 = .252 .23 .23
Bubbling Pressure 3 = .1115 .13 .15
Field Capacity 3 = .12 .13 .14
Wilting Point 3 = .08 .07 .05
Bulk Density 3 = 1300. 1400. 1450.
Vertical Conductivity 3 = 5.7e-05 5.5e-05 5.0e-05
Thermal Conductivity 3 = 7.11 6.92 8.01
Thermal Capacity 3 = 1.4e6 1.4e6 1.4e6
Mannings n 3 = 0.12

################ SOIL 4-SANDY CLAY LOAM
###
Soil Description 4 = HydroC
Lateral Conductivity 4 = 7.069e-04
Exponential Decrease 4 = 3.35
Maximum Infiltration 4 = 6.52e-04
Capillary Drive 4 = 0.2
Surface Albedo 4 = 0.22

Number of Soil Layers 4 = 3
Porosity 4 = .34 .34 .34
Pore Size Distribution 4 = .242 .23 .22
Bubbling Pressure 4 = .2589 .27 .28
Field Capacity 4 = .215 .23 .25
Wilting Point 4 = .097 .077 .057
Bulk Density 4 = 1300. 1400. 1500.
Vertical Conductivity 4 = 2.5e-05 2.5e-05 2.0e-05
Thermal Conductivity 4 = 7.11 6.92 8.01
Thermal Capacity 4 = 1.4e6 1.4e6 1.4e6
Mannings n 4 = 0.08

################ SOIL 5-CLAY/SILTY CLAY LOAM
##
Soil Description 5 = HydroD
Lateral Conductivity 5 = 2.0375e-04
Exponential Decrease 5 = 3.35
Maximum Infiltration 5 = 3.5e-04
Capillary Drive 5 = 0.2
Surface Albedo 5 = 0.22
Number of Soil Layers 5 = 3
Porosity 5 = .36 .36 .36
Pore Size Distribution 5 = .165 .15 .14
Bubbling Pressure 5 = .36 .37 .38
Field Capacity 5 = .31 .29 .27
Wilting Point 5 = .14 .15 .16
Bulk Density 5 = 1100. 1250. 1400.
Vertical Conductivity 5 = 3.8e-6 3.7e-6 3.0e-6
Thermal Conductivity 5 = 7.11 6.92 8.1
Thermal Capacity 5 = 1.4e6 1.4e6 1.4e6
Mannings n 5 = 0.05

################ SOIL 6 ##
old number 14 cod
Soil Description 6 = SL SILTY LOAM SIL
Lateral Conductivity 6 = 0.01
Exponential Decrease 6 = 3.3
Maximum Infiltration 6 = 1.0e-5
Capillary Drive 6 = 0.20
Surface Albedo 6 = 0.1
Number of Soil Layers 6 = 3
Porosity 6 = .45 .50 .50
Pore Size Distribution 6 = .21 .19 .19
Bubbling Pressure 6 = .15 .18 .18
Field Capacity 6 = .19 .28 .28
Wilting Point 6 = .10 .16 .16
Bulk Density 6 = 1510. 1380. 1380.
Vertical Conductivity 6 = 0.000034 0.000072 0.000072 #1.8e-5
Thermal Conductivity 6 = 7.114 6.923 7.0
Thermal Capacity 6 = .0000014 .0000014 .0000014
Mannings n 6 = 0.02 #0.012-0.033

################ SOIL 7 ##
old number 22 cod
Soil Description 7 = SILTY LOAM
Lateral Conductivity 7 = .01

Exponential Decrease 7 = 3.0
Maximum Infiltration 7 = 1.0e-5
Capillary Drive 7 = 0.11
Surface Albedo 7 = 0.1
Number of Soil Layers 7 = 3
Porosity 7 = .50 .50 .50
Pore Size Distribution 7 = .19 .19 .19
Bubbling Pressure 7 = .18 .18 .18
Field Capacity 7 = .28 .28 .287
Wilting Point 7 = .16 .16 .16
Bulk Density 7 = 1380. 1380. 1380.
Vertical Conductivity 7 = 0.000072 0.000072 0.000072 #4.0e-5
Thermal Conductivity 7 = 7.114 6.923 7.0
Thermal Capacity 7 = .0000014 .0000014 .0000014
Mannings n 7 = 0.02 #0.012-0.033

##
VEGETATION INFORMATION SECTION
##
(VEGETATION)

Vegetation Map File = ../input/more_lclu100.bin

Number of Vegetation Types = 15 # Number of different vegetation types

################ VEGETATION 1 ##
Vegetation Description 1 = Conifer
Impervious Fraction 1 = 0.0
Detention Fraction 1 = 0.0
Detention Decay 1 = 0.0
IMPERVIOUS SURFACE ROUTING FILE =
Overstory Present 1 = TRUE
Understory Present 1 = TRUE
Fractional Coverage 1 = 0.47
Hemi Fract Coverage 1 =
Trunk Space 1 = 0.50
Clumping Factor 1 =
Leaf Angle A 1 =
Leaf Angle B 1 =
Scattering Parameter 1 =
Aerodynamic Attenuation 1 = 2.0
Radiation Attenuation 1 = 0.46
Max Snow Int Capacity 1 = 0.04
Snow Interception Eff 1 = 0.6
Mass Release Drip Ratio 1 = 0.4
Height 1 = 22.0 1.0
Overstory Monthly LAI 1 = 2.0 2.0 2.6 3.0 3.2 3.2 3.2 3.2 3.0 3.0 2.6 2.0
Understory Monthly LAI 1 = 0.01 0.01 0.01 0.5 0.5 1.5 1.5 2.0 1.5 0.5 0.5 0.01
Maximum Resistance 1 = 1500. 1000.
Minimum Resistance 1 = 165. 75.
Moisture Threshold 1 = 0.24 0.16
Vapor Pressure Deficit 1 = 4000. 4000.
Rpc 1 = .108 .108
Overstory Monthly Alb 1 = 0.11 0.11 0.11 0.11 0.11 0.11 0.11 0.11 0.11 0.11 0.11 0.11
Understory Monthly Alb 1 = 0.5 0.5 0.5 0.5 0.2 0.2 0.2 0.2 0.2 0.2 0.2 0.5
Number of Root Zones 1 = 3

Root Zone Depths 1 = 0.2 0.45 0.25
Overstory Root Fraction 1 = 0.35 0.40 0.25
Understory Root Fraction 1 = 0.6 0.4 0.0

Vegetation Description 2 = Deciduous Forest
Impervious Fraction 2 = 0.0
Detention Fraction 2 = 0.0
Detention Decay 2 = 0.0
IMPERVIOUS SURFACE ROUTING FILE =
Overstory Present 2 = TRUE
Understory Present 2 = TRUE
Fractional Coverage 2 = 0.47
Hemi Fract Coverage 2 =
Clumping Factor 2 =
Leaf Angle A 2 =
Leaf Angle B 2 =
Scattering Parameter 2 =
Trunk Space 2 = 0.6
Clumping Factor 2 =
Leaf Angle A 2 =
Leaf Angle B 2 =
Scattering Parameter 2 =
Trunk Space 2 =
Aerodynamic Attenuation 2 = 2.0
Radiation Attenuation 2 = 0.579
Max Snow Int Capacity 2 = 0.002
Snow Interception Eff 2 = 0.1
Mass Release Drip Ratio 2 = 0.4
Height 2 = 23.0 1.0
Overstory Monthly LAI 2 = 1.1 1.1 1.5 3.0 3.5 4.0 4.5 4.5 4.0 3.0 2.5 1.1
Understory Monthly LAI 2 = 0.01 0.01 0.2 0.5 1.0 1.5 1.5 1.5 1.0 0.5 0.2 0.01
Maximum Resistance 2 = 2500. 1000.
Minimum Resistance 2 = 165. 75.
Moisture Threshold 2 = 0.24 0.16
Vapor Pressure Deficit 2 = 4000. 4000.
Rpc 2 = 0.108 0.108
Overstory Monthly Alb 2 = .1 .1 .1 .1 .18 .18 .18 .18 .18 .18 .18 .1
Understory Monthly Alb 2 = 0.5 0.5 0.5 0.5 0.2 0.2 0.2 0.2 0.2 0.2 0.2 0.5
Number of Root Zones 2 = 3
Root Zone Depths 2 = 0.2 0.40 0.10
Overstory Root Fraction 2 = 0.3 0.60 0.10
Understory Root Fraction 2 = 0.8 0.2 0.00

Vegetation Description 3 = Brush/transitional
Impervious Fraction 3 = 0.0
Detention Fraction 3 = 0.0
Detention Decay 3 = 0.0
Overstory Present 3 = TRUE
Understory Present 3 = TRUE
Fractional Coverage 3 = 0.47
Hemi Fract Coverage 3 =
Clumping Factor 3 =
Leaf Angle A 3 =
Leaf Angle B 3 =
Scattering Parameter 3 =
Trunk Space 3 = 0.8

Aerodynamic Attenuation 3 = 2.0
Radiation Attenuation 3 = 0.579
Max Snow Int Capacity 3 = 0.002
Snow Interception Eff 3 = 0.1
Mass Release Drip Ratio 3 = 0.4
Height 3 = 12.0 0.5
Overstory Monthly LAI 3 = 0.15 0.15 0.15 0.5 2.5 3.5 3.5 3.5 3.0 2.5 .15 .15
Understory Monthly LAI 3 = 0.01 0.01 0.2 0.5 0.5 0.8 0.8 1.1 0.8 0.25 0.02 0.01
Maximum Resistance 3 = 2500. 1000.
Minimum Resistance 3 = 165 75
Moisture Threshold 3 = 0.24 0.16
Vapor Pressure Deficit 3 = 4000. 4000.
Rpc 3 = .108 .108
Overstory Monthly Alb 3 = .1 .1 .1 .1 .18 .18 .18 .18 .18 .18 .18 .1
Understory Monthly Alb 3 = 0.5 0.5 0.5 0.5 0.2 0.2 0.2 0.2 0.2 0.2 0.2 0.5
Number of Root Zones 3 = 3
Root Zone Depths 3 = 0.2 0.45 0.10
Overstory Root Fraction 3 = 0.5 0.5 0.0
Understory Root Fraction 3 = 1.0 0.0 0.0

Vegetation Description 4 = Mixed Forest
Impervious Fraction 4 = 0.0
Detention Fraction 4 = 0.0
Detention Decay 4 = 0.0
IMPERVIOUS SURFACE ROUTING FILE =
Overstory Present 4 = TRUE
Understory Present 4 = TRUE
Fractional Coverage 4 = 0.47
Hemi Fract Coverage 4 =
Clumping Factor 4 =
Leaf Angle A 4 =
Leaf Angle B 4 =
Scattering Parameter 4 =
Trunk Space 4 = 0.6
Clumping Factor 4 =
Leaf Angle A 4 =
Leaf Angle B 4 =
Scattering Parameter 4 =
Trunk Space 4 =
Aerodynamic Attenuation 4 = 2.0
Radiation Attenuation 4 = 0.579
Max Snow Int Capacity 4 = 0.002
Snow Interception Eff 4 = 0.1
Mass Release Drip Ratio 4 = 0.4
Height 4 = 22.0 1.0
Overstory Monthly LAI 4 = 1.5 1.5 1.5 2.5 3.0 3.5 3.5 3.5 3.5 2.5 2.0 1.5
Understory Monthly LAI 4 = 0.01 0.01 0.2 1.0 1.5 1.8 1.8 1.8 1.0 1.0 0.2 0.01
Maximum Resistance 4 = 2500. 1000.
Minimum Resistance 4 = 165. 75.
Moisture Threshold 4 = 0.24 0.16
Vapor Pressure Deficit 4 = 4000. 4000.
Rpc 4 = 0.108 0.108
Overstory Monthly Alb 4 = .1 .1 .1 .1 .18 .18 .18 .18 .18 .18 .18 .1
Understory Monthly Alb 4 = 0.5 0.5 0.5 0.5 0.2 0.2 0.2 0.2 0.2 0.2 0.2 0.5
Number of Root Zones 4 = 3
Root Zone Depths 4 = 0.2 0.45 0.25

Overstory Root Fraction 4 = 0.4 0.40 0.20
Understory Root Fraction 4 = 0.8 0.20 0.00

Vegetation Description 5 = Forested Wetland
Impervious Fraction 5 = 0.0
Detention Fraction 5 = 0.0
Detention Decay 5 = 0.0
Overstory Present 5 = TRUE
Understory Present 5 = TRUE
Fractional Coverage 5 = 0.75
Hemi Fract Coverage 5 = 0.5
Clumping Factor 5 =
Leaf Angle A 5 =
Leaf Angle B 5 =
Scattering Parameter 5 =
Trunk Space 5 = 0.4
Aerodynamic Attenuation 5 = 0.5
Radiation Attenuation 5 = 0.2
Max Snow Int Capacity 5 = 0.003
Snow Interception Eff 5 = 0.6
Mass Release Drip Ratio 5 = 0.4
Height 5 = 15.0 0.5
Overstory Monthly LAI 5 = .5 .5 .5 1.0 2.0 4.0 4.0 4.0 4.0 2.0 1.5 .5
Understory Monthly LAI 5 = .5 .5 .5 1.0 1.0 2.3 2.3 2.3 2.3 1.0 1.0 .5
Maximum Resistance 5 = 1000 600.
Minimum Resistance 5 = 280 200.
Moisture Threshold 5 = 0.33 0.33
Vapor Pressure Deficit 5 = 4000 4000
Rpc 5 = 0.108 0.108
Overstory Monthly Alb 5 = 0.15 0.15 0.15 0.15 0.15 0.14 0.14 0.14 0.14 0.15 0.15 0.15
Understory Monthly Alb 5 = 0.18 0.18 0.18 0.18 0.18 0.18 0.18 0.18 0.18 0.18 0.18 0.18
Number of Root Zones 5 = 3
Root Zone Depths 5 = 0.2 0.40 0.10
Overstory Root Fraction 5 = 0.40 0.50 0.10
Understory Root Fraction 5 = 0.8 0.20 0.00

Vegetation Description 6 = non-forested wetland
Impervious Fraction 6 = 0.0
Detention Fraction 6 = 0.0
Detention Decay 6 = 0.0
Overstory Present 6 = TRUE
Understory Present 6 = TRUE
Fractional Coverage 6 = 0.8
Hemi Fract Coverage 6 =
Clumping Factor 6 =
Leaf Angle A 6 =
Leaf Angle B 6 =
Scattering Parameter 6 =
Trunk Space 6 = 0.5
Aerodynamic Attenuation 6 = 0.5
Radiation Attenuation 6 = 0.2
Max Snow Int Capacity 6 = 0.003
Snow Interception Eff 6 = 0.6
Mass Release Drip Ratio 6 = 0.4
Height 6 = 8.0 0.5
Overstory Monthly LAI 6 = 0.2 0.2 0.5 1.5 2.0 2.5 2.5 2.5 2.0 1.0 0.5 0.2

Understory Monthly LAI 6 = 0.01 0.01 0.5 1.0 1.0 1.5 2.0 2.0 1.5 0.5 0.2 0.01
Maximum Resistance 6 = 2000. 600.
Minimum Resistance 6 = 500. 280.
Moisture Threshold 6 = 0.33 0.13
Vapor Pressure Deficit 6 = 4000 4000
Rpc 6 = .108 .108
Overstory Monthly Alb 6 = 0.24 0.24 0.23 0.22 0.21 0.20 0.20 0.20 0.22 0.23 0.24 0.24
Understory Monthly Alb 6 = 0.24 0.24 0.23 0.22 0.21 0.20 0.20 0.20 0.22 0.23 0.24 0.24
Number of Root Zones 6 = 3
Root Zone Depths 6 = 0.20 0.40 0.1
Overstory Root Fraction 6 = 0.50 0.30 0.20
Understory Root Fraction 6 = 1.0 0.00 0.00

Vegetation Description 7 = not assigned
Impervious Fraction 7 = 0.0
Detention Fraction 7 = 0.0
Detention Decay 7 = 0.0
Overstory Present 7 = FALSE
Understory Present 7 = FALSE
Fractional Coverage 7 = 0.0
Hemi Fract Coverage 7 = 0.0
Clumping Factor 7 =
Leaf Angle A 7 =
Leaf Angle B 7 =
Scattering Parameter 7 =
Trunk Space 7 = 0.0
Aerodynamic Attenuation 7 = 0.0
Radiation Attenuation 7 = 0.0
Max Snow Int Capacity 7 = 0.00
Snow Interception Eff 7 = 0.75
Mass Release Drip Ratio 7 = 0.0
Height 7 = 0.0 0.0
Overstory Monthly LAI 7 = 0.0 0.0 0.0 0.0 0.0 0.0 0.0 0.0 0.0 0.0 0.0 0.0
Understory Monthly LAI 7 = 0.0 0.0 0.0 0.0 0.0 0.0 0.0 0.0 0.0 0.0 0.0 0.0
Maximum Resistance 7 = 00. 00.
Minimum Resistance 7 = 0. .
Moisture Threshold 7 = 0.0 0.0
Vapor Pressure Deficit 7 = 4000 4000
Rpc 7 = .108 .108
Overstory Monthly Alb 7 = 0.8 0.8 0.8 0.8 0.22 0.21 0.21 0.21 0.21 0.22 0.24 0.26
Understory Monthly Alb 7 = 0.175 0.175 0.175 0.175 0.175 0.175 0.175 0.175 0.175 0.175 0.175 0.175
Number of Root Zones 7 = 3
Root Zone Depths 7 = 0.2 0.3 0.2
Overstory Root Fraction 7 = 0.0
Understory Root Fraction 7 = 0.0

Vegetation Description 8 = Pasture/hay
Impervious Fraction 8 = 0.0
Detention Fraction 8 = 0.0
Detention Decay 8 = 0.0
Overstory Present 8 = FALSE
Understory Present 8 = TRUE
Fractional Coverage 8 = 0.9
Hemi Fract Coverage 8 =
Clumping Factor 8 =
Leaf Angle A 8 =

Leaf Angle B 8 =
Scattering Parameter 8 =
Trunk Space 8 = 0.0
Aerodynamic Attenuation 8 = 1.0
Radiation Attenuation 8 = 0.4
Max Snow Int Capacity 8 = 0.0
Snow Interception Eff 8 = 0.0
Mass Release Drip Ratio 8 = 0.0
Height 8 = 1.0
Overstory Monthly LAI 8 = 0.0 0.0 0.0 0.0 0.0 0.0 0.0 0.0 0.0 0.0 0.0 0.0
Understory Monthly LAI 8 = 0.01 0.01 0.01 1.0 2.0 4.0 4.5 5.0 4.5 2.0 1.0 0.01
Maximum Resistance 8 = 1000
Minimum Resistance 8 = 50
Moisture Threshold 8 = 0.25
Vapor Pressure Deficit 8 = 4000.
Rpc 8 = .108
Overstory Monthly Alb 8 = 0.0 0.0 0.0 0.0 0.0 0.0 0.0 0.0 0.0 0.0 0.0 0.0
Understory Monthly Alb 8 = 0.2 0.4 0.4 0.2 0.18 0.16 0.16 0.16 0.16 0.16 0.18 0.18
Number of Root Zones 8 = 3
Root Zone Depths 8 = 0.25 0.15 0.01
Overstory Root Fraction 8 = 0.80 0.20 0.00
Understory Root Fraction 8 = 1.0 0.00 0.00

Vegetation Description 9 = Orchard (not assigned)
Impervious Fraction 9 = 0.0
Detention Fraction 9 = 0.0
Detention Decay 9 = 0.0
Overstory Present 9 = TRUE
Understory Present 9 = FALSE
Fractional Coverage 9 = 0.5
Hemi Fract Coverage 9 =
Clumping Factor 9 =
Leaf Angle A 9 =
Leaf Angle B 9 =
Scattering Parameter 9 =
Trunk Space 9 = 0.5
Aerodynamic Attenuation 9 = 1.0
Radiation Attenuation 9 = 0.4
Max Snow Int Capacity 9 = 0.0
Snow Interception Eff 9 = 0.0
Mass Release Drip Ratio 9 = 0.0
Height 9 = 12.0
Overstory Monthly LAI 9 = 2.0 2.0 2.0 2.0 2.0 6.5 6.5 6.5 6.5 2.0 2.0 2.0
Understory Monthly LAI 9 = 2.0 2.0 2.0 2.0 2.0 6.5 6.5 6.5 6.5 2.0 2.0 2.0
Maximum Resistance 9 = 600
Minimum Resistance 9 = 220
Moisture Threshold 9 = 0.24
Vapor Pressure Deficit 9 = 4000
Rpc 9 = .108
Overstory Monthly Alb 9 = 0.8 0.8 0.8 0.8 0.22 0.21 0.21 0.21 0.21 0.22 0.24 0.26
Understory Monthly Alb 9 = 0.175 0.175 0.175 0.175 0.175 0.175 0.175 0.175 0.175 0.175 0.175 0.175
Number of Root Zones 9 = 3
Root Zone Depths 9 = 0.20 0.30 0.20
Overstory Root Fraction 9 = 0.60 0.30 0.10
Understory Root Fraction 9 = 1.0 0.00 0.00

Vegetation Description 10 = Roads/transportation
Impervious Fraction 10 = 0.0
Detention Fraction 10 = 0.0
Detention Decay 10 = 0.0
Overstory Present 10 = FALSE
Understory Present 10 = FALSE
Fractional Coverage 10 =
Hemi Fract Coverage 10 =
Clumping Factor 10 =
Leaf Angle A 10 =
Leaf Angle B 10 =
Scattering Parameter 10 =
Trunk Space 10 =
Aerodynamic Attenuation 10 =
Radiation Attenuation 10 =
Max Snow Int Capacity 10 =
Snow Interception Eff 10 =
Mass Release Drip Ratio 10 =
Height 10 = 0.2
Overstory Monthly LAI 10 =
Understory Monthly LAI 10 = 0.01 0.01 0.01 0.01 0.01 0.01 0.01 0.01 0.01 0.01 0.01 0.01
Maximum Resistance 10 = 600
Minimum Resistance 10 = 70
Moisture Threshold 10 = 0.24
Vapor Pressure Deficit 10 = 4000
Rpc 10 = .108
Overstory Monthly Alb 10 =
Understory Monthly Alb 10 = 0.19 0.19 0.19 0.19 0.19 0.19 0.19 0.19 0.19 0.19 0.19 0.19
Number of Root Zones 10 = 3
Root Zone Depths 10 = 0.20 0.20 0.20
Overstory Root Fraction 10 = 0.60 0.20 0.20
Understory Root Fraction 10 = 1.0 0.00 0.00

Vegetation Description 11 = Agriculture/Mixed Open
Impervious Fraction 11 = 0.0
Detention Fraction 11 = 0.0
Detention Decay 11 = 0.0
Overstory Present 11 = FALSE
Understory Present 11 = TRUE
Fractional Coverage 11 =
Hemi Fract Coverage 11 =
Clumping Factor 11 =
Leaf Angle A 11 =
Leaf Angle B 11 =
Scattering Parameter 11 =
Trunk Space 11 =
Aerodynamic Attenuation 11 =
Radiation Attenuation 11 =
Max Snow Int Capacity 11 =
Snow Interception Eff 11 =
Mass Release Drip Ratio 11 =
Height 11 = 2.0
Overstory Monthly LAI 11 =
Understory Monthly LAI 11 = 0.01 0.01 0.01 0.5 1.5 3.0 3.5 3.5 3.5 2.0 0.5 0.01
Maximum Resistance 11 = 100.
Minimum Resistance 11 = 60.

Moisture Threshold 11 = 0.25
Vapor Pressure Deficit 11 = 4000.
Rpc 11 = .108
Overstory Monthly Alb 11 =
Understory Monthly Alb 11 = 0.5 0.5 0.5 0.5 0.2 0.2 0.2 0.2 0.2 0.2 0.2 0.5
Number of Root Zones 11 = 3
Root Zone Depths 11 = 0.20 0.30 0.20
Overstory Root Fraction 11 = 0.70 0.20 0.10
Understory Root Fraction 11 = 0.6 0.40 0.00

Vegetation Description 12 = Barren
Impervious Fraction 12 = 0.0
Detention Fraction 12 = 0.0
Detention Decay 12 = 0.0
Overstory Present 12 = FALSE
Understory Present 12 = FALSE
Fractional Coverage 12 =
Hemi Fract Coverage 12 =
Clumping Factor 12 =
Leaf Angle A 12 =
Leaf Angle B 12 =
Scattering Parameter 12 =
Trunk Space 12 =
Aerodynamic Attenuation 12 =
Radiation Attenuation 12 =
Max Snow Int Capacity 12 =
Snow Interception Eff 12 =
Mass Release Drip Ratio 12 =
Height 12 = 0.0
Overstory Monthly LAI 12 =
Understory Monthly LAI 12 = 0
Maximum Resistance 12 = 0
Minimum Resistance 12 = 0
Moisture Threshold 12 = .1
Vapor Pressure Deficit 12 = 0
Rpc 12 = 0
Overstory Monthly Alb 12 =
Understory Monthly Alb 12 = 0.17 0.17 0.17 0.17 0.17 0.17 0.17 0.17 0.17 0.17 0.17 0.17
Number of Root Zones 12 = 3
Root Zone Depths 12 = 0.20 0.20 0.30
Overstory Root Fraction 12 = 0
Understory Root Fraction 12 = 0

Vegetation Description 13 = Residential
Impervious Fraction 13 = 0.0
Detention Fraction 13 = 0.0
Detention Decay 13 = 0.0
Overstory Present 13 = FALSE
Understory Present 13 = FALSE
Fractional Coverage 13 =
Hemi Fract Coverage 13 =
Clumping Factor 13 =
Leaf Angle A 13 =
Leaf Angle B 13 =
Scattering Parameter 13 =
Trunk Space 13 =

Aerodynamic Attenuation 13 =
Radiation Attenuation 13 =
Max Snow Int Capacity 13 =
Snow Interception Eff 13 =
Mass Release Drip Ratio 13 =
Height 13 = 0
Overstory Monthly LAI 13 =
Understory Monthly LAI 13 = 0
Maximum Resistance 13 = 0
Minimum Resistance 13 = 0
Moisture Threshold 13 = 3
Vapor Pressure Deficit 13 = 0
Rpc 13 = 0
Overstory Monthly Alb 13 =
Understory Monthly Alb 13 =
Number of Root Zones 13 = 3
Root Zone Depths 13 = 0.2 0.2 0.3
Overstory Root Fraction 13 =
Understory Root Fraction 13 =

Vegetation Description 14 = Water
Impervious Fraction 14 = 0.0
Detention Fraction 14 = 0.0
Detention Decay 14 = 0.0
Overstory Present 14 = FALSE
Understory Present 14 = FALSE
Fractional Coverage 14 =
Hemi Fract Coverage 14 =
Clumping Factor 14 =
Leaf Angle A 14 =
Leaf Angle B 14 =
Scattering Parameter 14 =
Trunk Space 14 =
Aerodynamic Attenuation 14 =
Radiation Attenuation 14 =
Max Snow Int Capacity 14 =
Snow Interception Eff 14 =
Mass Release Drip Ratio 14 =
Height 14 =
Overstory Monthly LAI 14 = 0.0 0.0 0.0 0.0 0.0 0.0 0.0 0.0 0.0 0.0 0.0 0.0
Understory Monthly LAI 14 = 0.0 0.0 0.0 0.0 0.0 0.0 0.0 0.0 0.0 0.0 0.0 0.0
Maximum Resistance 14 =
Minimum Resistance 14 =
Moisture Threshold 14 = 3
Vapor Pressure Deficit 14 =
Rpc 14 =
Overstory Monthly Alb 14 = 0.00 0.00 0.00 0.00 0.00 0.00 0.00 0.00 0.00 0.00 0.00 0.00
Understory Monthly Alb 14 = 0.00 0.00 0.00 0.00 0.00 0.00 0.00 0.00 0.00 0.00 0.00 0.00
Number of Root Zones 14 = 3
Root Zone Depths 14 = 0.20 0.20 0.30
Overstory Root Fraction 14 = 0.00 0.00 0.00
Understory Root Fraction 14 = 0.00 0.00 0.00

Vegetation Description 15 = Commercial/Industrial
Impervious Fraction 15 = 0.0
Detention Fraction 15 = 0.0

Detention Decay 15 = 0.0
Overstory Present 15 = FALSE
Understory Present 15 = FALSE
Fractional Coverage 15 =
Hemi Fract Coverage 15 =
Clumping Factor 15 =
Leaf Angle A 15 =
Leaf Angle B 15 =
Scattering Parameter 15 =
Trunk Space 15 =
Aerodynamic Attenuation 15 =
Radiation Attenuation 15 =
Max Snow Int Capacity 15 =
Snow Interception Eff 15 =
Mass Release Drip Ratio 15 =
Height 15 = 0
Overstory Monthly LAI 15 =
Understory Monthly LAI 15 = 0
Maximum Resistance 15 = 0
Minimum Resistance 15 = 0
Moisture Threshold 15 = 0
Vapor Pressure Deficit 15 = 0
Rpc 15 = 0
Overstory Monthly Alb 15 =
Understory Monthly Alb 15 =
Number of Root Zones 15 = 3
Root Zone Depths 15 = 0.10 0.20 0.30
Overstory Root Fraction 15 =
Understory Root Fraction 15 =

Vegetation Description 16 = Other Agricultural/Open
Impervious Fraction 16 = 0.0
Detention Fraction 16 = 0.0
Detention Decay 16 = 0.0
Overstory Present 16 = FALSE
Understory Present 16 = FALSE
Fractional Coverage 16 =
Hemi Fract Coverage 16 =
Clumping Factor 16 =
Leaf Angle A 16 =
Leaf Angle B 16 =
Scattering Parameter 16 =
Trunk Space 16 =
Aerodynamic Attenuation 16 =
Radiation Attenuation 16 =
Max Snow Int Capacity 16 =
Snow Interception Eff 16 =
Mass Release Drip Ratio 16 =
Height 16 = 0
Overstory Monthly LAI 16 =
Understory Monthly LAI 16 = 0
Maximum Resistance 16 = 0
Minimum Resistance 16 = 0
Moisture Threshold 16 = 0
Vapor Pressure Deficit 16 = 0
Rpc 16 = 0

Overstory Monthly Alb 16 =
Understory Monthly Alb 16 =
Number of Root Zones 16 = 3
Root Zone Depths 16 = 0.10 0.20 0.30
Overstory Root Fraction 16 = 0.0
Understory Root Fraction 16 = 0.0

##
MODEL OUTPUT SECTION
##
(OUTPUT) # Information what to output when
Output Directory = ../output/out_c146_bE14r42_MWM32_weathgen_f49_2012_second/
Initial State Directory = ../baseline_first/out_c146_b92r41_MWM45_weathgen_f49_2012_first/

################ PIXEL DUMPS ##

Number of Output Pixels = 25

For each pixel make a key-entry pair as indicated below, varying the
number for the output pixel (1, .. , Number of Output Pixel)

North Coordinate 1 = 197413.88
East Coordinate 1 = 480707.33
Name 1 = Moretown_turb

North Coordinate 2 = 186557.73
East Coordinate 2 = 473148.23
Name 2 = Millbrook_turb

North Coordinate 3 = 192068.133
East Coordinate 3 = 477099.914
Name 3 = Shepherd_bankturb

North Coordinate 4 = 185487.695
East Coordinate 4 = 473292.313
Name 4 = Lareau_bank

North Coordinate 5 = 183724.04
East Coordinate 5 = 472991.658
Name 5 = Folsom_turb

North Coordinate 6 = 187440.735
East Coordinate 6 = 474740.735
Name 6 = HiBridge_turb

North Coordinate 7 = 188386.436
East Coordinate 7 = 469152.756
Name 7 = Mansfield_rd

North Coordinate 8 = 188184.15
East Coordinate 8 = 468921.359
Name 8 = NMansfield_culvert

North Coordinate 9 = 180482.259
East Coordinate 9 = 745351.549

Name 9 = CiderHill_culvert

North Coordinate 10 = 194727.788
East Coordinate 10 = 471533.085
Name 10 = Sharpshooter_rd

North Coordinate 11 = 194666.406
East Coordinate 11 = 471506.625
Name 11 = Sharpshooter_culvert

North Coordinate 12 = 193171.021
East Coordinate 12 = 472876.829
Name 12 = Randell

North Coordinate 13 = 176620.858
East Coordinate 13 = 474377.880
Name 13 = 3Way_intersink

North Coordinate 14 = 185694.736
East Coordinate 14 = 476877.469
Name 14 = SkiValley

North Coordinate 15 = 187925.365
East Coordinate 15 = 472024.978
Name 15 = BraggHill

North Coordinate 16 = 193579.797
East Coordinate 16 = 471810.902
Name 16 = NFayston

North Coordinate 17 = 193551.222
East Coordinate 17 = 471606.114
Name 17 = NFayston_culv

North Coordinate 18 = 177799.645
East Coordinate 18 = 475106.190
Name 18 = Senor

North Coordinate 19 = 177986.970
East Coordinate 19 = 475199.323
Name 19 = Senor_culv

North Coordinate 20 = 193577.43
East Coordinate 20 = 471799.67
Name 20 = NFayston_sink

North Coordinate 21 = 187929.72
East Coordinate 21 = 472025.994
Name 21 = BraggHill_sink

North Coordinate 22 = 186511.416
East Coordinate 22 = 468588.621
Name 22 = Barton

North Coordinate 23 = 185748.348
East Coordinate 23 = 476919.168

```
Name                23 = SkiValley_sink

North Coordinate        24 = 183374.29
East Coordinate         24 = 473554.95
Name                24 = Rolston

North Coordinate        25 = 179458.239
East Coordinate         25 = 471664.26
Name                25 = Free_turb


################ MODEL STATE ####################################################
Number of Model States     =  0          # Number of model states to dump

# For each model state make a key-entry pair as indicated below, varying the
# number for the model state dump (1, .. , Number of Model States)

State Date            1 = 06/01/2011-00  # Time for model state dump
State Date            2 = 09/30/2011-21  # Time for model state dump
State Date            3 = 04/01/2012-00  # Time for model state dump
State Date            4 = 09/30/2012-21  # Time for model state dump
State Date            5 = 09/30/2013-21  # Time for model state dump
#State Date           4 = 01/01/2001-00  # Time for model state dump
################ MODEL MAPS #####################################################

Number of Map Variables    = 0          # Number of different variables for
                                # which you want to output maps

# For each of the variables make a block like the one that follows, varying
# the number of the variable (n = 1, .. , Number of Map Variables)

Map Variable          1 = 504        # ID of the variable to output
Map Layer             1 = 1
Number of Maps          1 = 1
Map Date 1            1 = 10/31/2010-00
#Map Date 2            1 = 10/01/2010-00
#Map Date 3            1 = 12/13/1995-09
#Map Date 4            1 = 12/13/1995-12
#Map Date 5            1 = 12/13/1995-15
#Map Date 6            1 = 12/13/1995-18
#Map Date 7            1 = 12/13/1995-21
#Map Date 8            1 = 12/14/1995-00
#Map Date 9            1 = 12/14/1995-03
#Map Date 10           1 = 12/14/1995-06
#Map Date 11           1 = 12/14/1995-09
#Map Date 12           1 = 12/14/1995-12


Map Variable          2 = 901        # ID of the variable to output
Map Layer             2 = 1
Number of Maps          2 = 1
Map Date 1            2 = 10/31/2010-00
#Map Date 2            2 = 10/01/2010-00
#Map Date 3            2 = 8/13/1999-09
#Map Date 4            2 = 8/13/1999-12
#Map Date 5            2 = 8/13/1999-15
```

```
#Map Date 6             2 = 8/13/1999-18
#Map Date 7             2 = 8/13/1999-21
#Map Date 8             2 = 8/14/1999-00
#Map Date 9             2 = 8/14/1999-03
#Map Date 10            2 = 8/14/1999-06
#Map Date 11            2 = 8/14/1999-09
#Map Date 12            2 = 8/14/1999-12

Map Variable            3 = 504         # ID of the variable to output
Map Layer               3 = 1
Number of Maps          3 = 2
Map Date 1              3 = 04/15/2010-00
Map Date 2              3 = 10/01/2010-00
#Map Date 3             3 = 12/13/1999-09
#Map Date 4             3 = 12/13/1999-12
#Map Date 5             3 = 12/13/1999-15
#Map Date 6             3 = 12/13/1999-18
#Map Date 7             3 = 12/13/1999-21
#Map Date 8             3 = 12/14/1999-00
#Map Date 9             3 = 12/14/1999-03
#Map Date 10            3 = 12/14/1999-06
#Map Date 11            3 = 12/14/1999-09
#Map Date 12            3 = 12/14/1999-12

#Map Variable           4 = 901
#Map Layer              4 = 1
#Number of Maps         4 = 2
#Map Date 1             4 = 04/15/2010-00
#Map Date 2             4 = 10/01/2010-00
#Map Date 3             4 = 05/30/1995-15
#Map Date 4             4 = 11/29/1995-21
#Map Date 5             4 = 06/08/1996-15
#Map Date 6             4 = 05/17/1997-15
#Map Date 7             4 = 06/15/1997-15


################ MODEL IMAGES ###################################################

Number of Image Variables  = 0          # Number of variables for which you
                                # would like to output images

# For each of the variables make a block like the one that follows, varying
# the number of the variable (n = 1, .. , Number of Image Variables)

Image Variable      1 = 501             # ID of the variable to output
Image Layer         1 = 1               # If the variable exists for a number
                                                    # of layers, specify the layers here
                                                    # with the top layer = 1
Image Start         1 =                 # First timestep for which to output
                                # an image
Image End           1 =                 # Last timestep for which to output
                                # an image
Image Interval      1 =                 # Time interval between images (hours)
Image Upper Limit   1 =                 # All values in the output equal to or
                                # greater than this limit will be set
                                # to 255
```

```
Image Lower Limit     1 =              # All values in the output equal to or
                                       # smaller than this limit will be set
                                       # to 0
################ GRAPHIC IMAGES ##################################################

Number of Graphics      =  0           # Number of variables for which you
                                       # would like to output images
Graphics ID          1 = 2             # ID of the variable to output
Graphics ID          2 = 15
Graphics ID          3 = 21
Graphics ID          4 = 24
Graphics ID          5 = 25
Graphics ID          6 = 43
Graphics ID          7 = 44
Graphics ID          8 = 8
Graphics ID          9 = 2
Graphics ID         10 = 50
Graphics ID         11 = 1

# 1          SWE (mm)
# 2          Water Table Depth (mm)
# 3          Digital Elevation Model (m)
# 4          Vegetation Class (index #)
# 5          Soil Class (index #)
# 6          Soil Depth (mm)
# 7          Precipitation at current time step (mm/time step)
# 8          Incoming Shortwave (Beam and Diffuse) (W/sqm)
# 9          Intercepted Snow (mm)
# 10         Snow Surface Temp (C)
# 11         Cold Content of snow entire snow pack (kJ)
# 12         Snow Melt (as Outflow minus Precip, can be negative) (mm/time step)
# 13         Snow Pack Outflow (mm/time step)
# 14         Saturated Subsurface Flow (mm/time step)
# 15         Overland Flow(mm)
# 16         Total Evapotranspiration (soil + all veg layers)
# 17         Ground Snow pack vapor flux (mm)
# 18         Intercepted snow pack vapor flux (mm)
# 19    Soil Moisture (Surface Layer) % of saturation (i.e. porosity)
# 20    Soil Moisture (2nd Layer) % of saturation (i.e. porosity)
# 21    Soil Moisture (3rd Layer) % of saturation (i.e. porosity)
# 22    Accumulated Precip (mm)
# 23    air temperature (C)
# 24    wind speed (m/s)
# 25    relative humidity
# 26    Prism Precip Field (mm)
# 31    Overstory Transpiration (mm)
# 32    Understory Transpirtation (mm)
# 33    Soil Evaporation (mm)
# 34    Overstory Evaporation (mm)
# 35    Understory Evaportation (mm)
# 41    Sky View Factor (%)
# 42    Shade Map (%)
# 43    Direct Beam Shortwave Rad (W/sqm)
# 44    Diffuse Beam Shortwave Rad (W/sqm)
# 45    Aspect (degrees)
# 46    Slope (percent)
```

```
# 50    Channel Subsurface Interception (mm)
# 51    Road Subsurface Interception (mm)
# WARNING Use soil mositure layers with caution, to minimize calculations during redraw
# DHSVM does not check to make sure that the assigned soil layer exists

################################################################################
# END OF INPUT FILE
################################################################################
(End)                       # This is probably not needed, but
                          # just in case (to close the previous
                          # section)
```

```
##############################################################################
# MASS WASTING MODEL INPUT FILE FORMAT
##############################################################################
# The following is the input format for Mass Wasting Model for DHSVM.  It is #modeled
# on the .ini files in windows.
# The file is organized in sections (...), which contain key = entry pairs.
# The file is free format, in that correct reading of the file is not dependent
# on spaces and/or the order of the key-entry pairs within a section.
# The keys are not case sensitive.  The entries are case sensitive as far as
# they deal with filenames on a UNIX platform.
# Comments are preceded by a '#', and run from the occurrence of '#' till the
# end of the line. Thus you can comment out an entire line (like in this
# header), or you can place a comment after an entry.
# It is important to place the key-entry pair in the correct section, since it
# will not be found if it is in another section.
# Since it will only use the keys that it requires you do not have to worry
# about empty entries for keys that are not needed.
# The key-entry pair format will also allow more specific error messages, since
# it is now easier to automate the process of reporting exactly which key is
# missing or cannot be read.  This should be an improvement over the cryptic
# "error in input file" type of message.
##############################################################################
# SEDIMENT OPTIONS SECTION
##############################################################################
(SEDOPTIONS)                    # Sediment Model Options
Mass Wasting       = FALSE        # TRUE or FALSE
Surface Erosion    = TRUE         # TRUE or FALSE
Channel Routing    = TRUE         # TRUE or FALSE
Road Erosion       = TRUE

##############################################################################
# PARAMETER SECTION
##############################################################################
(PARAMETERS)                    # Model Options
Mass wasting spacing =  25       # Resolution of mass wasting in m
Maximum Iterations = 10          # 0 for deterministic mode
                                 # Number > 0 for stochastic mode
Channel Parent d50 = 0.05        # currently not used
Channel Parent d90 = 1.0         # currently not used
Debris Flow d50 = 0.15           # in mm
Debris Flow d90 = 3.0            # in mm

##############################################################################
# TIME SECTION
##############################################################################
(SEDTIME)
# These are based on roads. May need to modify for other scenarios

MWM Time Steps     = 0           # Number of time to run the mass wasting model

Mass Wasting Date  1 = 06/08/1996-15
Mass Wasting Date  2 = 05/17/1997-15
Mass Wasting Date  3 = 06/15/1997-15
Mass Wasting Date  4 = 06/14/1997-00
Mass Wasting Date  5 = 07/06/1997-00
```

```
SE Time Steps       = 1             # Number of periods to run the surface
                                    # erosion model
Erosion Start     1 = 10/01/2011-21   # Surface Erosion start time (MM/DD/YYYY-#HH)
Erosion End       1 = 09/30/2012-21   # Surface Erosion end time (MM/DD/YYYY-HH)
Erosion Start     2 = 03/30/2010-00
Erosion End       2 = 04/25/2010-00
Erosion Start     3 = 10/01/2010-00
Erosion End       3 = 10/23/2010-00
Erosion Start     4 = 12/10/2010-00
Erosion End       4 = 12/15/2010-00


##########################################################################################
# ELEVATION INFORMATION SECTION
##########################################################################################
(FINEDEM)                           # Terrain information

DEM File        = ../input/more_dem25m.bin     # Fine resolution DEM.
MASK File       = ../input/more_msk25.bin  # Fine resolution mask

##########################################################################################
# SEDIMENT INFORMATION SECTION
##########################################################################################
(SEDIMENT)                          # Soil information

Number of Soil Types = 5                # Number of soil types specifed in
                                    # configuration file

# Descriptions and parameters should correspond to those specified in the
# configuration file

################ SOIL 1, water ###########################################
Soil Description          1  = WATER (as clay)
Kindex                  1  = -999.         #1/J
d50                     1  = .001          #mm
Soil Cohesion Distribution  1  = NORMAL
SC Mean                 1  = 2000.         #kPa
SC Dev                  1  = 0.            #kPa
Angle of Internal Friction Distribution   1 = NORMAL
AIF Mean                1  = 45.           #degrees
AIF Dev                 1  = 0.            #degrees

################ SOIL 2, HydroA ##########################################################
Soil Description          2   = SANDY LOAM
Kindex                  2   = 40.
d50                     2   = 0.17
Soil Cohesion Distribution  2   = NORMAL
SC Mean                 2   = 10.
SC Dev                  2   = 2.
Angle of Internal Friction Distribution   2 = UNIFORM
AIF Min                 2   = 30.
AIF Max                 2   = 42.

################ SOIL 3, HydroB
##########################################################
```

```
Soil Description          3  = LOAM/SILT LOAM
Kindex                  3  = 38.
d50                   3  = 0.005
Soil Cohesion Distribution  3  = NORMAL
SC Mean                 3  = 12.
SC Dev                  3  = 2.
Angle of Internal Friction Distribution   3 = UNIFORM
AIF Min                 3  = 29.
AIF Max                 3  = 38.

################ SOIL 4, HydroC ################################################
Soil Description          4   = SANDY CLAY LOAM
Kindex                  4   = 35.
d50                   4   = 0.001
Soil Cohesion Distribution  4   = NORMAL
SC Mean                 4   = 16.
SC Dev                  4   = 2.
Angle of Internal Friction Distribution   4 = UNIFORM
AIF Min                 4   = 33.
AIF Max                 4   = 45.

############### SOIL 5, HydroD
############################################################
Soil Description          5   = CLAY LOAM, SANDY/SILTY CLAY
Kindex                  5   = 35.       # 1/J
d50                   5   = 0.0005       # mm
Soil Cohesion Distribution  5   = NORMAL
SC Mean                 5   = 22.       # kPa
SC Dev                  5   = 2.        # kPa
SC Min                  5   =          # kPa
#SC Max                  5   =          # kPa
#SC Mode                 5   =          # kPa
Angle of Internal Friction Distribution   5 = UNIFORM
#AIF Mean                5   =          # degrees
#AIF Dev                 5   =          # degrees
AIF Min                 5   = 33.       # degrees
AIF Max                 5   = 45.       # degrees
#AIF Mode                5   =          # degrees

################ SOIL 6 ########################################################
Soil Description          6  = SILTY LOAM
Kindex                  6  = 28.
d50                   6  = .04
Soil Cohesion Distribution  6  = NORMAL
SC Mean                 6  = 16.
SC Dev                  6  = 6.
Angle of Internal Friction Distribution   6 = UNIFORM
AIF Min                 6  = 29.
AIF Max                 6  = 37.

################ SOIL 7 ########################################################
Soil Description          7  = SILTY LOAM
Kindex                  7  = 28.
d50                   7  = .04
Soil Cohesion Distribution  7  = NORMAL
SC Mean                 7  = 16.
```

SC Dev 7 = 6.
Angle of Internal Friction Distribution 7 = UNIFORM
AIF Min 7 = 29.
AIF Max 7 = 37.

################ SOIL 8 ##
Soil Description 8 = LOAMY FINE SAND
Kindex 8 = 62.
d50 8 = .25
Soil Cohesion Distribution 8 = NORMAL
SC Mean 8 = 15.
SC Dev 8 = 7.
Angle of Internal Friction Distribution 8 = UNIFORM
AIF Min 8 = 31.
AIF Max 8 = 42.

################ SOIL 11 ###
Soil Description 11 = FINE SANDY LOAM
Kindex 11 = 32.
d50 11 = .2
Soil Cohesion Distribution 11 = NORMAL
SC Mean 11 = 18.
SC Dev 11 = 4.5
Angle of Internal Friction Distribution 11 = UNIFORM
AIF Min 11 = 31.
AIF Max 11 = 39.

################ SOIL 13 ###
Soil Description 13 = LOAM
Kindex 13 = 30.
d50 13 = .1
Soil Cohesion Distribution 13 = NORMAL
SC Mean 13 = 22.
SC Dev 13 = 8.
Angle of Internal Friction Distribution 13 = UNIFORM
AIF Min 13 = 29.
AIF Max 13 = 38.

################ SOIL 22 ###
same as 13
Soil Description 22 = ORGANIC (as loam)
Kindex 22 = 30.
d50 22 = .1
Soil Cohesion Distribution 22 = NORMAL
SC Mean 22 = 22.
SC Dev 22 = 8.
Angle of Internal Friction Distribution 22 = UNIFORM
AIF Min 22 = 29.
AIF Max 22 = 38.

################ SOIL 23 ###
Soil Description 23 = BEDROCK
Kindex 23 = -999.
d50 23 = 2.
Soil Cohesion Distribution 23 = NORMAL
SC Mean 23 = 2000.

```
SC Dev                  23  = 0.
Angle of Internal Friction Distribution   23 = NORMAL
AIF Mean                23  = 45.
AIF Dev                 23  = 0.

################ SOIL 24 ############################################################
# same as 23
Soil Description          24  = WATER (as clay)
Kindex                  24  = -999.
d50                   24  = 2.
Soil Cohesion Distribution  24  = NORMAL
SC Mean                 24  = 2000.
SC Dev                  24  = 0.
Angle of Internal Friction Distribution   24 = NORMAL
AIF Mean                24  = 45.
AIF Dev                 24  = 0.

################ SOIL 25 ############################################################
# same as 23
Soil Description          25  = ROCK (frag)
Kindex                  25  = -999.
d50                   25  = .2
Soil Cohesion Distribution  25  = NORMAL
SC Mean                 25  = 2000.
SC Dev                  25  = 0.
Angle of Internal Friction Distribution   25 = NORMAL
AIF Mean                25  = 45.
AIF Dev                 25  = 0.


#############################################################################
# VEGETATION INFORMATION SECTION
#############################################################################
(VEGETATION)

Number of Vegetation Types = 15          # Number of different vegetation types
                           # configuration file

# Descriptions and parameters should correspond to those specified in the
# configurataion file

################ VEGETATION 1 ######################################################

Vegetation Description      1 = conifer
Root Cohesion Distribution  1 = TRIANGULAR            # NORMAL, UNIFORM or TRIANGULAR
RC Mode                  1 = 5.5                 # kPa
RC Min                  1 = 2.                  # kPa
RC Max                  1 = 12.                 # kPa
Vegetation Surcharge Distribution   1   = UNIFORM       # NORMAL, UNIFORM or TRIANGULAR
VS Min                  1 = 48.9                # kg/m2
VS Max                  1 = 195.4               # kg/m2

################ VEGETATION 2 ######################################################

Vegetation Description      2 = deciduous forest
Root Cohesion Distribution  2 = TRIANGULAR            # NORMAL, UNIFORM or TRIANGULAR
```

RC Mode 2 = 5.5 # kPa
RC Min 2 = 2. # kPa
RC Max 2 = 12. # kPa
Vegetation Surcharge Distribution 2 = UNIFORM # NORMAL, UNIFORM or TRIANGULAR
VS Min 2 = 48.9 # kg/m2
VS Max 2 = 195.4 # kg/m2

################ VEGETATION 3 ##

Vegetation Description 3 = brush
Root Cohesion Distribution 3 = TRIANGULAR # NORMAL, UNIFORM or TRIANGULAR
RC Mode 3 = 5.5 # kPa
RC Min 3 = 2. # kPa
RC Max 3 = 12. # kPa
Vegetation Surcharge Distribution 3 = UNIFORM # NORMAL, UNIFORM or TRIANGULAR
VS Min 3 = 48.9 # kg/m2
VS Max 3 = 195.4 # kg/m2

################ VEGETATION 4 ##

Vegetation Description 4 = mixed forest
Root Cohesion Distribution 4 = TRIANGULAR
RC Mode 4 = 5.5
RC Min 4 = 2.
RC Max 4 = 12.
Vegetation Surcharge Distribution 4 = UNIFORM
VS Min 4 = 48.9
VS Max 4 = 195.4

################ VEGETATION 5 ##

Vegetation Description 5 = forested wetland
Root Cohesion Distribution 5 = TRIANGULAR
RC Mode 5 = 5.5
RC Min 5 = 2.
RC Max 5 = 12.
Vegetation Surcharge Distribution 5 = UNIFORM
VS Min 5 = 48.9
VS Max 5 = 195.4

################ VEGETATION 6 ##

Vegetation Description 6 = non-forested wetland
Root Cohesion Distribution 6 = TRIANGULAR
RC Mode 6 = 5.5
RC Min 6 = 2.
RC Max 6 = 12.
Vegetation Surcharge Distribution 6 = UNIFORM
VS Min 6 = 48.9
VS Max 6 = 195.4

################ VEGETATION 7 ##

Vegetation Description 7 = COOL_of3
Root Cohesion Distribution 7 = TRIANGULAR
RC Mode 7 = 8.4

RC Min 7 = 4.2
RC Max 7 = 12.6
Vegetation Surcharge Distribution 7 = UNIFORM
VS Min 7 = 48.9
VS Max 7 = 195.4

################ VEGETATION 8 ##

Vegetation Description 8 = pasture/hay
Root Cohesion Distribution 8 = TRIANGULAR
RC Mode 8 = 0.5
RC Min 8 = 0.1
RC Max 8 = 2.0
Vegetation Surcharge Distribution 8 = UNIFORM
VS Min 8 = 0.0
VS Max 8 = 5.0

################ VEGETATION 9 ##

Vegetation Description 9 = orchard
Root Cohesion Distribution 9 = TRIANGULAR
RC Mode 9 = 10.
RC Min 9 = 5.
RC Max 9 = 15.
Vegetation Surcharge Distribution 9 = UNIFORM
VS Min 9 = 0.0
VS Max 9 = 5.0

################ VEGETATION 10 ###

Vegetation Description 10 = roads
Root Cohesion Distribution 10 = NORMAL
RC Mean 10 = 2000.
#RC Min 10 = 0.
RC Dev 10 = 0.
Vegetation Surcharge Distribution 10 = NORMAL
VS Mean 10 = 0.
VS Dev 10 = 0.

################ VEGETATION 11 ###

Vegetation Description 11 = agriculture
Root Cohesion Distribution 11 = TRIANGULAR
RC Mode 11 = 0.5
RC Min 11 = 0.1
RC Max 11 = 2.0
Vegetation Surcharge Distribution 11 = UNIFORM
VS Min 11 = 48.9
VS Max 11 = 195.4

################ VEGETATION 12 ###

Vegetation Description 12 = barren
Root Cohesion Distribution 12 = NORMAL
RC Mean 12 = 0.
RC Dev 12 = 0.

#RC Max 12 = 23.
Vegetation Surcharge Distribution 12 = NORMAL
VS Mean 12 = 0.
VS Dev 12 = 0.

################ VEGETATION 13 ##

Vegetation Description 13 = residential
Root Cohesion Distribution 13 = NORMAL
RC Mean 13 = 2000.
RC Dev 13 = 0.
#RC Max 13 = 23.
Vegetation Surcharge Distribution 13 = NORMAL
VS Mean 13 = 0.
VS Dev 13 = 0.

################ VEGETATION 14 ##

Vegetation Description 14 = water
Root Cohesion Distribution 14 = NORMAL
RC Mean 14 = 2000.
RC Dev 14 = 0.
#RC Max 14 = 23.
Vegetation Surcharge Distribution 14 = NORMAL
VS Mean 14 = 0.
VS Dev 14 = 0.

################ VEGETATION 15 ##

Vegetation Description 15 = commercial/industrial
Root Cohesion Distribution 15 = NORMAL
RC Mean 15 = 2000.
RC Dev 15 = 0.
#RC Max 15 = 23.
Vegetation Surcharge Distribution 15 = NORMAL
VS Mean 15 = 0.
VS Dev 15 = 0.

################ VEGETATION 16 ##

Vegetation Description 16 = other ag
Root Cohesion Distribution 16 = TRIANGULAR
RC Mode 16 = 0.5
RC Min 16 = 0.1
RC Max 16 = 2.0
Vegetation Surcharge Distribution 16 = UNIFORM
VS Min 16 = 0.0
VS Max 16 = 5.0

################ VEGETATION 17 ##

Vegetation Description 17 = Forest_si2
Root Cohesion Distribution 17 = TRIANGULAR
RC Mode 17 = 14.5
RC Min 17 = 6.
RC Max 17 = 23.

Vegetation Surcharge Distribution 17 = UNIFORM
VS Min 17 = 48.9
VS Max 17 = 195.4

################ VEGETATION 18 ##

Vegetation Description 18 = Forest_si3
Root Cohesion Distribution 18 = TRIANGULAR
RC Mode 18 = 14.5
RC Min 18 = 6.
RC Max 18 = 23.
Vegetation Surcharge Distribution 18 = UNIFORM
VS Min 18 = 48.9
VS Max 18 = 195.4

################ VEGETATION 19 ##

Vegetation Description 19 = HDWD1
Root Cohesion Distribution 19 = TRIANGULAR
RC Mode 19 = 5.5
RC Min 19 = 2.
RC Max 19 = 13.
Vegetation Surcharge Distribution 19 = UNIFORM
VS Min 19 = 48.9
VS Max 19 = 195.4

################ VEGETATION 20 ##

Vegetation Description 20 = HDWD2
Root Cohesion Distribution 20 = TRIANGULAR
RC Mode 20 = 5.5
RC Min 20 = 2.
RC Max 20 = 13.
Vegetation Surcharge Distribution 20 = UNIFORM
VS Min 20 = 48.9
VS Max 20 = 195.4

################ VEGETATION 21 ##

Vegetation Description 21 = HDWD3
Root Cohesion Distribution 21 = TRIANGULAR
RC Mode 21 = 5.5
RC Min 21 = 2.
RC Max 21 = 13.
Vegetation Surcharge Distribution 21 = UNIFORM
VS Min 21 = 48.9
VS Max 21 = 195.4

################ VEGETATION 22 ##

Vegetation Description 22 = MOIST_int1
Root Cohesion Distribution 22 = TRIANGULAR
RC Mode 22 = 14.5
RC Min 22 = 6.
RC Max 22 = 23.
Vegetation Surcharge Distribution 22 = UNIFORM

VS Min 22 = 48.9
VS Max 22 = 195.4

################ VEGETATION 23 ##

Vegetation Description 23 = MOIST_int2
Root Cohesion Distribution 23 = TRIANGULAR
RC Mode 23 = 14.5
RC Min 23 = 6.
RC Max 23 = 23.
Vegetation Surcharge Distribution 23 = UNIFORM
VS Min 23 = 48.9
VS Max 23 = 195.4

################ VEGETATION 24 ##

Vegetation Description 24 = MOIST_int3
Root Cohesion Distribution 24 = TRIANGULAR
RC Mode 24 = 14.5
RC Min 24 = 6.
RC Max 24 = 23.
Vegetation Surcharge Distribution 24 = UNIFORM
VS Min 24 = 48.9
VS Max 24 = 195.4

################ VEGETATION 26 ##

Vegetation Description 26 = MOIST_ofms3
Root Cohesion Distribution 26 = TRIANGULAR
RC Mode 26 = 14.5
RC Min 26 = 6.
RC Max 26 = 23.
Vegetation Surcharge Distribution 26 = UNIFORM
VS Min 26 = 48.9
VS Max 26 = 195.4

################ VEGETATION 27 ##

Vegetation Description 27 = MOIST_ofss2
Root Cohesion Distribution 27 = TRIANGULAR
RC Mode 27 = 14.5
RC Min 27 = 6.
RC Max 27 = 23.
Vegetation Surcharge Distribution 27 = UNIFORM
VS Min 27 = 48.9
VS Max 27 = 195.4

################ VEGETATION 29 ##

Vegetation Description 29 = agriculture
Root Cohesion Distribution 29 = TRIANGULAR
RC Mode 29 = 1.5
RC Min 29 = 1.
RC Max 29 = 2.
Vegetation Surcharge Distribution 29 = UNIFORM
VS Min 29 = 0.

VS Max 29 = 5.

################ VEGETATION 30 ##

Vegetation Description 30 = grassland
Root Cohesion Distribution 30 = TRIANGULAR
RC Mode 30 = 1.5
RC Min 30 = 1.
RC Max 30 = 2.
Vegetation Surcharge Distribution 30 = UNIFORM
VS Min 30 = 0.
VS Max 30 = 5.

################ VEGETATION 31 ##

Vegetation Description 31 = shrubland
Root Cohesion Distribution 31 = TRIANGULAR
RC Mode 31 = 4.
RC Min 31 = 2.
RC Max 31 = 6.
Vegetation Surcharge Distribution 31 = UNIFORM
VS Min 31 = 0.
VS Max 31 = 5.

################ VEGETATION 32 ##

Vegetation Description 32 = Water
Root Cohesion Distribution 32 = NORMAL
RC Mean 32 = 2000.
RC Dev 32 = 0.
Vegetation Surcharge Distribution 32 = NORMAL
VS Mean 32 = 0.
VS Dev 32 = 0.

################ VEGETATION 33 ##

Vegetation Description 33 = rock
Root Cohesion Distribution 33 = NORMAL
RC Mean 33 = 2000.
RC Dev 33 = 0.
Vegetation Surcharge Distribution 33 = NORMAL
VS Mean 33 = 0.
VS Dev 33 = 0.

################ VEGETATION 34 ##

Vegetation Description 34 = barren
Root Cohesion Distribution 34 = NORMAL
RC Mean 34 = 0.
RC Dev 34 = 0.
Vegetation Surcharge Distribution 34 = NORMAL
VS Mean 34 = 0.
VS Dev 34 = 0.

###########NOT IN BASIN###

```
################ VEGETATION 13 ################################################

Vegetation Description      13 = blank1
Root Cohesion Distribution  13 = TRIANGULAR
RC Mode                  13 = 7.
RC Min                  13 = 4.
RC Max                  13 = 14.
Vegetation Surcharge Distribution   13  = UNIFORM
VS Min                  13 = 48.9
VS Max                  13 = 195.4

################ VEGETATION 25 ################################################

Vegetation Description      25 = barren
Root Cohesion Distribution  25 = TRIANGULAR
RC Mode                  25 = 7.
RC Min                  25 = 4.
RC Max                  25 = 14.
Vegetation Surcharge Distribution   25  = UNIFORM
VS Min                  25 = 48.9
VS Max                  25 = 195.4

################ VEGETATION 28 ################################################

Vegetation Description      28 = barren
Root Cohesion Distribution  28 = TRIANGULAR
RC Mode                  28 = 7.
RC Min                  28 = 4.
RC Max                  28 = 14.
Vegetation Surcharge Distribution  28   = UNIFORM
VS Min                  28 = 48.9
VS Max                  28 = 195.4

###############################################################################
# STREAM CLASS INFORMATION SECTION
###############################################################################
(STREAMCLASS)

Number of Stream Classes = 5          # Number of different vegetation types
                              # configuration file

# Descriptions and parameters should correspond to those specified in the
# configuration file

################ STREAMCLASS 1 ################################################

Stream Class Description      1 = Order1
Radius of Curvature Distribution  1 = NORMAL            # NORMAL, UNIFORM or TRIANGULAR
RaC Mean                  1 = 70.0                  # m
RaC Dev                  1 = 30.0                  # m
RaC Min                      1 = 10.0
RaC Max                  1 = 150.0
Bank Soil Cohesion Distribution  1  = NORMAL
BSC Mean                  1  = 27.
BSC Dev                  1  = 3.0
Bank Angle of Internal Friction Distribution   1 = NORMAL
```

BAIF Mean 1 = 33.
BAIF Dev 1 = 2.0
Bank Bulk Density Distribution 1 = UNIFORM
BDEN Min 1 = 1700.
BDEN MAX 1 = 2500.
Bank d50 Distribution 1 = NORMAL
Bd50 Mean 1 = .2
Bd50 Dev 1 = .10
Bank Toe d50 Distribution 1 = NORMAL
BTd50 Mean 1 = .2
BTd50 Dev 1 = .10

################ STREAMCLASS 2 ##

Stream Class Description 2 = Order2
Radius of Curvature Distribution 2 = NORMAL # NORMAL, UNIFORM or TRIANGULAR
RaC Mean 2 = 90.0 # m
RaC Dev 2 = 40.0 # m
RaC Min 2 = 15.0
RaC Max 2 = 250.0
Bank Soil Cohesion Distribution 2 = NORMAL
BSC Mean 2 = 25.0
BSC Dev 2 = 3.0
Bank Angle of Internal Friction Distribution 2 = NORMAL
BAIF Mean 2 = 33.
BAIF Dev 2 = 2.0
Bank Bulk Density Distribution 2 = UNIFORM
BDEN Min 2 = 1600.
BDEN Max 2 = 2500.
Bank d50 Distribution 2 = NORMAL
Bd50 Mean 2 = .20
Bd50 Dev 2 = .1
Bank Toe d50 Distribution 2 = NORMAL
BTd50 Mean 2 = .20
BTd50 Dev 2 = .1

################ STREAMCLASS 3 ##

Stream Class Description 3 = Order3
Radius of Curvature Distribution 3 = NORMAL # NORMAL, UNIFORM or TRIANGULAR
RaC Mean 3 = 100. # m
RaC Dev 3 = 65.0 # m
RaC Min 3 = 15.0
RaC Max 3 = 300.0
Bank Soil Cohesion Distribution 3 = NORMAL
BSC Mean 3 = 20.0
BSC Dev 3 = 5.0
Bank Angle of Internal Friction Distribution 3 = NORMAL
BAIF Mean 3 = 33.
BAIF Dev 3 = 2.0
Bank Bulk Density Distribution 3 = UNIFORM
BDEN Min 3 = 1500.
BDEN Max 3 = 1950.
Bank d50 Distribution 3 = NORMAL
Bd50 Mean 3 = .17

Bd50 Dev 3 = .1
Bank Toe d50 Distribution 3 = NORMAL
BTd50 Mean 3 = .17
BTd50 Dev 3 = .1

################ STREAMCLASS 4 ##

Stream Class Description 4 = Order4
Radius of Curvature Distribution 4 = NORMAL # NORMAL, UNIFORM or TRIANGULAR
RaC Mean 4 = 190.0 # m
RaC Dev 4 = 140.0 # m
RaC Min 4 = 50.0
RaC Max 4 = 450.0
Bank Soil Cohesion Distribution 4 = NORMAL
BSC Mean 4 = 17.0
BSC Dev 4 = 7.5
Bank Angle of Internal Friction Distribution 4 = NORMAL
BAIF Mean 4 = 33.
BAIF Dev 4 = 3.0
Bank Bulk Density Distribution 4 = UNIFORM
BDEN Min 4 = 1500.
BDEN Max 4 = 1850.
Bank d50 Distribution 4 = NORMAL
Bd50 Mean 4 = .16
Bd50 Dev 4 = .05
Bank Toe d50 Distribution 4 = NORMAL
BTd50 Mean 4 = .16
BTd50 Dev 4 = .05

################ STREAMCLASS 5 ##

Stream Class Description 5 = Order5
Radius of Curvature Distribution 5 = NORMAL # NORMAL, UNIFORM or
TRIANGULAR
RaC Mean 5 = 350. # m
RaC Dev 5 = 120.0 # m
RaC Min 5 = 75.0
RaC Max 5 = 500.0
Bank Soil Cohesion Distribution 5 = NORMAL
BSC Mean 5 = 13.0
BSC Dev 5 = 8.5
Bank Angle of Internal Friction Distribution 5 = NORMAL
BAIF Mean 5 = 31.
BAIF Dev 5 = 4.0
Bank Bulk Density Distribution 5 = UNIFORM
BDEN Min 5 = 1450.
BDEN Max 5 = 1800.
Bank d50 Distribution 5 = NORMAL
Bd50 Mean 5 = .15
Bd50 Dev 5 = .05
Bank Toe d50 Distribution 5 = NORMAL
BTd50 Mean 5 = .15
BTd50 Dev 5 = .05

################ STREAMCLASS 6 ##

```
Stream Class Description      6 = Order6
Radius of Curvature Distribution  6 = UNIFORM          # NORMAL, UNIFORM or TRIANGULAR
RaC Min                  6 = 8.5                 # m
RaC Max                  6 = 20.                 # m
Bank Soil Cohesion Distribution  25  = NORMAL
BSC Mean                 25  = 2000.
BSC Dev                  25  = 0.
Bank Angle of Internal Friction Distribution   25 = NORMAL
BAIF Mean                25  = 45.
BAIF Dev                 25  = 0.

################ STREAMCLASS 7 ################################################

Stream Class Description      7 = Order7
Radius of Curvature Distribution  7 = UNIFORM          # NORMAL, UNIFORM or TRIANGULAR
RaC Min                  7 = 10.5                # m
RaC Max                  7 = 20.                 # m
Bank Soil Cohesion Distribution  25  = NORMAL
BSC Mean                 25  = 2000.
BSC Dev                  25  = 0.
Bank Angle of Internal Friction Distribution   25 = NORMAL
BAIF Mean                25  = 45.
BAIF Dev                 25  = 0.

################ STREAMCLASS 8 ################################################

Stream Class Description      8 = Order8
Radius of Curvature Distribution  8 = UNIFORM          # NORMAL, UNIFORM or TRIANGULAR
RaC Mean                 8 = 20.5                # m
RaC Dev                  8 = 20.                 # m
Bank Soil Cohesion Distribution  25  = NORMAL
BSC Mean                 25  = 2000.
BSC Dev                  25  = 0.
Bank Angle of Internal Friction Distribution   25 = NORMAL
BAIF Mean                25  = 45.
BAIF Dev                 25  = 0.

################ STREAMCLASS 9 ################################################

Stream Class Description      9 = Order9
Radius of Curvature Distribution  9 = UNIFORM          # NORMAL, UNIFORM or TRIANGULAR
RaC Mean                 9 = 50.5                # m
RaC Dev                  9 = 20.                 # m
Bank Soil Cohesion Distribution  25  = NORMAL
BSC Mean                 25  = 2000.
BSC Dev                  25  = 0.
Bank Angle of Internal Friction Distribution   25 = NORMAL
BAIF Mean                25  = 45.
BAIF Dev                 25  = 0.

###############################################################################
# END OF INPUT FILE
###############################################################################
(End)                        # This is probably not needed, but
                             # just in case (to close the previous
                             # section)
```